

VISION-BASED MEASUREMENT METHODS
FOR SCHOOLS OF FISH AND ANALYSIS OF THEIR BEHAVIORS

KEI TERAYAMA

This thesis was typeset with \LaTeX using classicthesis typography style developed by André Miede (<http://www.miede.de>). The package is located at <http://www.ctan.org/tex-archive/macros/latex/contrib/classicthesis/>

ABSTRACT

We present measurement methods for schools of fish with image processing technology and use them to analyze the behaviors of a large school of sardines.

Collective behaviors of animal groups such as crowds of people, flocks of birds and schools of fish are attractive not only from the viewpoint of animal behavior but also from the perspectives of statistical physics, behavioral economics, and engineering. However, behaviors of schools of fish, in particular large and dense schools, have not been sufficiently empirically analyzed and understood, compared to behaviors of other insects and animals such as ants, bees, and birds. It is mainly because there are difficulties in measuring the behaviors of such fish schools. Nevertheless, to investigate measurement technologies and mechanisms of schooling behavior is important not only for natural science but also for engineering because such technology and knowledge related to schooling behavior must be useful for developing systems to observe health and growth of schooling fishes in aquariums and fish farms, and improving their survival rate.

Based on this research background, we have developed measurement methods for large and dense schools of fish in this thesis. We also have recorded such schools of fish in an aquarium to conduct our research. For such schools, we can sometimes track the members manually even though there are occlusions. On the other hand, we often cannot track members of the schools, even using manual methods, due to frequent occlusions. It is hard to develop a measurement method that deals effectively with these different situations. Therefore, we divide the schools into two types: relatively sparse and relatively dense. And we propose measurement methods which are suitable for each type of density.

For relatively sparse type schools, we first track isolated members and develop a measuring method for each fish behavior. We also propose a multiple fish tracking method based on an appearance model that functions even if more than two fish are occluded.

For schools of the relatively dense type, it is hard to track individuals even using manual methods. However, tracking is not necessary for the measurement of behaviors of the school. We propose a method to estimate the speed distribution of collective motions with dense optical flow.

We analyze schooling behaviors of rotating sardines in the torus shape with the developed measurement methods. We first measure the length and speed distributions in a relatively sparse type school with one of the proposed methods. The speed structure of the school

and the time evolution of the structure are also analyzed. The speed structure we discovered where, outer fish always swim faster in a rotating school, is a new discovery of fish behavior and it is impossible to analyze the time evolution of the speed distributions for large school of fish without the proposed automatic measurement method.

ACKNOWLEDGEMENTS

First of all, I would like to thank my supervisor Prof. Hideki Tsuiki. Without his continuous support and warm encouragements throughout my undergraduate, master and doctoral courses, I could not have carried out this study. I also would like to thank my co-authors Prof. Masa-aki Sakagami and Prof. Hirohisa Hioki for giving me appropriate advices, constructive discussions and valuable comments.

My gratitude also goes to Lecturer Hitoshi Habe at Kinki University and Associate Prof. Kenichiro Shimatani at the Institute of Statistical Mathematics for giving me valuable comments and chances for discussions in their laboratories. It goes without saying that I am very thankful to Associate Prof. Takashi Sakuragawa and Professor Emeritus Masatsugu Kidode at Nara Advanced Institute of Science and Technology for their insightful comments and advices.

I also appreciate helpful contributions from and discussions with my collaborators Daisuke Tadokoro and Koki Hongo. A very warm thank you goes to Dr. Takahisa Toda, Mr. Yu Sengoku, Mr. Kento Miyajima, and Mr. Yasuyuki Tsukamoto for valuable discussions and warm encouragements in our laboratory. I also would like to thank all members in our laboratory.

I sincerely appreciate the cooperation of the Kujukushima Umikirara Aquarium in taking movies of schools of sardines.

Finally, I truly and deeply thank my family: my father Yusaku, my mother Tomoko, and my wife Suzuko. My parents have continuously supported my research life. I would especially like to thank my wife Suzuko, for always giving me warm encouragement and support. Without their support and patience, I could not continue my research.

CONTENTS

1	INTRODUCTION	1
1.1	The Goals of This Thesis	3
1.2	The Overview of This Thesis	5
2	RELATED WORKS	7
2.1	Collective Behaviors	7
2.2	Schooling Behaviors of fishes	8
2.3	Measurement Methods for Collective Motions	10
3	FILMED DATA OF SCHOOLS OF FISH USED IN THIS RESEARCH	15
3.1	A tank in the Kujukushima Umikirara Aquarium and Camera Setup	15
3.2	Filmed Data in the Tank	15
3.3	The Advantages of the School and the Water tank in the Kujukushima Umikirara Aquarium	17
4	TRACKING AND MEASUREMENT METHODS FOR ISOLATED FISH	21
4.1	Introduction	21
4.2	Tail Beat Frequency and Coast Phase	23
4.2.1	Tail Beat Frequency	23
4.2.2	Coast Phase	24
4.3	Our Method	25
4.3.1	Dataset	25
4.3.2	Tracking Method for Isolated Fish	25
4.3.3	Estimations of Fish Length, Tail Beat Frequency and Coast Phase	28
4.4	Experimental Results	31
4.4.1	Tracking Isolated Fish	31
4.4.2	Body Length and Tail Beat Frequency	31
4.4.3	Coast Phase	33
4.5	Conclusion	33
5	TRACKING METHOD FOR MULTIPLE FISH WITH AN APPEARANCE MODEL	35
5.1	Introduction	35
5.2	Tracking Methods for Multiple Objects	37
5.3	Our Method	38
5.3.1	Dataset	38
5.3.2	Appearance Model	39
5.3.3	Parameter Estimation with the Appearance Model	39
5.3.4	Tracking Multiple Fish	40
5.4	Experimental Results	42
5.5	Conclusion	44

6	VELOCITY DISTRIBUTION MEASUREMENT METHOD WITH OPTICAL FLOW FOR SCHOOL OF FISH	45
6.1	Introduction	45
6.2	Measurements of Collective Animal Behaviors	48
6.3	Speed Distribution Measurement with Optical Flow	49
6.4	Rotation Curve	51
6.4.1	Rotation Curve Estimation	51
6.4.2	Experimental Results	57
6.5	Applications of Rotation Curve Estimation Method	63
6.5.1	RC Estimation with a 20 minute Scene	64
6.5.2	Event Detection by School Flow Features	66
6.5.3	RC Estimation of School of Anchovies	68
6.6	Cake-Cut Distribution	70
6.6.1	Speed and Angle distribution on Cake-Cut Regions	70
6.7	Conclusion	74
7	VELOCITY STRUCTURES OF ROTATING FISH SCHOOLS AND THEIR EVOLUTIONS	75
7.1	Introduction	75
7.2	Distributions of Body length, Swimming Speed and Tail Beat Frequency in a Rotating School of Sardines	76
7.3	Rotation Curves of Sardine's Schools and Time Evolution of Their Velocity Structure	79
7.3.1	Time Development of Averaged Speed at the 9th Bin	80
7.3.2	Time Development of the Velocity Structure of the Rotating School	80
7.4	Existence of Averaged Tori over the Dynamical Time	82
7.5	Discussion and Conclusion	83
8	CONCLUSION	87
8.1	Summary	87
8.2	Future Work	89
A	LIST OF PUBLICATIONS	91
	BIBLIOGRAPHY	93

LIST OF FIGURES

- Figure 1 (a) A circular column of army ants (*Eciton praedator*). Source: adapted from [95]. (b) A flock of European Starlings (*Sturnus vulgaris*). Source: adapted from [10]. (c) A school of sardines. (d) Hundreds of people participating in a marathon. Source: adapted from [72]. 1
- Figure 2 A dense and large school of sardines in an aquarium 2
- Figure 3 (a) A part of a RS type school of sardines. (b) A part of a RD type school of sardines. 4
- Figure 4 Structure of this thesis. 5
- Figure 5 (a) A shoal of Surgeonfish. (b) A rotating school of sardines. (c) A school of Goldband Fusilier. (d) A school of Sixfinger threadfin. Couzin *et al.* called (a) a swarm, (b) a torus, (c) a dynamical parallel group and (d) a highly parallel group [29]. (a) by Uxbona, (c) by Brocken Inaglory, and (d) a public domain image. 9
- Figure 6 (a) Two fish are separated. (b) Two fish are occluded. (c) During an occlusion, trajectories of two fish are crossing. (d) During an occlusion, trajectories of two fish are not crossing. (e) Three fish are occluded. (f) Dense school of sardines. Occlusions occur everywhere. 12
- Figure 7 (a) Measuring the position of a fish with an image of fish and their shadows (modified from [66]). (b) An overview of measuring positions with a stereo camera. (c) Measuring the position of a fish with a mirror (modified from [46]). 13
- Figure 8 (a) The open air tank at the aquarium. (b) The tank filmed from a side through thick glass 16
- Figure 9 Camera setup. 16
- Figure 10 (a) Larger fishes in the white ellipse are chub mackerels. (b) A hammerhead shark in the white ellipse is approaching the school of sardines. (c) A rotating school of sardines in a solid torus shape. (d) The hole size of the rotation center is large. (e) The hole size is small. (f) An image of the school taken from a side. (g) A banded houndshark is covering the school. 18

- Figure 11 A snapshot sequence of a 60 second movie in which the school of sardines is attacked and distorted by a hammerhead shark and recovers its form. 19
- Figure 12 A RS type school of sardines taken from the bottom of a tank at the Kujukushima Umikirara Aquarium. 22
- Figure 13 The tail endpoint (blue line) along the axis perpendicular to the line that passes through the area centroid and the head end-point of an isolated fish. The detail is shown in Section 4.3. The orange line is the sinusoid estimated from the first 20 position data. The difference between the two lines are not ignorable, because the tail beat frequency (the blue line) changes over time. 24
- Figure 14 (a) An example of a tail beat cycle of a fish in the school (Figure 12). (b) An example of a fish in coast phase in the school 25
- Figure 15 (a) An isolated fish in the school. (b) The binarized image of (a). (c) The thinned image of (b). (d) The white point is the centroid of the area. The yellow points are the endpoints of the line (c). The red points are the three points that divide the line (c) into quarters. 26
- Figure 16 The overview of the reference points. 28
- Figure 17 An overview of the position of the tail endpoint. 29
- Figure 18 The estimated results of tail endpoint positions and tail beat frequencies with the particle filter for the data in Figure 13. 31
- Figure 19 (a) A school of sardines taken from the bottom of a tank at the Kujukushima Umikirara Aquarium. (b) A magnified view of (a). 36
- Figure 20 An example of Type B scene. Two fish in the ellipses are crossing once. Fish in each yellow ellipse are overlapping. 38
- Figure 21 Part of the appearance model. Note that these templates are grayscale images. 39
- Figure 22 (a) Original image. (b) Image drawn from the estimated parameters of (a). (c) Image of occluded fish. (d) Image drawn from the estimated parameters of (c) with our method 40
- Figure 23 Framework of multiple fish tracking 41

- Figure 24 Tracking results. The top row shows the ground-truth of the fish trajectories. The second to the fourth rows show the trajectories of the FP-LK method. The fifth to seventh rows show the trajectories of the proposed method. The numbers in the images are frame numbers. We set the number of first frame in each scene as 0. 43
- Figure 25 (a) Rotating schools of sardines taken from the side and (b) the bottom of a tank at the Kujukushima Umikirara Aquarium, and (c) an overview of the RC of the school 47
- Figure 26 Speed measurement with optical flow: (a) measuring the speed of a moving element, (b) the speed of moving elements that move together and (c) measuring the mean speed of moving elements in the blue region 50
- Figure 27 RC estimation framework 52
- Figure 28 Optical flows of a frame in scene C: blue lines show flows that satisfy the conditions, red lines are flows that do not satisfy the direction condition, and yellow lines are extremely slow and fast flows 54
- Figure 29 Overview of center estimation 56
- Figure 30 Snapshots of simulation scenes D-1, D-2 and D-3 58
- Figure 31 RCs Estimated by our method for simulation scenes 60
- Figure 32 Snapshots of scenes and the estimated manually-tracked RCs: (a), (c), and (e) are snapshots of scenes A, B, and C, respectively. Red crosses are the centers estimated by our method. (b), (d), and (f) show the estimated RCs and number of tracked fish in each bin for scenes A, B, and C, respectively. 62
- Figure 33 (a) Yellow lines are the 152 trajectories of the manually-tracked sardines in scene A. (b) Blue points represent tracked data for each sardine from (a), and the red line shows the average speed of each bin, i.e., rotation curve. 63
- Figure 34 RCs estimated by our method and manually-tracked RCs. The 20th bin's value of B by our method was not computed because the ratio of the school flows was less than α . 64
- Figure 35 (a), (b) and (c) are snapshots of the long term scene at 153s, 24s and 898s respectively. 65
- Figure 36 RC time series of sardines 66

- Figure 37 10s averaged time series of CER and 1s averaged time series of SDMD and differential of SDMD. 67
- Figure 38 Rotating school of anchovies from the bottom of the tank 69
- Figure 39 (a) White lines are the 172 trajectories of manually-tracked anchovies in Figure 38. (b) Estimated RCs by manual tracking and our method. 69
- Figure 40 (a) RC time evolution of the anchovies and (b) CER, SDMD and differential of SDMD time series of the anchovies 70
- Figure 41 Snapshots of the school of anchovies. (a), (b) and (c) are snapshots of the scene at 34s, 54s and 65s respectively. 71
- Figure 42 An overview of the velocity distribution on the cake-cuts. 72
- Figure 43 Snapshots of scenes and the result of the speed and velocity distributions by hand and by our method: (a), (c), and (e) are snapshots of scenes A, B, and C, respectively. (b), (d), and (f) show the estimated speed and angle in each cut for scenes A, B, and C, respectively. 73
- Figure 44 A large and dense school of sardines 76
- Figure 45 (a) A snapshot of the RSS. (b) The trajectories of the isolated fish in the RSS obtained by the tracking method in Section 4.3.2. 77
- Figure 46 (a) The frequency distribution of body lengths of the RSS. (b) The body length distribution against the radial distance from the rotation center. (c) The plotted speeds [BL/s] against the body length [pixel]. 78
- Figure 47 (a) The plotted speeds [BL/s] against the radial distance [BL] from the center. The red line shows the averaged speed of each bin. (b) The plotted speeds [each body length/s] against the radial distance [BL] from the center. The red line is the averaged speed of each bin. 79
- Figure 48 (a) A short term time series of the averaged speed at the 9th bin. (b) The time series of the averaged speed at the 9th bin for the long video. 81
- Figure 49 (a) Long term evolution of 60s averaged velocities at several radius. (b) Long term evolution of 600s averaged velocities at several radius. 82

- Figure 50 (a) The variances of the averaged velocity distributions over time τ . (b) Log-Log plot of the variance of the averaged velocity distributions over time τ at $r = 9$ BL. 84
- Figure 51 Velocity correlation function at $r = 9$ BL 85

LIST OF TABLES

Table 1	Measurement Results of Body Length and Tail Beat Frequency	32
Table 2	Parameters of Our Method	40
Table 3	Quantitative Comparison of Tracking Errors (Percentage of the BL)	44
Table 4	parameters of our method	55
Table 5	simulation scenes	59
Table 6	Center estimation results	59
Table 7	RC estimation results	61
Table 8	Basic data of schools of sardines and RC estimation results	61
Table 9	The CER and SDMD values of the first frame of the scene A, B and C and the snapshots	68
Table 10	The estimation result of angles and speeds.	72

ACRONYMS

BL	Body Length
CER	Center Estimation Residuals
DOD	Degree Of the Deformation of fish body
FP-LK	Feature Points and tracks them using the Lucas-Kanade method
MPF	Mixture Particle Filter
RC	Rotation Curve
RD	Relatively Dense
RE	Relative Error
RMSE	Root Mean-Square Error
RMSRE	Root Mean Square of the Relative Errors
RS	Relatively Sparse
RSS	Relatively Sparse Scene
SDMD	Standard Deviation of the Mean Distances
SSD	Sum of the Squared Distance

INTRODUCTION

Collective behavior is a widely observed phenomenon in nature. Prominent examples of such behavior are swarms of insects, flocks of birds, schools of fish and crowds of people. Figure 1 shows examples of a colony of army ants (Figure 1(a)), a flock of European starlings (Figure 1(b)), a school of sardines (Figure 1(c)), and a crowd of people (Figure 1(d)).

These behaviors have been intensively investigated using the methods of biology, physics, mathematics, and engineering. Over 2400 years ago, it is said that Aristotle first observed schooling behavior in the sea [105]. Over the past few decades, various collective behaviors have been empirically studied through observations in outdoor fields and laboratories [80, 12, 9, 77], mathematical models [7, 91, 78, 110], and simulation experiments [54, 28, 29]. This research has par-

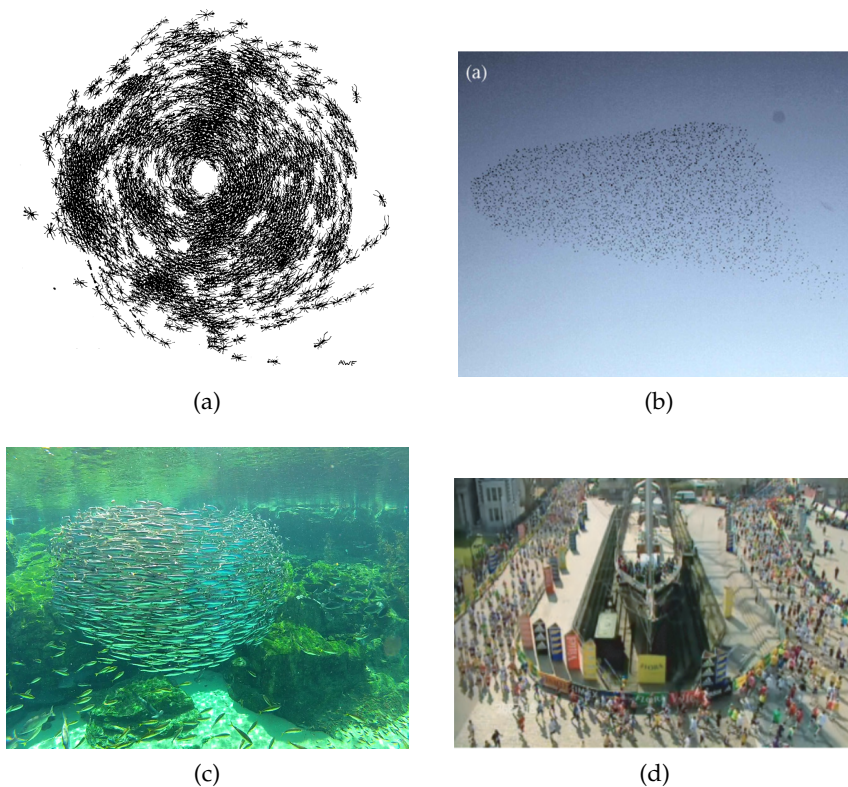


Figure 1: (a) A circular column of army ants (*Eciton praedator*). Source: adapted from [95]. (b) A flock of European Starlings (*Sturnus vulgaris*). Source: adapted from [10]. (c) A school of sardines. (d) Hundreds of people participating in a marathon. Source: adapted from [72].



Figure 2: A dense and large school of sardines in an aquarium

tially clarified schooling mechanisms, advantages of collective behavior, and the origin of collective motions [81, 86, 67, 111]. However, the questions of why and how animals behave as flocks, herds, and schools still remain unanswered today.

Behaviors of fish schools or shoals, which are frequently observed in aquariums, in fish farms, and in nature, also have been studied [96, 90, 112]. The local interactions between individuals in the school, and the global shape and functions of the school have been investigated through observation [80, 60, 99]. And numerous mathematical models of fish schooling and corresponding simulations have been studied [78, 55, 31, 13].

However, behaviors of schools of fish, in particular large and dense schools as shown in Figure 2, have not been sufficiently empirically analyzed and understood, compared to the behaviors of other insects and animals such as ants, bees, and birds. It is mainly because there are difficulties in measuring the behaviors of such fish schools: video filming underwater is more difficult than on land and frequent occlusions usually occur as shown in Figure 1(c) and Figure 2. Nevertheless, to investigate the mechanisms and functions of schooling behavior is important not only for natural science but also for engineering because such knowledge related to schooling behavior must be useful for developing systems to observe health and growth of

schooling fishes in aquariums and fish farms, and improving their survival rate.

In response to this problem, a lot of measuring methods, in particular multi-target tracking methods, have been proposed in the field of computer vision [97, 57, 24, 6]. Tracking individuals in a group is a naive but important way to measure behaviors of the group. For schools of fish, multi-target tracking methods have been studied [59, 39, 20, 34, 89]. However, for a dense and large school of fish as shown in Figure 2, the proposed methods are insufficient to measure behaviors and track individuals in the school for analysis of fish behaviors.

Based on this background, it is essential to establish automatic measurement methodologies for schooling behaviors in order to advance research on fish schooling. Moreover, measurement methodologies for dense and large groups such as schools of fish must be fundamental methods for automatic monitoring of schools in an aquarium or fish farm, and for other collective behaviors like those of crowds of people. These are the motivations of this thesis.

1.1 THE GOALS OF THIS THESIS

Based on this research background and our aforementioned motivations, we set out to develop measurement methods for a large and dense school of fish in this thesis. However, an immediate problem we encountered is that the density of fish schools change, as shown in Figure 3. For the situation in Figure 3(b) individual tracking is hard even manually. Therefore, we assume that there are two types of school density as follows,

RELATIVELY SPARSE (RS), there are a certain number of isolated fish and we can manually track most of them if occlusion of multiple fish occur. Figure 3(a) shows a typical example of type RS.

RELATIVELY DENSE (RD), isolated fish are very few and we cannot reliably track individuals in a group, even using manual tracking. We show the example of the type RD in Figure 3(b).¹

We have developed measurement methods which are suitable for each type of density.

We first track the isolated fish in a RS type school and develop a measuring method for each fish behavior (such as tail beat frequency and coast phase). These features are essential for modeling deformation of a fish body and for discussion of energy consumption in the school.

¹ It is of course impossible to classify schools precisely into one of the two types. We need to select the method suitable for the purposes of analysis based on the appearance of the school.



(a)



(b)

Figure 3: (a) A part of a RS type school of sardines. (b) A part of a RD type school of sardines.

Tracking isolated fish in a RS type school is not so difficult, however individual tracking becomes difficult when occlusions occur, even in the case of type RS. We also propose a tracking method which is based on an appearance model. We can track fish with this method even if more than two fish are occluded.

For a school of the RD type, it is hard to track individuals even manually. However, tracking is not necessary for the measurement of behaviors of the school. We propose a method based on dense optical flow to estimate the speed distribution of collective motions. In order to measure and detect different information about the behavior, we also propose several kinds of divisions of space.

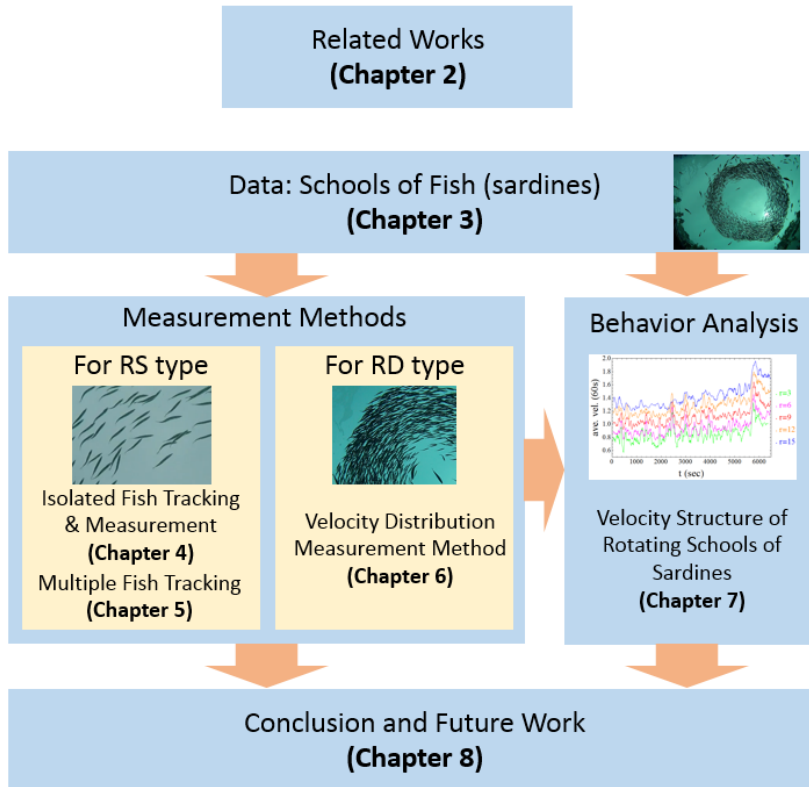


Figure 4: Structure of this thesis.

The second goal of this thesis is to find and analyze characteristic features of schools of fish. We focus on sardine and anchovy schools, usually observed rotating in solid torus. With the proposed measurement methods, we first measure fundamental features of the school, such as body length distribution. With these measures we are able to determine the speed structure of the rotating school and analyze the time development of the structure.

1.2 THE OVERVIEW OF THIS THESIS

This thesis consists of 8 Chapters. Figure 4 depicts a schematic structure of this thesis.

In Chapter 1, we present the background and motivations of this thesis. The goals of this thesis are also stated.

In Chapter 2, we introduce related works on collective behaviors in Section 2.1 and schooling behaviors of fish in Section 2.2. We also review measurement methods for collective behaviors and their limits in Section 2.3.

In order to conduct our research, we have collected videos of schools of fish that are large (over 2000 individuals) and close to those found in their natural environment. The details of the filmed data are de-

scribed in Chapter 3. Fundamental data such as filmed data are summarized. We also provide some snapshots as examples of the video footage used in our research.

In Chapter 4, for schools of the RS type, we track the isolated fish and measure their behaviors such as tail beat frequency and coast phase. We also review related work on fish swimming and swimming mechanics.

In Chapter 5, for schools of the RS type, we propose a tracking method which is based on an appearance model and can track fish even if more than two fish are occluded.

In Chapter 6, for schools of the RD type, we propose a method to estimate the speed distribution of collective motions with dense optical flow. In order to measure and detect different behavior information, we also propose several kinds of divisions of space.

In Chapter 7, we analyze schooling behaviors of rotating sardines in a torus shape with the developed measurement methods. We first measure the length and speed distributions in a RS type school with the proposed method in Chapter 4. The speed structure of the school and the time evolution of the structure are analyzed.

In Chapter 8, we conclude the thesis and discuss future work.

RELATED WORKS

In this chapter, we first briefly review research into collective behaviors in Section 2.1. In particular, we introduce research related to schools of fish in Section 2.2 and measurement methods of fish behavior in Section 2.3.

2.1 COLLECTIVE BEHAVIORS

Collective behaviors have been observed and studied for various animals such as bacteria [61, 30], insects [27, 12], birds [50, 9, 42], and fish [47, 13, 45]. Collective motions of human crowds have also been investigated [49, 43, 36].

A large number of models have been proposed to understand the mechanisms of collective behavior. Rules of schooling mechanisms were studied in earlier work on such models. For example, Partridge *et al.* analyzed schools of saithe (*Pollachius virens*) and found that members match the heading and swimming speeds of at least their first two nearest neighbors [80]. Aoki also proposed a model of fish schooling and conducted simulations to examine the schooling mechanism in 1982 [7].

Reynolds proposed a well-known flocking model called “boid” in 1987 [91]. The boid model has the only three local rules:

1. collision avoidance: avoid collisions with neighbors
2. alignment: attempt to match velocity with neighbors
3. cohesion: attempt to stay close to neighbors.

Each particle (bird) interacts only with their neighbors according to the above rules and thereby the collective of particles form a virtual flock. Reynolds demonstrated that group leadership and global information are not necessary for schooling behaviors with his simple model.

The boid model triggered research into mathematical models of collective behaviors [78, 31, 32, 29]. Viscek *et al.* proposed a statistical physics type model with perturbations [110]. Several properties of the model, e.g. the order-disorder phase transition, have been intensively investigated with theoretical analysis and simulations [23]. The above models in which each particle in collective groups is self driven and interacts with other particles is called the self-propelled particles (SPP) approach. Toner and Tu have proposed nonequilibrium continuum dynamical models as another modeling approach to collective behaviors. [106, 107].

Various features of collective behaviors such as the role of leaders [16, 102], their forms in escaping from predators [81, 56] and information transmission in collective groups have been studied [90, 101, 99]. The role of leaders and decision making of animal groups are attractive topics [26]. For instance, Couzin *et al.* showed that a minority of informed individuals in a group can affect the behaviour of the whole group [28] and Nagy *et al.* showed the existence of hierarchy in a pigeon flock recorded by small GPS devices [77]. Transmission of information in various groups have been investigated [90, 101]. Recently, in investigating schools of fish, Strandburg-Peshkin *et al.* recorded information transmission in a school of golden shiners in a shallow tank and suggested that each member of the school interacts with other fish as far as the member can see [99].

In addition to animal groups, non-living systems such as shaken metallic rods, robots, and boats have been studied. For example, traffic congestion has been focused on as a kind of collective motion of vehicles, and various mathematical model of congestion have been proposed [85, 76, 11]. As a result related to traffic jams, Sugiyama *et al.* showed that a bottleneck, which was thought to cause a traffic jam, is only a trigger and not the essential origin of a traffic jam with both analysis of their optical velocity model and experiments on a circuit using real cars [100].

The findings in collective behavior research have been widely used in other areas. The boid model has been employed to easily create collective motions in computer graphics [52] and for other purposes such as data visualization [75]. For crowds of people, strategies of avoidance of dangerous crowd pressure and human stampedes have been proposed with models of human crowds [43, 44]. Recently, strategies for autonomous control of robots [41, 74], Unmanned Aerial Vehicles (UAVs) [51, 94], and cars [3] have been developed based on research into collective animal behaviors.

2.2 SCHOOLING BEHAVIORS OF FISHES

Schooling behaviors are observed in many kinds of fishes. Shaw estimated that more than 25% of the approximately 27,000 species of the teleosts adopt shoaling behaviors throughout their life and over 50% do as juveniles [96]. Among schools of fish, huge shoals containing tens of millions of fish and extending for many kilometers have been observed [71].

A number of reasons for schooling behaviors have been proposed [81, 86]. The benefits of being a member of a fish school in reducing the effectiveness of predator's attack have been studied for a long time [70, 88]. Pitcher *et al.* demonstrated that predators in a shoal find prey more efficiently with experiments [87]. Moreover, the energetic benefits from the hydrodynamical interactions of swimming

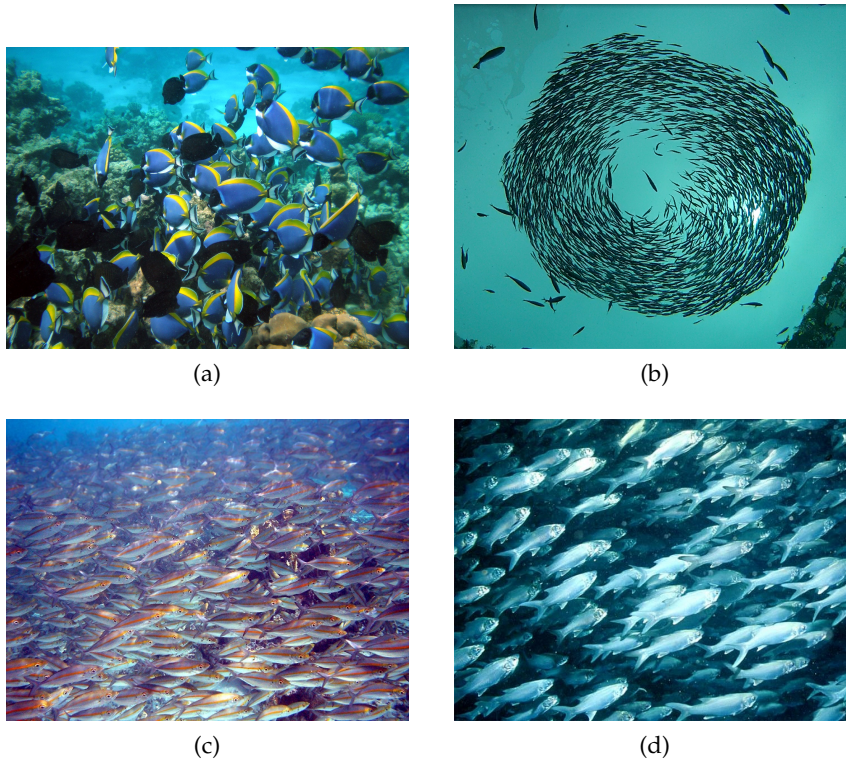


Figure 5: (a) A shoal of Surgeonfish. (b) A rotating school of sardines. (c) A school of Goldband Fusilier. (d) A school of Sixfinger threadfin. Couzin *et al.* called (a) a swarm, (b) a torus, (c) a dynamical parallel group and (d) a highly parallel group [29]. (a) by Uxbona, (c) by Brocken Inaglory, and (d) a public domain image.

in a school have been proposed and experimentally demonstrated [114, 67, 48].

Schools of fish take a variety of forms and dynamically change their forms, although the schools were traditionally thought to be leaderless and egalitarian systems [17, 63]. We show the four classes of school forms in Figure 5 according to the classification of [29].

In order to analyze and model such schooling behaviors, as early studies, the forms of schools of fish in a water tank and interactions between members in each school have been measured [18, 92, 93, 80]. Partridge and Pitcher also studied the sensory basis of fish schools in which members utilize both their lateral lines and vision [84]. The form of a school and distribution of individuals in a school have also been observed. For example, Partridge *et al.* showed that schools are usually oblong and fish do not position themselves at random within schools [83].

As stated in Section 2.1, large number of models of schooling have been proposed. With these models, we can create artificial schools in a computer without leaders or external global stimuli for their school organization [54, 55]. Couzin *et al.* demonstrated that simula-

tions with their model exhibited four characteristic collective behaviors, which are observed in nature as shown in Figure 5, when certain parameters were changed [29]. However, for numerous models and research based on simulations, it was difficult to decide which model is fitting to describe a real school, because sufficient observational research was not available and the characteristics of social interaction between individuals was not well understood.

Recently, researchers have observed collective behavior, information transmission among schools, and form and density distributions of schools in detail. Based on these observations, previously proposed models of collective behavior have been modified and novel models have been proposed. Some examples of such observations include transition from disordered to correlated motion of a school of young Tilapia [13], monitoring of oceanic fish shoals with a kind of sonar echo [71] and interactions between two or three fish [60]. Strandburg-Peshkin *et al.* measured information transmission among a shoal of golden shiners in a shallow tank and evaluated the proposed models with their observations. In a separate school, Bumann *et al.* observed the highest density distribution of individuals in a school is often at the front [19]. The origin of density distribution and size sorting have been also observed [64, 47, 45].

2.3 MEASUREMENT METHODS FOR COLLECTIVE MOTIONS

A number of devices and techniques to measure collective motions have been developed. According to the purposes of researches or the types of collective groups, researchers have chosen or developed many devices: cameras (photo) [17], video cameras [83, 80], sonar echoes [71, 58], and GPS devices [16, 77]. For example, Cavagna *et al.* have measured the 3D positions of individual European starlings within flocks of up to 2,600 birds using a stereo camera [22]. Here, we review measurement methods specially proposed for fish behavior analysis and outline their limits.

The initial measurements for fish schools were manual and laborious [18, 80]. For example, in 1980s, the 3-D positions of schools of 20-30 saithe were recorded manually with their manual plotter system [82, 83]. Even recently, some researchers have used manual detection by clicking on the screen at the position of the fish, frame by frame [73, 34].

However, automatic or semi-automatic measurement methods are essential because manual analyses would be complicated, time-consuming and sometimes even impossible. For the last several decades, measurement methods, in particular individual tracking methods, for schools of fish have been developed in collaboration with image analysis and computer vision. Tracking each member of a school is a naive but effective way for the analysis of schooling behavior. In the field of

computer vision, object tracking is an important task and has various applications such as automatic surveillance, robotics, and collective motion analysis [69, 97, 57, 24, 25]. For multi-target tracking, Vermaak *et al.* introduced mixture particle filter (MPF) [109] and many extended algorithms based on the MPF have been proposed [79, 62, 14]. In this field, tracking methods for multiple objects in highly dense groups have recently been proposed [116, 6, 68].

For example, Ylief *et al.* tracked two fish with color tags [117] and Suzuki *et al.* tracked 25 individuals using a mathematical model [103]. Recently, fish schools of up to 100 individuals have been multitracked for several minutes [13, 33]. Moreover, there is an open source tracking system SwisTrack [4] and commercial tracking systems such as EthoVision[1] and VideoTrack now available [5].

The major problem of individual tracking in fish schools is occlusion, as stated in [34]. An occlusion is the phenomenon of two or more tracked target images becoming one during a time period. Figure 6(a) and 6(b) show examples of separated fish and occluded fish. For occlusion events as shown in Figure 6(c) and 6(d), tracking algorithms need to identify each fish after occlusions. Individual identification is quite difficult when three or more fish are superimposed as shown in Figure 6(e) and 6(f).

Many solutions for the occlusion problem have been proposed. The simplest but most widely used way (even these days) is to leave fish in a shallow tank. This strategy can reduce occlusions [99, 89]. In order to avoid occlusions in a video filmed from one direction, two strategies have been proposed. The first one is using lights and shadows as shown in Figure 7(a). From the fish images and their shadows, we can continue tracking from one direction even if occlusions occur [66]. The second strategy is the stereo camera technique, which uses two or more video cameras to detect 3D positions. Figure 7(b) shows an overview of stereo camera. For instance, Viscido *et al.* tracked groups of 30 giant danios with stereo camera [113]. Hemelrijk *et al.* utilized a mirror and measured the 3D positions of 60 mullets with one camera as shown in Figure 7(c) [46]. As another approach for occlusions, some researchers have presented estimation methods to determine whether two fish have crossed (Figure 6(c)) or not (Figure 6(d)) from the information gathered in previous and later observations [59, 33].

Several researchers have measured not only the positions and directions of tracked fish but also their postures with parameterized deformable models [39, 20]. Ukita *et al.* tracked goldfish and measured their postures with the stick and ellipse model [108].

From the above, a number of auto measurement tracking methods of schooling behaviors of fish have been developed, particularly for fish schools in shallow tanks. The positions of fish schools of up to 100 members have been measured with stereo cameras and light and shadows. However, measuring and tracking for real fish schools in

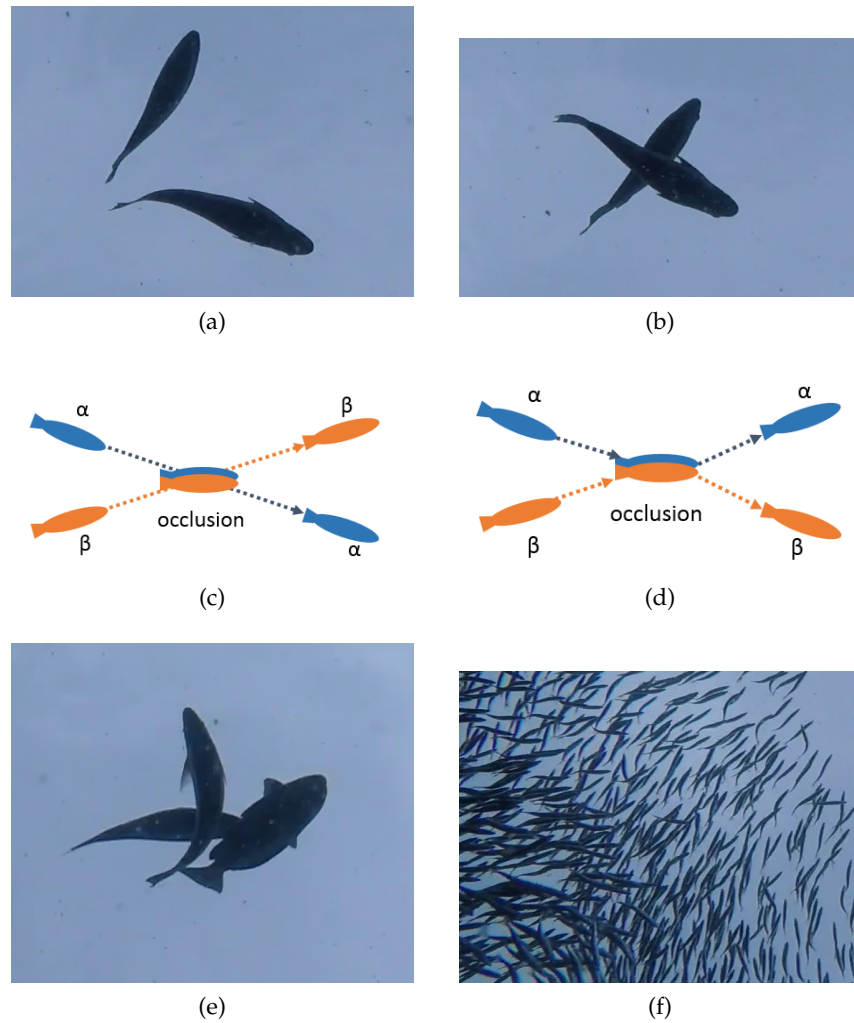
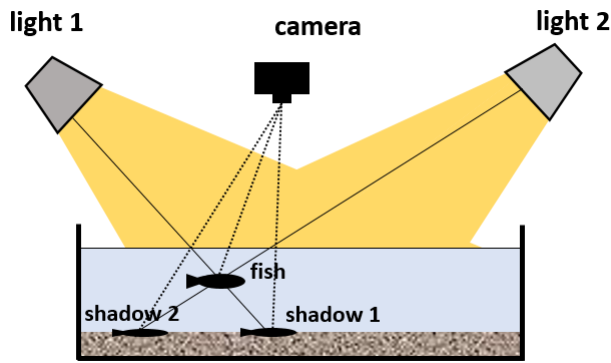
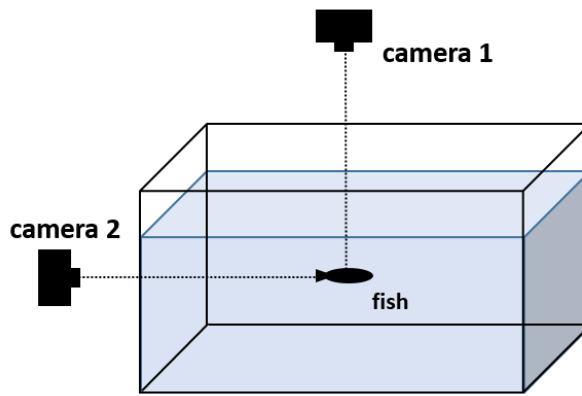


Figure 6: (a) Two fish are separated. (b) Two fish are occluded. (c) During an occlusion, trajectories of two fish are crossing. (d) During an occlusion, trajectories of two fish are not crossing. (e) Three fish are occluded. (f) Dense school of sardines. Occlusions occur everywhere.

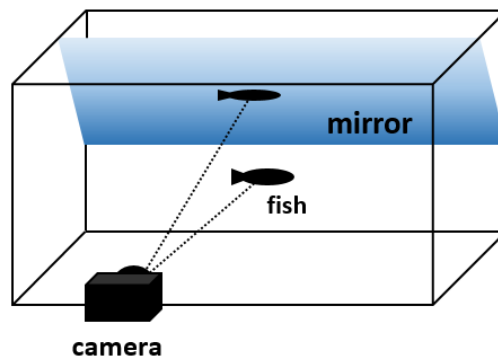
large tanks or fields as shown in Figure 7(f) are still quite difficult, because populations of these school are comprised of thousands of members and real fish schools are dense (That is, the distances between individuals are close). Despite these difficulties, analysis for large and complicated collective groups is important. In fact, from the observation of large (over 2000 individuals) flocks of European Starlings [22, 10], Cavagna *et al.* proposed a characteristic behavior type called “scale free” behavior, which suggests that individuals change their interaction ranges with neighbors according to the entire school size and that this may create dynamic behaviors of flocks, as if they were a single organism [21]. Developing measurement methods for large and dense schools of fish is essential in order to proceed schooling behavior research for larger and more complicated fish schools,



(a)



(b)



(c)

Figure 7: (a) Measuring the position of a fish with an image of fish and their shadows (modified from [66]). (b) An overview of measuring positions with a stereo camera. (c) Measuring the position of a fish with a mirror (modified from [46]).

and develop applied systems to observe health and growth of individuals of fish schools in fish farms and zoos.

FILMED DATA OF SCHOOLS OF FISH USED IN THIS RESEARCH

In this chapter, we first show our recording method for schools of fish in an aquarium 3.1. The filmed videos are used to conduct experiments for the proposed methods in 4 to 6 and analyze the behavior of schools of fish in Section 7. We present basic data of the filmed school. We show a school of sardines with some snapshots of the filmed data as examples in Section 3.2. In Section 3.3, the reasons why the school and aquarium are selected in our research are also stated.

3.1 A TANK IN THE KUJUKUSHIMA UMIKIRARA AQUARIUM AND CAMERA SETUP

We filmed videos of schools of sardines and anchovies in the largest open air tank at the Kujukushima Umikirara Aquarium, Nagasaki Japan [2].¹ The tank is 5 meters deep. Figure 8(a) shows the open air tank. We can see the water surface of the tank in Figure 8(a). Figure 8(b) shows the tank filmed from a side through thick glass.

We submerged commercially available video cameras (HERO2, HERO3, and HERO4 by GoPro, Inc.) to the bottom of the tank. The cameras were put in protective waterproof cases and trained upward. Figure 9 shows the overview of the camera setup. Note that the filmed images of the schools are projected 2D ones. We visited the aquarium about 10 times between March 2012 and March 2015 for recordings. We used a part of the filmed videos in our experiments and analysis in this thesis.

3.2 FILMED DATA IN THE TANK

Figure 10 shows snapshots of the school of sardines in the filmed videos. There is a large school (approximately 3000 individuals) of sardines (*Sardinops melanostictus*) in the tank throughout a year.

There are not only sardines in the tank but also other various kinds of fish, including jack mackerels, horse mackerels, chub mackerels, and largescale blackfishes as shown in Figure 10(a). We can also find many of the sardine's predators such as chub mackerels and hammerhead sharks in Figure 10(b). The sardines are usually rotating in a solid torus shape in the daytime as in Figure 10(c). The size of the hole in the center of the torus changes; the hole in Figure 10(d) is

¹ The videos are collected with Professor Masa-aki Sakagami at Kyoto University and his laboratory members.

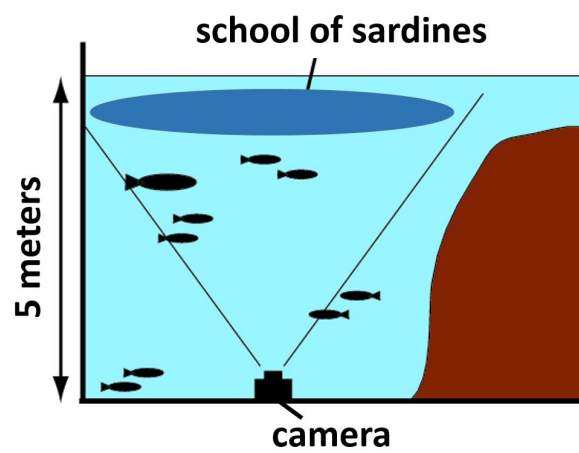


(a)



(b)

Figure 8: (a) The open air tank at the aquarium. (b) The tank filmed from a side through thick glass



(a)

Figure 9: Camera setup.

small, and the one in Figure 10(e) is large. The sardines are typically fairly flat and individuals in a school usually swim at a relatively equal depth as shown in Figure 10(f), which was filmed from the side.

The school of sardines in the video are often occluded by other fishes and sharks. We show some examples of such events. In Figure 10(a), larger fishes (horse mackerels and club mackerels) are overlapping on the school of sardines. Figure 10(g) shows an event of a banded houndshark covering the school. In order to measure and observe the behavior of the school of sardines, we need to exclude the effect of the occlusions or find such events in any way. The solution strategies for these problems are mainly shown in Chapter 6.

The shape of a school can sometimes be distorted, for example, by the attacks of large fish (predators). Figure 11 shows a snapshot sequence of a 60 second movie in which the school is attacked and distorted by a hammerhead shark and recovers its form. Figure 11(b) and 11(c) show the attack by the hammerhead shark. The forms of the school are drastically distorted in Figure 11(d), 11(e), 11(f), 11(g). The distorted school always returns to the solid torus shape within some dozens of seconds after the attack, as shown in Figure 11(h), 11(i), 11(j).

3.3 THE ADVANTAGES OF THE SCHOOL AND THE WATER TANK IN THE KUJUKUSHIMA UMIKIRARA AQUARIUM

The school and water tank in the Kujukushima Umikirara aquarium have been selected as research subjects because they have many advantages. In this section, we outline the reasons why the school and the aquarium have been selected.

The first advantage is that the tank is suitable for recording videos. Since it is an open air tank, we can obtain sufficient light for filming videos. Moreover, the water in the tank in the aquarium has high transparency and thus we can obtain clear videos.

The second advantage is the large rotating school of sardines. In the tank, there are thousands of sardines as stated in Section 3.2. As shown in Figure 10, the school is usually rotating in a solid torus form and the centroid of the rotating school is stable and stays within the visual field of the camera. Consequently, for a long time, we can take a movie of the whole school from a fixed camera in the bottom of the tank. Using the long movies taken from one camera, we can analyze changes of fish behaviors over time.

The third advantage is the environment of the tank. As stated in Section 3.2, there are many predators of sardines such as club mackerels and hammerhead sharks inside the tank. Moreover, birds, e.g. a kind of Scolopacidae, sometimes catch sardines with their long bills

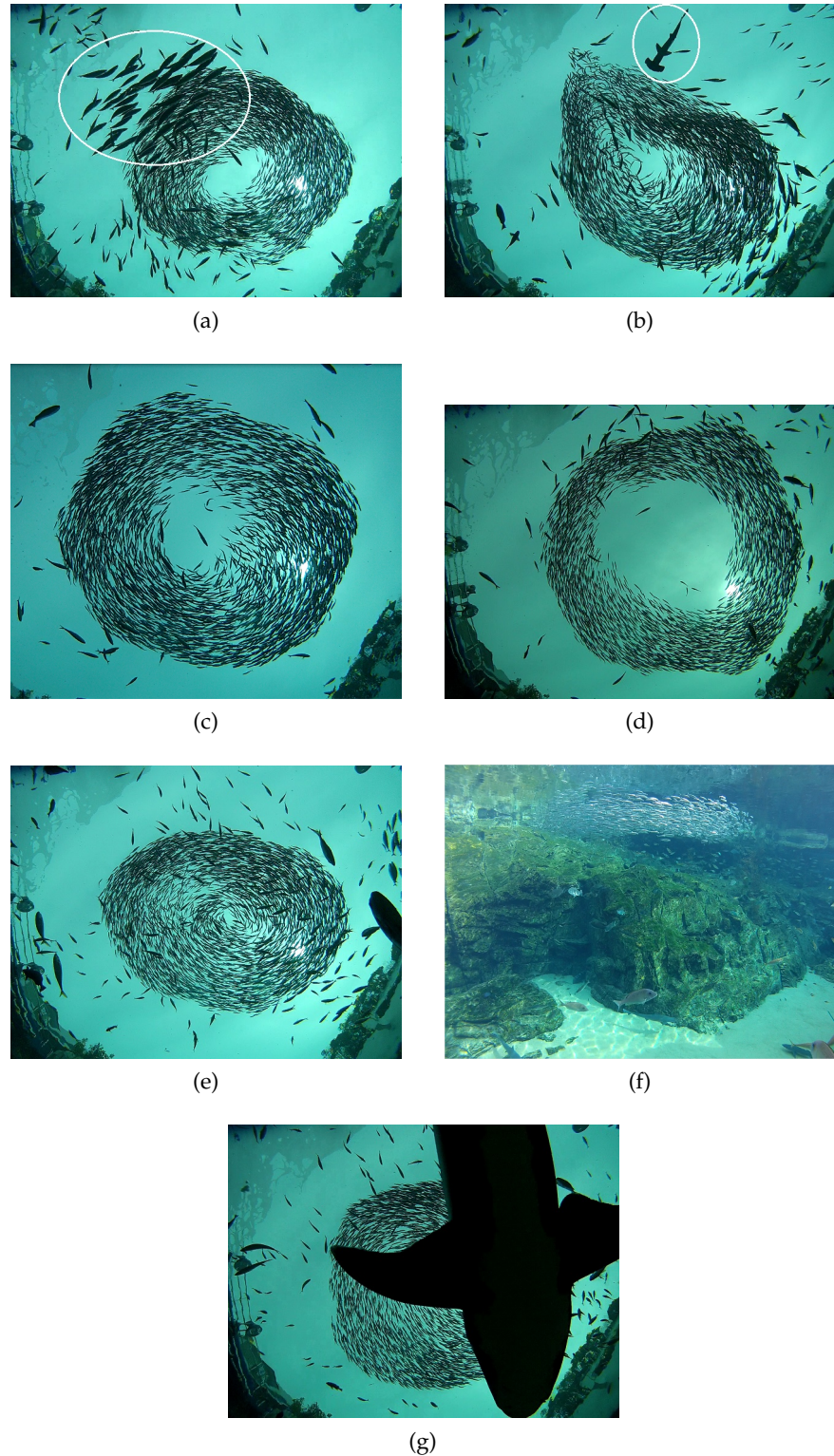


Figure 10: (a) Larger fishes in the white ellipse are chub mackerels. (b) A hammerhead shark in the white ellipse is approaching the school of sardines. (c) A rotating school of sardines in a solid torus shape. (d) The hole size of the rotation center is large. (e) The hole size is small. (f) An image of the school taken from a side. (g) A banded houndshark is covering the school.

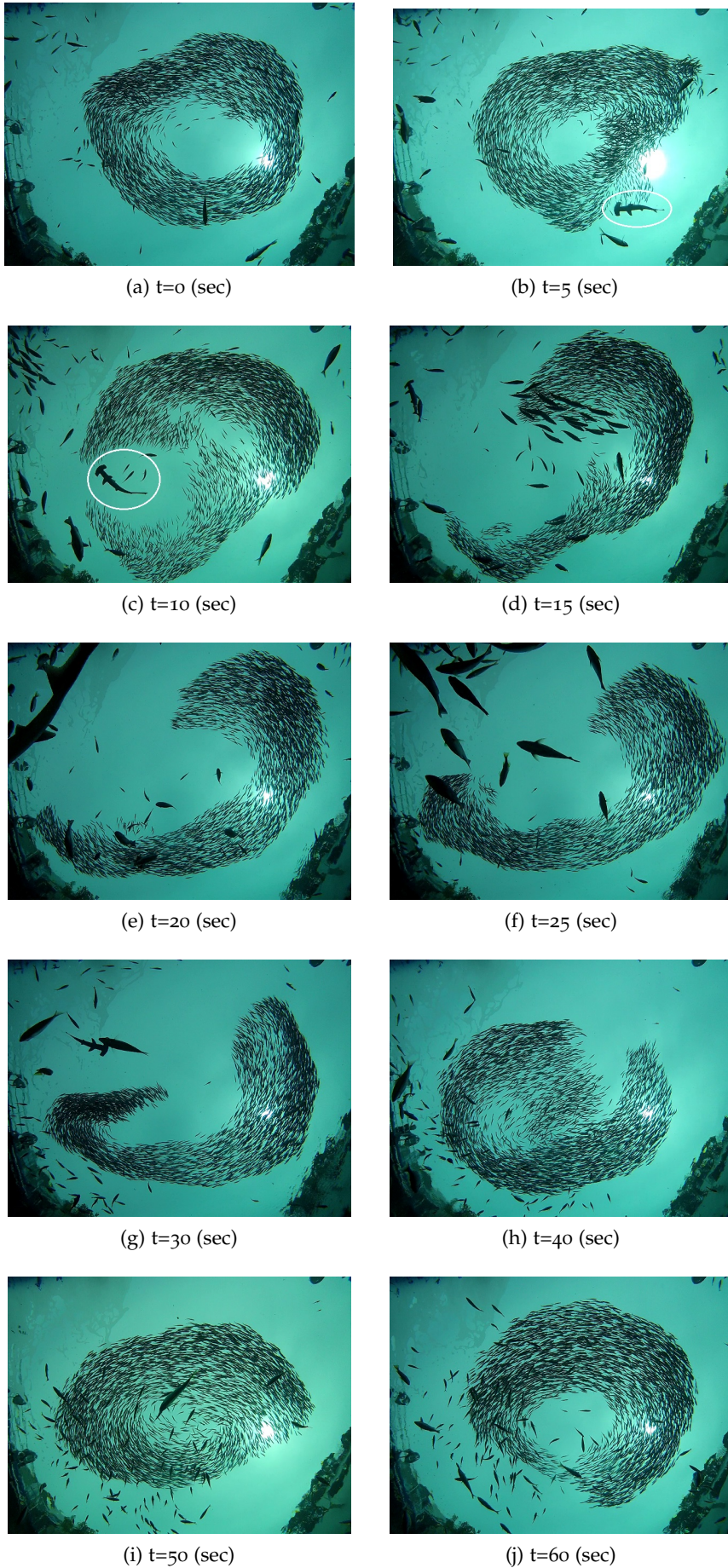


Figure 11: A snapshot sequence of a 60 second movie in which the school of sardines is attacked and distorted by a hammerhead shark and recovers its form.

in the open air tank. Therefore, the environment of the tank is closer to nature rather than these of tanks in laboratories.

From these advantages, we selected the Kujukushima Umikirara aquarium and the open air water tank in the aquarium to record the schools of fishes in this study.

TRACKING AND MEASUREMENT METHODS FOR ISOLATED FISH

In this chapter, we propose a measurement method of tail beat frequency and coast phase of fish swimming for isolated fish in a RS type school of fish. For analysis of fish swimming behaviors, features that represent fish movements, e.g. tail beat frequency and coast phase, have been commonly used. We propose a measurement method for such features using particle filter and apply the method to a large school of fish in an aquarium. Experimental results show that the tail beat frequencies and the coast phases are measured with our method accurately enough for further analysis of fish behaviors. The average of the differences of the tail beat frequencies was 0.126 (Hz) and the precision and recall of the classification for coast phase detection were 0.945 and 0.879 respectively.

The research of this chapter have been done with Prof. Hioki Hirohisa and Prof. Masa-aki Sakagami at Kyoto University. The author of this thesis designed research, developed methods, and performed experiments.

4.1 INTRODUCTION

In the field of biological research, the mechanics of fish swimming has been investigated over many years [112]. Researchers have focused on features that characterize fish swimming such as swimming speed, tail beat frequency, and stride length in a beat to analyze swimming mechanics [8, 53]. These features have been utilized to study mechanics of swimming and behavior of an isolated fish or a small group of fishes through observational experiments and theoretical analysis [67].

Recently, behaviors of fish schools and other collective motions of animals have been studied [111], as stated in Chapter 2. For example, it is known that schooling behavior reduce energy consumption [98]. However, for large and dense real schools of fish, the effects of schooling and the interactions between individuals have not been understood well enough. To promote the research of behaviors of fish schools, it is important to develop methods for measuring features of fish swimming. Such measurement method could be applied to fishes in fish farms to manage their health and growth.

In this study, as a first step to measure features of fish in a large RS type school, we focus on tail beat frequency and coast phase among various features of fish swimming and measure those two features

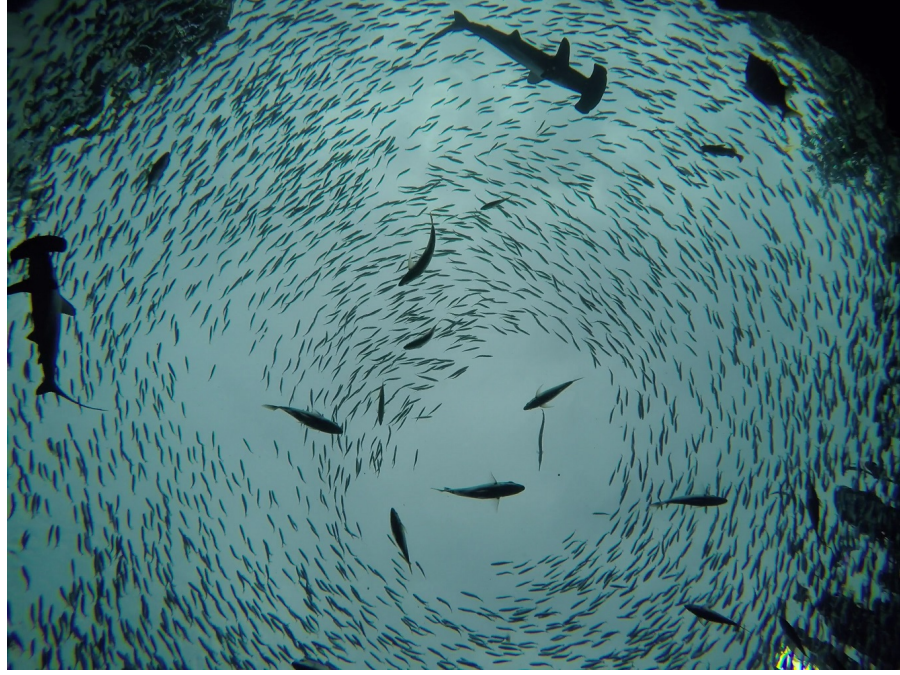


Figure 12: A RS type school of sardines taken from the bottom of a tank at the Kujukushima Umikirara Aquarium.

for isolated fish in a large school. Tail beat frequency is the number of beats per second. Coast phase refers to one of characteristic swimming states of fish in which the body is kept motionless and straight [112].

For measuring these features, it is required to track individuals in a school. Although much progress has been made for the object tracking issue [34], it is still quite difficult to track all the individuals in a large group like a school of fish shown in Figure 12. Even so, we can still obtain useful information for analyzing fish behaviors in a school if we can track a certain number of fish in the school. Since tracking isolated fish is easier than occluded multiple fish, we focus on isolated fish and measure their behaviors in this study.

To track each fish and measure tail beat frequency and coast phase, we first extract the silhouettes of isolated fish and calculate their centroids, which are tracked with a particle filter [40]. For measuring features for each tracked fish, we locate several reference points on a line obtained by thinning the silhouette of the fish in each frame. Such reference points are also used to estimate the body length of the fish, which is employed as the unit length for normalizing measured data.

From the measured data, we calculate the movements of tail tips and then estimate the tail beat frequencies of each fish with another particle filter. In order to detect coast phases for tracked fish, we devised a feature that represents the degree of deformation of fish body.

In our experiments, we tracked 126 silhouettes as targets in a video, among which 109 silhouettes were extracted as ones corresponding to isolated fish by considering their sizes and shapes. We also manually tracked the same 126 silhouettes and found that 110 out of them could be tracked as isolated fish. For the 110 fish, 108 out of them were correctly tracked by our method whereas 2 fish were missed. Aside from them, 1 silhouette was wrongly tracked. The precision and recall of the result of tracking were thus 0.991 and 0.981 respectively.

For the same 110 fish, we detected coast phases by our method and by hand. The tail beat frequencies were also measured by our method and by hand for 20 fish selected out of them. The average error of the estimated tail beat frequency was 0.126 (Hz) and the precision and recall of the classification of coast phase detection were 0.945 and 0.879 respectively.

From these experimental results, for isolated fish, we find that our method can accurately track targets and our method enables us to obtain the tail beat frequencies and detect coast phases that are accurately enough for analyzing fish behavior further.

The remainder of this chapter is organized as follows. In Section 4.2, we review previous work related to tail beat frequency and coast phase. Section 4.3 presents the dataset and the details of our method for tracking isolated fish and measuring fish behaviors. We then show experimental results in Section 4.4. Finally, we summarize this chapter and give directions for future work in Section 4.5.

4.2 TAIL BEAT FREQUENCY AND COAST PHASE

In this section, we briefly review previous work related to tail beat frequency and coast phase. At the same time, we give the definitions of tail beat frequency and coast phase employed in this study.

4.2.1 Tail Beat Frequency

Bainbridge showed that swimming speed of a fish depends on the distance covered per tail beat cycle (the stride length) and the tail beat frequency [8]. From the research, the relationships between swimming speed, the stride length, body length, and amplitude and frequency of tail beat have been studied by many researchers [112, 53, 67]. Tail beat frequency and other features are recently used for analysis of fish behaviors from the observational and theoretical viewpoints [48]. The effect of schooling behaviors on tail beat frequency also have been studied [98, 38, 104].

The issue of tracking multiple fish and measuring their postures and tail beat frequency have been studied based on images [34, 57] and sonar echoes [58, 65]. However, there is a problem in measurement of tail beat frequency in most of these research. Fourier trans-

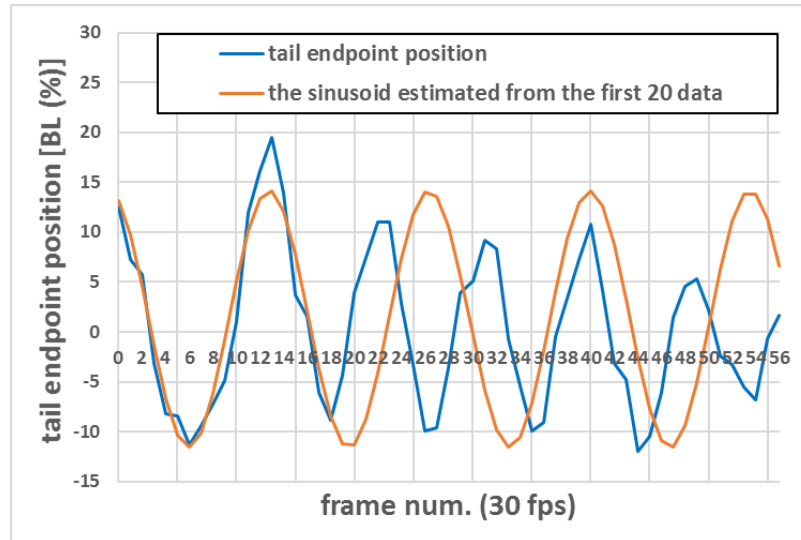


Figure 13: The tail endpoint (blue line) along the axis perpendicular to the line that passes through the area centroid and the head end-point of an isolated fish. The detail is shown in Section 4.3. The orange line is the sinusoid estimated from the first 20 position data. The difference between the two lines are not ignorable, because the tail beat frequency (the blue line) changes over time.

formation was simply used for computing tail beat frequency. However the tail beat frequency generally changes over time as shown in Figure 13.

In this study, we define tail beat frequency as the number of beats per second [53]. Figure 14(a) shows a typical tail beat cycle of a fish. In our experiments, the tail beat frequency of a fish is estimated using the average cycle time obtained from three tail beats.

4.2.2 Coast Phase

Burst-and-coast (or kick-and-glide) swimming behavior is commonly observed among several species of fish [112]. It consists of cyclic bursts of swimming and a coast phase in which the fish body is kept motionless and straight. Figure 14(b) shows a fish in coast phase. It is known that burst-and-coast swimming is important for fishes because such a way of swimming is superior, in respect of energy consumption, to the steady swimming at the same average speed [115]. Fish *et al.* have measured the effect of schooling for burst-and-coast swimming [38].

In this study, a fish is defined to be in coast phase when the fish keeps the body motionless and straight for 0.2 seconds.

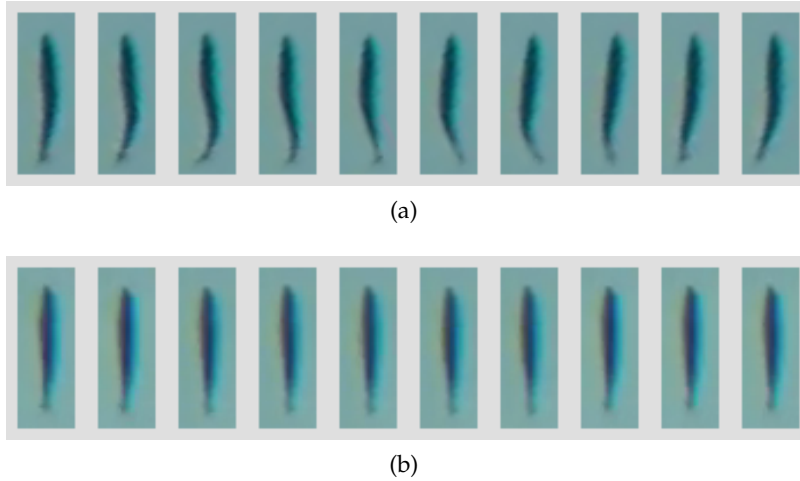


Figure 14: (a) An example of a tail beat cycle of a fish in the school (Figure 12). (b) An example of a fish in coast phase in the school

4.3 OUR METHOD

In this section, we first describe how we obtained the video data used for our experiments. We then explain the details of our method: the tracking method for isolated fish, the measurement method of tail beat frequency and the detection method for coast phase.

4.3.1 Dataset

We used the recorded videos (30 fps) of a school of sardines at the Kujukushima Umikirara Aquarium as explained in Chapter 3. The video was taken by HERO4 video camera in March 2015. The population of the school was approximately 3000. We selected a three second scene from a video (90 frames) and used it for experiments. Figure 12 shows a snapshot of the scene.

For computing feature values of fish in our experiments, we use the estimated body length (BL) of each fish as unit of measure and normalize the feature values of the fish by the BL, because each fish can be different in size.

4.3.2 Tracking Method for Isolated Fish

We track isolated fish in a school by particle filter [40]. Fish are extracted as silhouettes from each frame and their centroids are used for tracking.

In order to track fish for a scene in a video, we first binarize each frame of the scene and extract candidate regions of isolated fish by calculating the area size of regions. Figure 15(a) and Figure 15(b) show an isolated fish and its binarized image. We select the regions whose

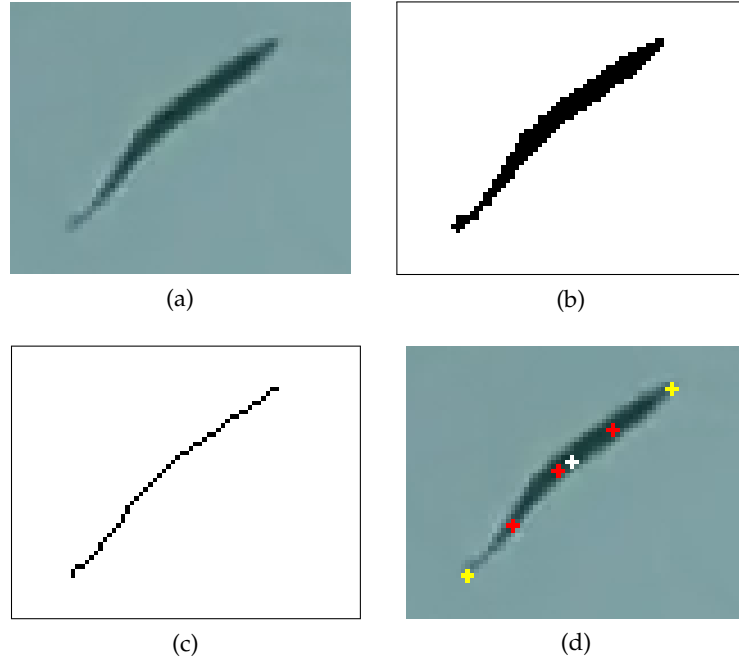


Figure 15: (a) An isolated fish in the school. (b) The binarized image of (a). (c) The thinned image of (b). (d) The white point is the centroid of the area. The yellow points are the endpoints of the line (c). The red points are the three points that divide the line (c) into quarters.

area sizes are in a range $[l, m]$ and calculate the area centroids of them. For specifying an appropriate range of size, we picked up a number of isolated fish from the scene in advance and select a rather wide range of $l = 120$ and $m = 500$ not to miss the fish.

To track the area centroids of targets, we use the sampling importance resampling algorithm introduced in [40]. We define the state as $s^i = (x, y, v_x, v_y)^{tr}$, in which (x, y) is the coordinates of the area centroid and (v_x, v_y) is the motion parameters. The particle set is $S = \{s^i \mid i = 1, \dots, N\}$ where N is the size of sample set. The motion model is defined as

$$s_t^i = \begin{pmatrix} 1 & 0 & 1 & 0 \\ 0 & 1 & 0 & 1 \\ 0 & 0 & 1 & 0 \\ 0 & 0 & 0 & 1 \end{pmatrix} s_{t-1}^i + \begin{pmatrix} w_{C_x} \\ w_{C_y} \\ w_{C_{v_x}} \\ w_{C_{v_y}} \end{pmatrix} \quad (1)$$

where $w_{C_x}, w_{C_y}, w_{C_{v_x}}, w_{C_{v_y}}$ are noises that follows the distribution $N(0, 1)$. For the measurement position y_t , we evaluate the likelihood of each prior sample and obtain a normalized weight w_t^i for each sample s_t^i

$$w_t^i = \frac{pO(y_t \mid s_t^i)}{\sum_{j=1}^N pO(y_t \mid s_t^j)}. \quad (2)$$

Here, we define $p_O(y_t | s_t^i)$ as

$$p_O(y_t | s_t^i) = \exp\left(-\frac{\|y_t - Hs_t^i\|^2}{\sigma_c^2}\right) \quad (3)$$

where observation model H extract the position of the state, that is,

$$H = \begin{pmatrix} 1 & 0 & 0 & 0 \\ 0 & 1 & 0 & 0 \end{pmatrix}. \quad (4)$$

We set $\sigma_c = 5$ from the preliminary experiment. The number of particle is 1000.

For the initial parameters of the particle filter, we search a candidate (C_1) in the first frame of the scene and the nearest candidate (C_2) to the C_1 in the second frame. If the distance between C_1 and C_2 is less than 15 pixels (approximately $2/7$ BL), we provide the position of C_1 and the amount of shift between C_1 and C_2 as initial parameters and begin the tracking process. In order to make our tracking results stable, we track a candidate in a frame only when it is close enough to one of centroid points that are estimated from preceding frames using the particle filter. For each pair of the centroid of a candidate and an estimated point in a frame, when the distance between the two points is less than 15 pixels, we presume that a candidate is moved from the candidate in the previous frame and then we track the candidate. Otherwise we do not track the candidate.

The time series of silhouettes for one tracking process is called a silhouette sequence in this chapter. Because fish can overlap each other, a silhouette does not necessarily corresponds to a certain isolate fish. For this reason, we may fail to track fish correctly if we simply take the centroids of all the silhouettes extracted. We have to extract only silhouettes those expected to be corresponded to isolated fish. In this chapter, a silhouette sequence is said to be valid when it corresponds to an isolated fish. We call a silhouette sequence of an isolated fish valid sequence.

In order to extract valid sequences and exclude invalid sequences resulting from overlaps between fish, we introduce the following two conditions. The first condition is that the area of the tracked isolated fish in a frame must be in the range of 60% to 140% of that in the preceding frame. The second condition is constraints on the fish body proportion. The area of a fish is expected to be proportional to the square of its body length (How to estimate the body length is explained in Section 4.3.3). Therefore, when the area of the tracked image is much smaller than expected, the tracked image may not be an isolated fish. In this study, if the equation

$$\alpha < \frac{bl^2}{13.5} \quad (5)$$

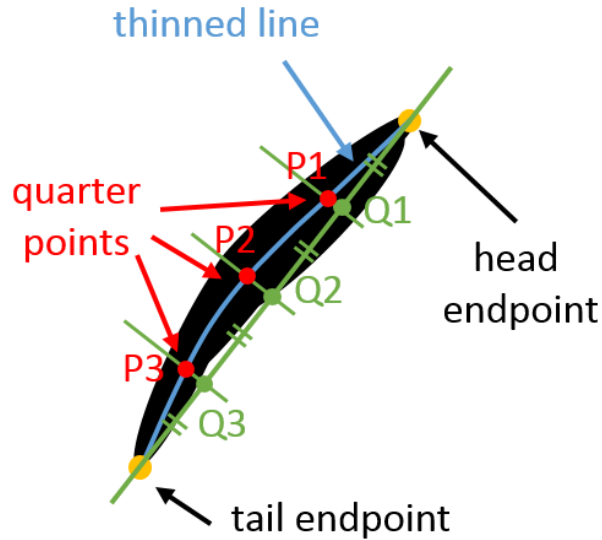


Figure 16: The overview of the reference points.

is satisfied, we discard the silhouette as invalid one. Here, α is the area, bl is the body length, and the value 13.5 is derived from a preliminary experiment.

4.3.3 Estimations of Fish Length, Tail Beat Frequency and Coast Phase

During the tracking process, for each tracked fish, we measure posture data that are retrieved from several reference points of the fish. We then estimate the body length, tail beat frequency and coast phase of each fish from the posture data.

4.3.3.1 Locating Reference Points

As reference points of a fish, we extract its head point, tail point, and other three points that are called quarter points in this chapter. The overview of the quarter points and the reference points is shown in Figure 16. For this purpose, we first obtain a skeleton line of the fish by applying a simple thinning algorithm [35] to its silhouette. The end point of the skeleton near the head is taken as the head point and the other end point is taken as the tail point. These two points are respectively called head endpoint and tail endpoint in this chapter. The other three reference points are those that divide the skeleton line into quarters. Let us denote the three points P_1 , P_2 and P_3 . These are called the quarter points in this chapter. They are located as follows. We first compute the three points (Q_1 , Q_2 , and Q_3) that divide the line segment (l) between the endpoints into quarters. We then project the points Q_1 , Q_2 and Q_3 respectively along the direction perpendicular to the line l and find the intersection points with the thinned line

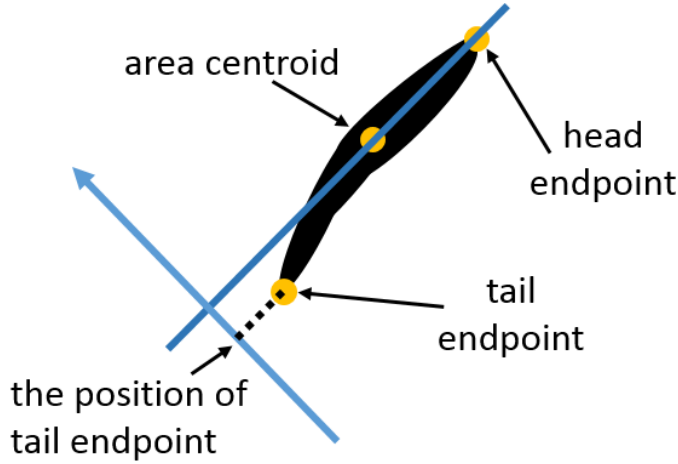


Figure 17: An overview of the position of the tail endpoint.

as the points P_1 , P_2 and P_3 . Figure 15(c) and Figure 15(d) show the thinned line of the candidate area and the points on the line l .

4.3.3.2 Estimation of Body Length

We can estimate the body length of a fish from the distance between the head and tail endpoints. Although the distance varies as the fish beats its tail, it would become close to the body length when the body of the fish is stretched straight and the distance takes maximal values.

Here, we do not simply take the maximum value with considering measurement error. The body length is hence computed as the average value of top 10% of distances measured during tracking.

4.3.3.3 Estimation of Tail Beat Frequency

In order to calculate the tail beat frequency of a tracked fish, we calculate the position of the tail end-point along the axis perpendicular to the line that passes through the area centroid and the head endpoint. Figure 17 depicts how we measure the position of the tail endpoint. An example of the time series of the tail endpoint is shown in Figure 13. Note that the values of the position of the tail endpoint are normalized by the body length of the fish.

From the time series of the tail endpoint position, we estimate the tail beat frequency with another particle filter. The details of the particle filter are as follows. To capture the nonstationary frequency of tail beats, we define the state as $s_F^i = (a, f, b, d)^{tr}$ and consider that each particle moves along the following sine curve

$$a \sin\left(\frac{2\pi ft}{30} + b\right) + d. \quad (6)$$

The system model is define as

$$s_{F_t}^i = s_{F_{t-1}}^i + \begin{pmatrix} w_{F_a} \\ w_{F_f} \\ w_{F_b} \\ w_{F_d} \end{pmatrix} \quad (7)$$

where $w_{F_a}, w_{F_f}, w_{F_b}$ and w_{F_d} are noises and $w_{F_a} \sim N(0, 0.3), w_{F_f} \sim N(0, 0.3/\pi), w_{F_b} \sim N(0, 0.1)$ and $w_{F_d} \sim N(0, 0.1)$. For the measurement position y_t of the tail tip, we calculate the weight $w_{F_t}^i$ of each particle as

$$w_{F_t}^i = \frac{p_F(y_t | s_t^i)}{\sum_{j=1}^N p_F(y_t | s_t^j)}. \quad (8)$$

Here, we define $p_F(y_t | s_t^i)$ as

$$p_F(y_t | s_t^i) = \exp\left(-\frac{(y_t - h_F(s_{F_t}^i))^2}{\sigma_F^2}\right) \quad (9)$$

where observation model h_F is defined as,

$$h_F(s_{F_t}^i) = a' \sin\left(\frac{2\pi f' t}{30} + b'\right) + d' \quad (10)$$

for $s_{F_t}^i = (a', f', b', d')^{\text{tr}}$. We set $\sigma_F = 3$ in this study. We use 2000 particles. For the initial value of parameters, we fit the above sine curve to the first 20 frame data with least squares method. The estimated parameters of the sine curve are used as initial values. We estimate the tail beat frequency in each frame by calculating the weighted average of frequency parameters of the particles based on the weights of the particles. Figure 18 shows the estimated tail beat frequencies for the data in Figure 13. From Figure 18, we can see that our method enables us to estimate the tail beat frequencies that change over time.

4.3.3.4 Detection of Coast Phase

To detect coast phases, we introduce a feature that represents the degree of the deformation of fish body. We call the feature DOD. It is calculated by averaging the squared distances between the quarter points P_1, P_2 and P_3 to the line that passes through head and tail endpoints. For a tracked fish, if moving average of a prescribed number 6 of DOD value, i.e. the average of DOD values for 0.2 seconds¹, is less than th_i , the fish is supposed to be in a coast phase. In this chapter, we set $th_i = 0.4$ from a preliminary experiments.

¹ Note that the frame rate of the recorded videos is 30 fps.

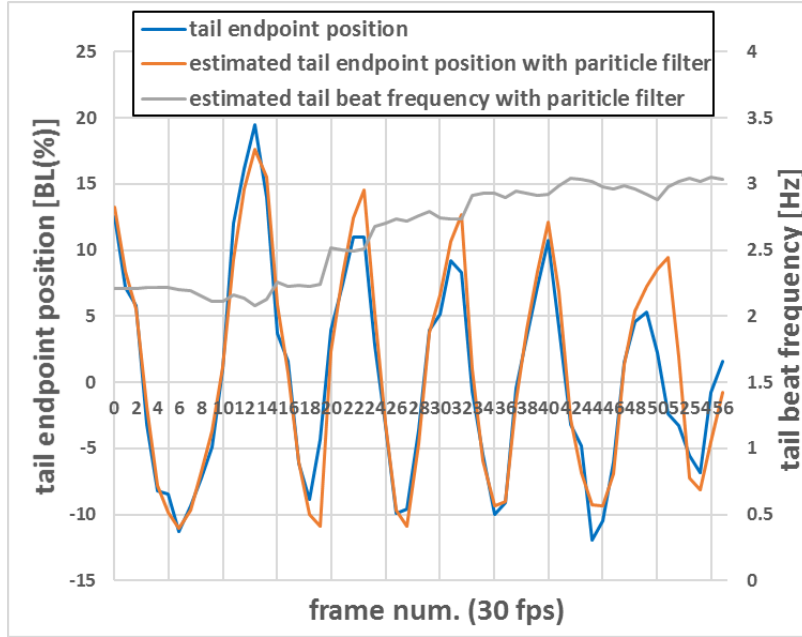


Figure 18: The estimated results of tail endpoint positions and tail beat frequencies with the particle filter for the data in Figure 13.

4.4 EXPERIMENTAL RESULTS

We have conducted experiments to demonstrate the effectiveness of our method. We first tracked isolated fish by our method and evaluated the accuracy of the result by manually tracking the same fish. We then measured body lengths and tail beat frequencies by our method, for which errors were computed by comparing the results with the data computed from manually estimated data. The results of detecting changes in tail beat frequency by our method are also shown. Finally, we present the accuracy of our detection method for coast phase.

4.4.1 Tracking Isolated Fish

In experiments, we first applied our tracking method (Section 4.3.2) to the three second scene (Section 4.3.1) and evaluated the accuracy of the result.

4.4.2 Body Length and Tail Beat Frequency

For the three second scene, we tracked 126 silhouettes (i.e., fish) by our method over 30 frames from the first frame. Out of them, 109 silhouette sequences were extracted as valid ones using the two conditions described in Section 4.3.2. After that, we manually tracked the same 126 silhouettes and checked whether all silhouettes of each sil-

houette sequence are isolated all through the tracking or not. We then confirmed that 110 silhouette sequences were valid ones that could be tracked. For the 110 valid sequences, 108 out of them were correctly tracked by our method whereas 2 valid sequences were missed. Aside from them, 1 invalid sequence was wrongly tracked. The precision and recall of the result of tracking were thus 0.991 and 0.981 respectively.

In order to evaluate the accuracies of estimated body length and tail beat frequency obtained by our method, we manually tracked 20 fish out of the 110 valid sequences mentioned above. During the tracking, we measured the head and tail points as ground-truth and computed the average body lengths from the head and tail points of ground-truth in the same way as described in Section 4.3.3. The tail beat frequencies from three beat cycles were also manually measured as ground-truth.

We measured the head positions, the body lengths and tail beat frequencies by our method (Section 4.3.3). The average and standard deviation (S.D.) of the body length differences by our method and ground-truth are 0.0172 (BL) and 0.0100 (BL) respectively. These results indicate that we can measure the body length of fish by our method accurately.

To evaluate our estimation method of tail beat frequency, we compared the values obtained by our method and those of ground-truth for the periods during which the ground-truth have been measured. For each tracked fish, we average the time series of tail beat frequencies computed by our method and calculated the difference of the tail beat frequencies between ground-truth and our method. The average and S.D. of the differences are 0.126 (Hz) and 0.154 (Hz).

The results are summarized in Table 1.

Table 1: Measurement Results of Body Length and Tail Beat Frequency

	difference between ground-truth and our method
ave. of body lengths	0.0172 (BL)
S.D. of body lengths	0.0100 (BL)
ave. of tail beat frequencies	0.126 (Hz)
S.D. of tail beat frequencies	0.154 (Hz)

4.4.3 *Coast Phase*

For the 110 valid sequences obtained in Section 4.4.1, we manually checked whether coast phases were observed. The definition of coast phase is as described in Section 4.2. As a result, we found coast phases for 29 valid sequences. On the other hand, our method detected that 33 valid sequences contained coast phases. The precision and recall of the classification result are 0.945 and 0.879. The results demonstrate that our method can practically detect coast phases.

4.5 CONCLUSION

In this chapter, we proposed the measurement method of tail beat frequency and the estimation method of coast phase for isolated fish in RS type schools of fish. For our experiments, we recorded a large school of sardines and applied our method to a scene taken from the movie. The average difference of the tail beat frequencies estimated by our method and those estimated manually was 0.126 (Hz). For estimation of coast phase, the precision and recall of the classification result were 0.945 and 0.879. These results indicate that our method is practical useful. We expect that our method is useful for observation of individual behaviors in school of fish.

TRACKING METHOD FOR MULTIPLE FISH WITH AN APPEARANCE MODEL

In this chapter, we propose a visual tracking method for fish schools of the type RS, i.e., there are a certain number of isolated fish and we can manually track most of them if occlusions of multiple fish occur as stated in Section 1.1. The accuracy of our method is evaluated with a scene of a school of sardines (Figure 19) filmed in the Kujukushima Umikirara Aquarium.

Most of the results presented in this chapter have been published in [IC1]. The research of this chapter have been done with Mr. Hongo Koki, Lecturer Hitoshi Habe at Kinki University and Prof. Masa-aki Sakagami. The author of this thesis designed research, developed methods, performed experiments and wrote the paper.

5.1 INTRODUCTION

Tracking multiple targets in a video arises in many important applications such as automatic surveillance, robotics, and collective motion analysis. A lot of tracking algorithms have been proposed [69, 97, 57, 24, 25], as stated in Chapter 2. Recently, tracking methods for multiple objects in highly dense group have been proposed [116, 6, 68]. However, it becomes quite difficult to track targets when they are homogeneous and occlusions occur frequently, such as the school of fish shown in Figure 19.

Many methods have been proposed for tracking a large number of unmarked fish under frequent occlusion [33, 34, 89]. Several researchers have measured not only the positions and directions of the tracked fish but also their postures with parameterized deformable models [39, 20]. However, as stated in Section 2.3, the targets in most of these studies are fishes in a shallow tank, and consequently, two fish at most are assumed to superimpose in occlusion cases. Viewed from one direction, more than two fish are generally superimposed in schools of fish, as in Figure 6(e) and 19(b).

As can be seen in Figure 19, fish overlap with each other in real fish schools, and occlusions frequently occur as a result. Moreover, the texture of fish is weak, and identification of individuals in the school is difficult because they are a highly homogeneous group and their appearances change according to their tail beats. For these reasons, it is difficult to track multiple fish in real scenes.

In this chapter, we solve this problem by considering appearances of occluded fish in the school. We first constructed an appearance



(a)



(b)

Figure 19: (a) A school of sardines taken from the bottom of a tank at the Kujukushima Umikirara Aquarium. (b) A magnified view of (a).

model that represents the nonrigid fish bodies. Because the members of the school are similar, each of them can be accurately represented by the model with suitable scaling. We confirmed that an isolated fish can be tracked with our appearance model. For occluded fish, we can estimate their states by matching all of the combinations of the possible positions allowing rotation and scaling of the models if we know the number of the fish. On the basis of the above ideas, we propose a tracking method for multiple fish, even if more than two member of them overlap with each other.

For the experiments, we collected 11 scenes of swimming sardines from a movie recorded at the Kujukushima Umikirara aquarium. In order to compare the tracking performance of our method, we have manually tracked the fish and have also carried out tracking using a basic tracking method [97, 69]. For multiple swimming fish that overlap with each other, our method practically tracked targets (80% for two fish and 100% for three fish) for the collected scenes, although tracking based on [97, 69] failed owing to occlusions. For the successfully tracked scenes, we also computed the difference in position between the tracked results and the ground-truth to measure the accuracy of our method. The average difference is less than 4% of the mean body length of the school, and these results indicate that our method is practical for tracking multiple fish.

This chapter is organized as follows: we first review works related to collective behavior of fish schools and tracking methods mainly used for fish in Section 5.2. Section 5.3 presents the dataset and the details of our method for tracking multiple fish. We then discuss the experimental results in Section 5.4. Finally, we summarize this chapter and state the plans for future work in Section 5.5.

5.2 TRACKING METHODS FOR MULTIPLE OBJECTS

We briefly review tracking methods for multiple objects, in particular schools of fish.

Tracking methods for multiple objects in a high dense group: Tracking individuals in a highly dense group is challenging because occlusions among individuals occur frequently, which makes it difficult to identify individuals. Recently proposed tracking algorithms have employed individual behavior models, i.e., spatiotemporal consistency models [116], global scene constraint models [6], and spatial pattern models [68].

Tracking methods for multiple fish: Tracking methods mainly for multiple fish have been proposed. Delcourt *et al.* tracked blobs in binarized fish school images, identifying the individuals using three parameters based on [59] for occlusions [33]. Butail *et al.* modeled the shape of each fish as a series of elliptical cross sections and reconstructed the full-body trajectories of eight fish with multiple cameras [20]. Fontaine *et al.* tracked multiple fish, estimating their postures by parameterized deformable model with an iterated Kalman filter [39]. Qian *et al.* detected the head regions with a Kalman filter and linked the trajectory fragments under time and space constraints [89].

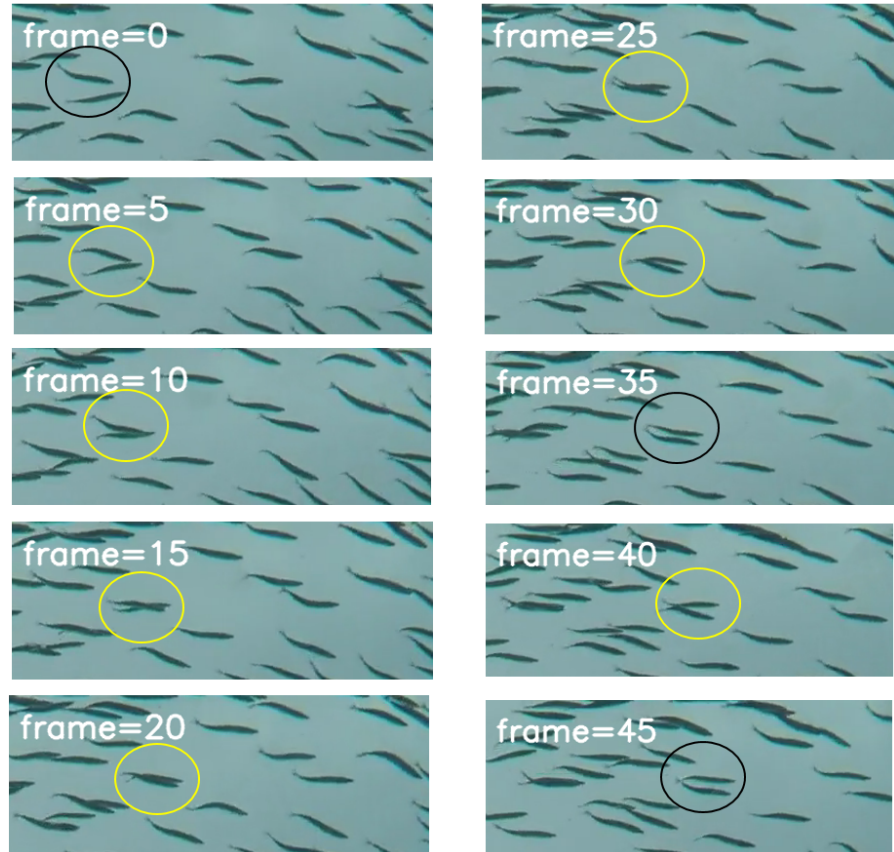


Figure 20: An example of Type B scene. Two fish in the ellipses are crossing once. Fish in each yellow ellipse are overlapping.

5.3 OUR METHOD

In this section, we explain the details of our method: the dataset used for the tracking experiments, our appearance model, and the tracking method for multiple fish.

5.3.1 Dataset

We recorded videos of a school of sardines in March 2015, as explained in Chapter 3. We used videos in which the school is relatively sparse as shown in Figure 19. The population of the school was approximately 3,000 individuals. The average apparent body length of the 30 sardines in the video is 58.67 pixels. In this chapter, we use the estimated mean body length (BL) as units of measure. The typical speed of the sardines in the aquarium is approximately 1-2 BL/s.

For our experiments, we extracted three types (A-C) of scenes from the movies as follows. Type A contains an isolated swimming fish during the scene. Type B contains two fish that cross once. Type C contains three fish that overlap with each other. We prepared one



Figure 21: Part of the appearance model. Note that these templates are grayscale images.

scene of Type A, five scenes of Type B and five scenes of Type C. Figure 20 shows an example of Type B scene. The top row in Figure 24 shows snapshots from scenes of Type A, B, and C and the trajectories of the tracked fish.

5.3.2 Appearance Model

We constructed an appearance model that represents nonrigid fish bodies. From the sequential images of a manually tracked fish, we extracted 20 template images whose directions, sizes, and positions of the center of gravity are aligned. Figure 21 shows part of the appearance model. Because all of the members of the school are similar to each other, we can approximately represent all of the fish images with this models by rotation, scaling their size, and fitting their thickness. Therefore, we can estimate the position and other states of each isolated member of the school by matching it with our appearance model.

5.3.3 Parameter Estimation with the Appearance Model

For an isolated fish in the school, we estimate its position, direction angle, posture (index number of our appearance model), scale, and thickness by applying template matching algorithm and our appearance model to the image. In this study, we employed the sum of the squared distance (SSD) as the similarity measure. Figure 22(a) and 22(b) show an example of the estimation for isolated fish. Table 2 is the list of parameters used in our method.

For a multiple fish occluded image, we cannot estimate the parameters of all of the members in the image by simply applying the above matching method. However, if we know the number of fish in the occluded fish image, we can also estimate the positions and other parameters of multiple fish by matching with all of the combination of parameters. Figure 22(c) and 22(d) show an example of parameter estimation for occluded fish. This matching method for occluded fish

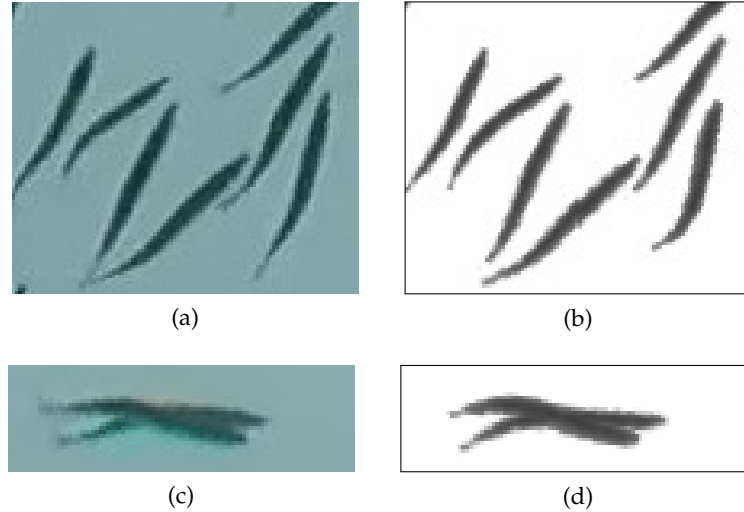


Figure 22: (a) Original image. (b) Image drawn from the estimated parameters of (a). (c) Image of occluded fish. (d) Image drawn from the estimated parameters of (c) with our method

enables us to extract their states unless the entire body is occluded by other fish.

5.3.4 Tracking Multiple Fish

We explain a multiple fish tracking procedure with our parameter estimation method. In this study, we first select fish to track and assign id numbers. We calculate the initial parameters with our parameter estimation method.

For frame t of a scene of Type A, we first estimate the position and angle of the tracked fish in frame t from previous five frames of data. We next apply our parameter estimation method. The position and direction angle are explored within $\pm\alpha$ pixels and $\pm\beta$ degrees on the basis of the estimated position and angle. The thickness is fixed through tracking. We renew the position and other parameters of frame t and repeat these processes.

Table 2: Parameters of Our Method

parameter	units	value explored
position	pixels	the entire image
direction angle	degrees	omnidirectional
scale	5%	95% - 120%
thickness	25%	75%, 100%
appearance model	1	1-20

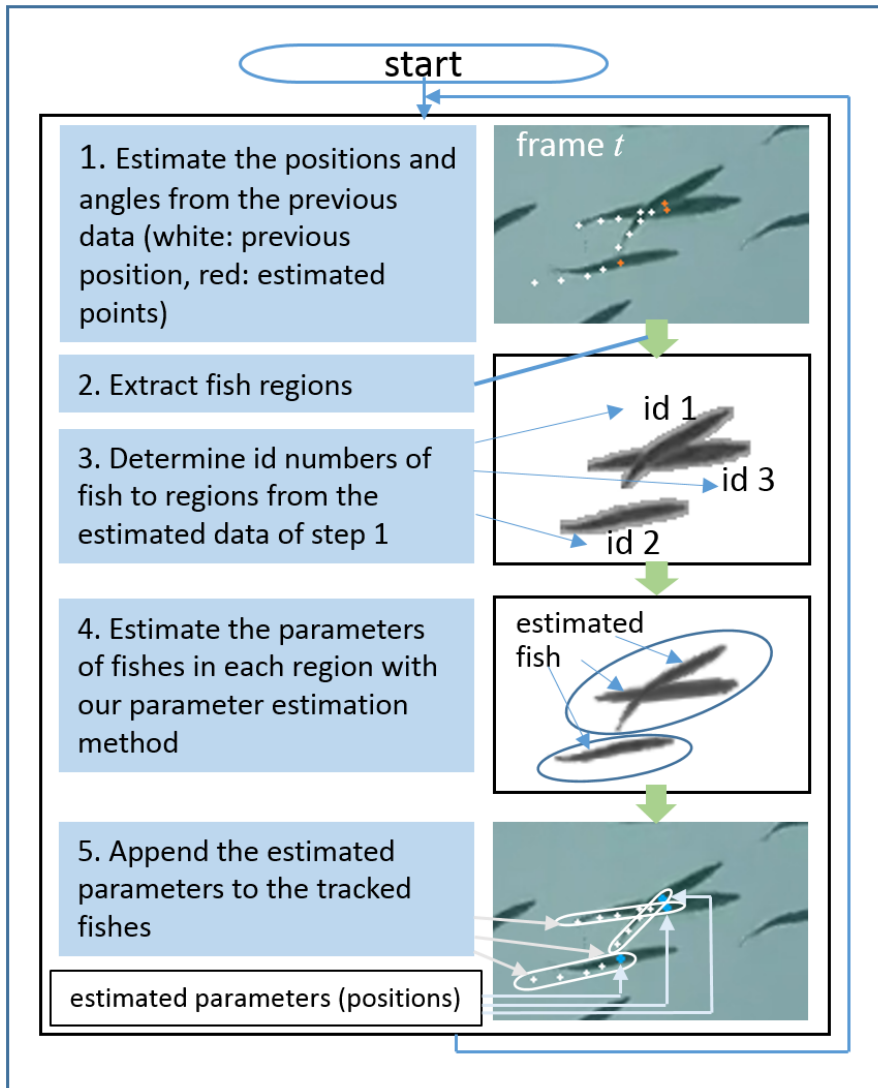


Figure 23: Framework of multiple fish tracking

For a scene of Type B and C, i.e., in the case of multiple fish tracking, we track them as follows. In frame t , we first estimate the temporal positions and directions from the previous data. We calculate the fish parameters in frame t with the parameter estimation method. Finally, we assign the parameters estimated from the calculated parameters to the tracked fish. Figure 23 shows the flowchart of the tracking process. The details are as follows.

1. We estimate the position and angle of each tracked fish at frame t from the previously estimated parameters. In this study, we calculate the parameters with extrapolation from five previous frames of data.
2. We binarize the t -th image and extract the fish regions. Note that there are regions that contain multiple fish. We dilate the

fish regions and extract regions of fish from the original t -th image using the dilated regions as masks.

3. For the separated regions prepared in the previous step, we assign the id numbers of the tracked fish to the regions. We calculate the similarity with average SSD between the region and the fish image drawn from each fish's parameters estimated in step 1. We assume that a region contains a tracked fish if the average SSD between them is less than γ .
4. For each region and assigned id number, we estimate the parameters of the fish with our parameter estimation method. For each fish of the assigned fish, the position and direction angle are explored within $\pm\alpha$ pixels $\pm\beta$ degrees on the basis of the estimated positions and angles of the fish. The thicknesses of assigned fish are fixed through tracking.
5. To append the estimated parameters to tracked fish data, we define the distance d_p between the parameters p and q of the fish as follows:

$$d_p(p, q) = \sqrt{(p_x - q_x)^2 + (p_y - q_y)^2 + (p_\theta - q_\theta)^2 + (p_s - q_s)^2}$$

where p_x , q_x , p_y and q_y are the positions, p_θ and q_θ are the direction angles, and p_s and q_s are the scales. We assign each estimated parameter to the nearest tracked fish data according to the distance.

In this study, we set α to 3, β to 6, and γ to 100.

5.4 EXPERIMENTAL RESULTS

We have conducted experiments to show the effectiveness of the proposed method. In order to compare the tracking performance of the proposed method, we manually prepared the ground-truth positions of the targets and have also carried out tracking using a simple method that extracts feature points[97] and tracks them using the Lucas-Kanade method[69]. We call the simple method 'FP-LK' for short.

FP-LK and the proposed method tracked successfully for the scene of Type A. For the scenes of occluded fish, the proposed method tracked targets practically (80% for Type B and 100% for for Type C), although FP-KL failed to track in the middle of tracking. Figure 24 shows typical examples of tracking results. Each column corresponds to a sequence of test images. The top of each column shows a ground-truth trajectory by which we can see how fish are swimming in the sequence. The remaining rows show the tracking results of FP-LK and the proposed method.

In Figure 24, we note that FP-LK often failed to track the target. For example, FP-LK cannot continue tracking until the end of sequence

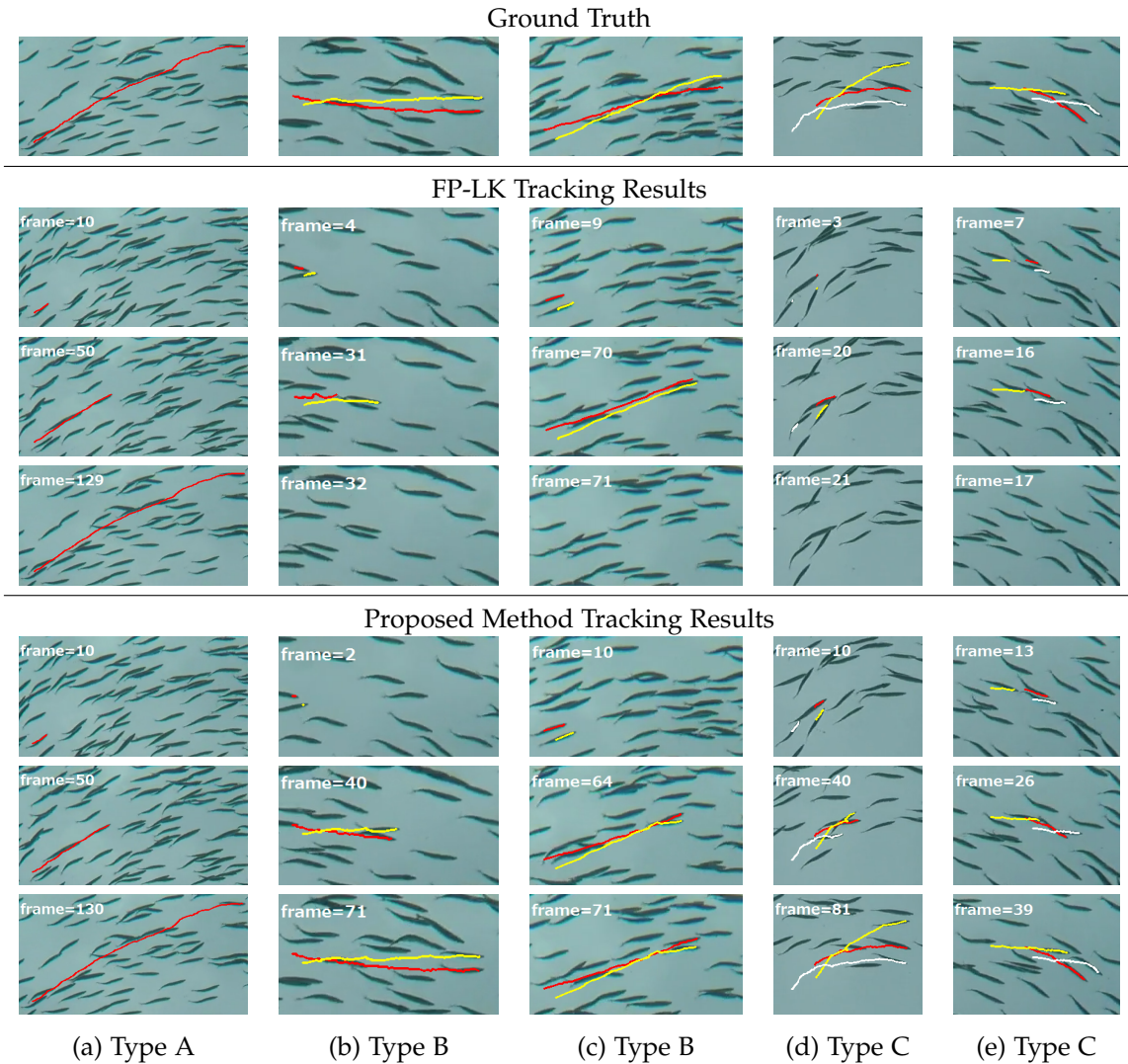


Figure 24: Tracking results. The top row shows the ground-truth of the fish trajectories. The second to the fourth rows show the trajectories of the FP-LK method. The fifth to seventh rows show the trajectories of the proposed method. The numbers in the images are frame numbers. We set the number of first frame in each scene as 0.

in (b) to (e), where multiple fish are tracked, because the fish bodies are very close to each other. On the other hand, the proposed method robustly track the target fish even for the challenging situations as (b), (d), and (e) in Figure 24, while the proposed method cannot correctly track the two fish in Figure 24 (c). The tracking for Figure 24 (c) was failed when the two fish were completely overlapped.

The errors of the tracking results are summarized in Table 3. We computed the distances between the successfully tracked results and the ground-truth in each frame. Their averages and variances are listed in the table. Note that the unit is the percentage of body length(BL). Moreover, we note that the errors of FP-LK for multiple tracking can-

Table 3: Quantitative Comparison of Tracking Errors (Percentage of the BL)

	Type A	Type B	Type C
FP-LK	2.83(0.66)	N/A	N/A
Proposed	2.66(1.21)	3.63(6.17)	3.58(3.56)

not be computed because it cannot track the targets until the end of the sequences. On the other hand, we can see that the proposed method provides sufficiently accurate trajectories.

5.5 CONCLUSION

In this chapter, we proposed an appearance-based tracking method for multiple fish. For the test scenes in which two or three fish overlap with each other, our tracking method exhibited practical performance (80% for Type B and 100% for Type C), although the FP-LK method failed in all the scenes. The trajectories tracked by our method were also accurate, because the average differences between the trajectories of our method and the ground-truth in the three scene types were less than 4% of the BL of the school.

Our future work includes improving the tracking performance by introducing a parametrised appearance model of fish, a probabilistic object tracking framework, and interaction models between fish to estimate the states in the next frame. It is also worth accelerating our algorithm in order to track thousands of fish in schools.

VELOCITY DISTRIBUTION MEASUREMENT METHOD WITH OPTICAL FLOW FOR SCHOOL OF FISH

We propose a measurement method for the mean speed distribution of collective motions of RD type schools of fish with optical flow in this chapter. Our method is applicable to highly dense homogeneous groups wherein individual movements are approximately uniform locally. To measure speed distributions, we partition a group into regions and estimate mean speeds in each region by extracting only flows that are relevant to collective motions and averaging them over a period of time. We experimentally find that our method works well even when we cannot reliably track individuals. We specifically apply our method to schools of sardines to measure a kind of speed distribution called rotation curve (RC). Experimental results obtained by simulation demonstrate that our method can estimate flows and RCs accurately. We also performed experiments with videos of real fish. The RCs were estimated by manual tracking and by our method. The results are approximately equal, and the average difference is less than 4% of the mean body length of fish in the observed schools. These results indicate that our method is practically useful for measuring RCs. We also applied the proposed method to another kind of fish school, a school of anchovies and measured another kind of velocity distribution, called cake-cut distribution. These results are also presented.

Most of the results presented in this chapter have been published in [J1] and [IC3]. The research of this chapter have been done with Prof. Horohisa Hioki and Prof. Masa-aki Sakagami. The author of this thesis designed the research, developed methods, performed experiments and wrote these paper.

6.1 INTRODUCTION

Measuring collective motions of a group is a fundamental step in mathematical modeling and analysis of collective behavior as stated in Chapter 2. In principle, we can measure collective motions of a group by tracking individuals separately. However, it becomes quite difficult to track individuals when they are homogeneous and their density in the group is high like RD type schools.

In this chapter, we find that estimating speed and velocity distribution of collective motions is possible, even when we cannot reliably track individuals of a group manually or automatically. In this

chapter, we propose a method to estimate the speed distribution of collective motions with dense optical flow from video. Our method is applicable to homogeneous groups where individual movements are approximately uniform locally and are stable for a sufficient time period.

To estimate the speed distribution of collective motions from a video, just computing a dense optical flow for the entire scene through all video frames is often insufficient. When we record a video of a group, we may observe noise and obstacles, i.e., objects that are not in the target group. Therefore, we must extract only the flows that are relevant to the target group and exclude other flows.

We can exclude the flows derived from noise and obstacles if we know approximately typical velocities in each region. We also exclude flows around the flows just excluded, because such flows can be affected by noise and obstacles. Once the flows relevant to the group are extracted from all frames successfully, we can compute the mean speed in each region by deriving the mean speed from the flows in the region for each frame and then take their mean value.

We have measured the rotation curve (RC) for rotating schools of sardines by our method. Figures 25(a) and 25(b) show snapshots of the schools of sardines whose RCs were estimated. RC is a kind of speed distribution for a group in rotational motion (Figure 25(c)). RC is defined as a plot of the mean speed of the rotational motion against the radial distance from its center. To estimate RCs automatically, the center point must be accurately located; therefore, we have developed an algorithm to compute the center point from flows.

As can be seen in Figures 25(a) and 25(b), fish swim in 3D space; thus, in the strictest sense, measuring 3D motions is required to estimate RCs, which is quite difficult. In this study, we estimate RCs from projected 2D images (Figure 25(b)) because schools of fish are typically fairly flat and fish generally swim at a relatively equal depth (see Figure 25(a)). Measurement of speed distribution for such collective motion is useful for roughly understanding the movement and features of groups and estimating parameters for mathematical models of group behavior that can be used to construct better models [78, 99]. Such measurement enable us to observe automatically the health and growth of individuals in a fish farm.

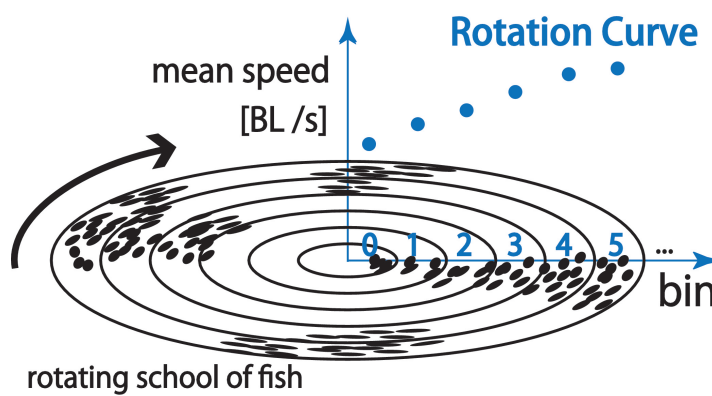
We first applied our method to a set of simulations. The correct parameters for schools of fish are known for such simulations; therefore, we can quantitatively evaluate our method by simulation. We also applied our methods to videos of schools of sardines. To identify the correct RCs for real schools of sardines, we manually tracked as many individual sardines as possible in a careful way. It was, however, quite difficult to track sardines stably because individuals frequently overlapped. This means that the RCs obtained by manual tracking are



(a)



(b)



(c)

Figure 25: (a) Rotating schools of sardines taken from the side and (b) the bottom of a tank at the Kujukushima Umikirara Aquarium, and (c) an overview of the RC of the school

inaccurate in the strictest sense. We estimated RCs using our method and compared the results with the manually-tracked RCs.

The experimental results demonstrate that our algorithm is accurate in simulation. For schools of sardines, the average relative errors of the RCs estimated by our method with respect to the RCs obtained by manual tracking were less than 4%, both RCs were thus approximately equal.

Our method was also applied to a 20 minute video of sardines. We could automatically compute RC time series of sardines for such a long scene. During taking a long video of a school, we cannot always expect to observe the school rotating in torus form stably. The shape of a school can be distorted, for example, by attacks of large fishes (predators). A part or all of the school becomes not observable to us when large fishes cross over near the camera. For finding those kinds of events automatically, we devised two features that are derived from flows. We could successfully detect noticeable events from the 20 minute video by those features.

In order to evaluate applicability of our method, we measured the RC time series of rotating school of a different kind of fish, anchovies in the same aquarium. We also detected events at the same time as for the case of sardines. The results indicate that our method is useful practically.

We cannot measure propagation of speed along to circumferential direction with the RC. To detect such propagations as a kind of information transfer, we also propose another kind of division of space, called cake-cut distribution, and measure speed and angle distribution on the division. We have conducted experiments to show the accuracy of the velocity (speed and direction) distribution on the division. The result is also presented.

In the rest of this chapter, we briefly review results from collective motion measurement in natural science in Section 6.2. Section 6.3 presents the basic idea of speed distribution measurement with optical flow. We present the details of our method for estimating RC and experimental results in Section 6.4. Applications of our method, including event detection, to a long time scene of sardines and to a school of anchovies are shown in Section 6.5. We introduce the cake-cut distribution and show the experimental results. Finally, we summarize this chapter and give directions for future work in Section 6.7.

6.2 MEASUREMENTS OF COLLECTIVE ANIMAL BEHAVIORS

In collective animal behavior research, tracking individuals of a group has often been performed manually as stated in Chapter 2. Cavagna *et al.* [22] measured the 3D positions of individual European starlings within flocks of up to 2,600 birds using a stereo camera. Tracking in-

dividuals in a shoal or school of fish is often more difficult than in flocks of birds because the density of a shoal or school of fish is typically higher than that of a flock of birds. For example, the average nearest neighbor distance of flocks of European starlings is reported as approximately 2.6 wing spans (5.3 body length) [10], whereas the average nearest neighbor distance of a school of sardines is approximately 0.3 body length, which was determined by a single frame from one of our videos.

In previous work, videos have been recorded in shallow tanks to avoid difficulties caused by overlap among fish [99]. Hemelrijk *et al.* [46] measured the 3D positions of dozens of mullets in a tank. However, to date, the features of collective motions of schools with thousands of fish, as shown in Figure 25(b), have not been investigated.

6.3 SPEED DISTRIBUTION MEASUREMENT WITH OPTICAL FLOW

Here, we propose a method to estimate the speed distribution of collective motions with dense optical flow. We find experimentally that our method is effective even when we cannot reliably track individuals. We assume that the directions and speeds of individuals in a group are approximately uniform locally.

To estimate the speed of an object, based on the dense optical flows of a proper density, we can compute the mean speed of the flows that are relevant to the object (Figure 26(a)). Similarly, we can estimate the mean speed of a group of objects that may overlap when they move together; thus, their velocities are approximately equal (Figure 26(b)).

Here, we discuss the basic idea of estimating the mean speed of collective motions, which is stable for a time period, by computing the dense optical flow. Assume we have T consecutive frames for collective motions of a group. We partition the group into regions and estimate the mean speeds in each region. We then estimate the mean speed in a region between frame 0 and frame $T-1$ by obtaining all flows in the region of each frame, computing the mean speed in the region of each frame, and then taking their mean value with time as follows:

$$\text{the mean speed} \sim \frac{1}{T} \sum_{0 \leq t < T} \left(\frac{1}{|F_t|} \sum_{i \in F_t} \text{flow}_i \right) \quad (11)$$

where F_t is the index set of the flows in the region at frame t , and flow_i is the size of the i th flow. Figure 26(c) shows the basic idea of speed estimation for a region.

It should be noted that obstacles, i.e., objects not in the target group, may be present in the same scene. At the same time, we usually observe various types of noises that can degrade flows. Therefore, we need to extract only the flows that are relevant to the target group and exclude other flows.

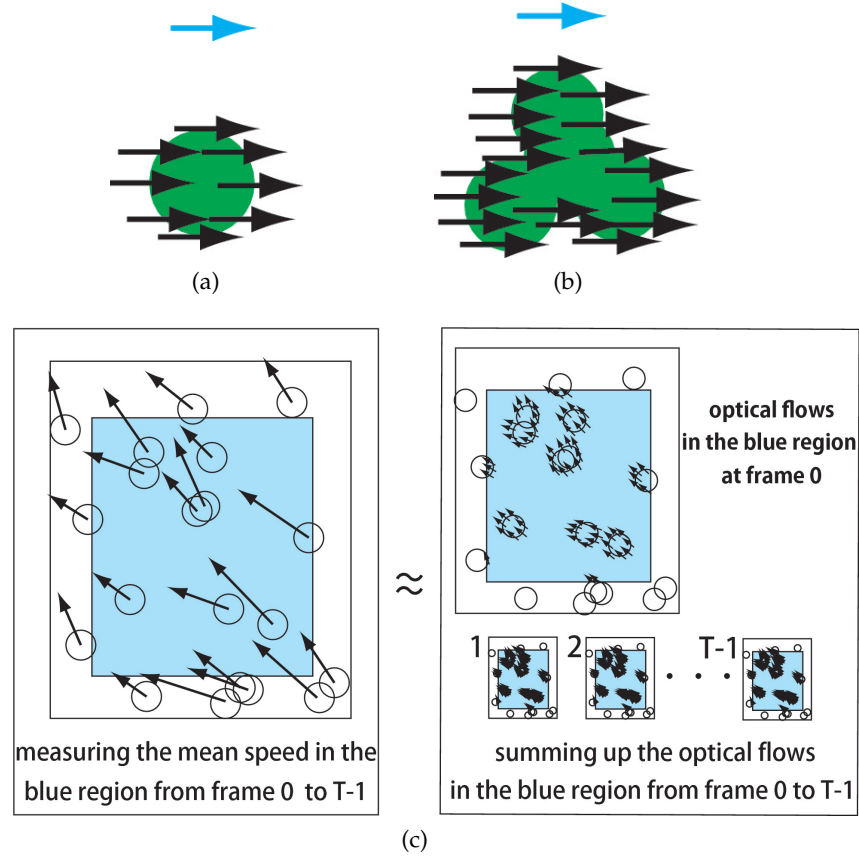


Figure 26: Speed measurement with optical flow: (a) measuring the speed of a moving element, (b) the speed of moving elements that move together and (c) measuring the mean speed of moving elements in the blue region

We assume that individuals in the group move together in a certain direction in a local area; therefore, if we know the direction, flows that move in apparently different directions can be excluded. If we know the typical speed of a measured individual, we can exclude flows that are too slow and too fast. Flows apparently irrelevant to the target group are thus excluded as those derived from noise and obstacles. We also exclude flows around them, because such flows can be affected by noise and obstacles. Under these conditions, it is expected that we can extract only the flows that are relevant to the target group, from which we compute the speed distribution of the group.

In this study, we measure RCs, which are a kind of speed distribution, for rotating schools of sardines to characterize the states of fish. For example, RCs can be used to evaluate Niwa's mathematical model [78] of fish schooling. A definition of RC and methods to estimate it are described in Section 6.4.

6.4 ROTATION CURVE

RC is a speed distribution defined for groups in rotational motion. The RC for a group is given as a plot of the mean speed of rotational motion against the radial distance from its center. RC was originally introduced to understand the structures of disk galaxies. The RCs of visible stars and gases in disk galaxies are useful for analyzing such galaxies, and the results support the dark matter hypothesis [15].

In this study, we estimate RCs of rotating schools of sardines. They are typically relatively flat, and individuals in a school usually swim at a relatively equal depth. Therefore, we estimate RCs from 2D motions observed in video frames. We divide the region of a school into concentric annulus-shaped areas of equal width. In this study, each of these areas is used as a bin. The RC is then taken as a plot of the mean speeds of fish for each bin. Figure 25(c) illustrates the RC of a school of fish.

We use the estimated mean BL of fish as the unit of distance. The speed is measured in BL/s. The width of each bin is set to 1 BL. Note that BL values vary relative to the characteristics of each unique school of fish.

6.4.1 *Rotation Curve Estimation*

Here, we provide an overview of the RC estimation process, which is based on the method introduced in Section 6.3. Figure 27 shows a flowchart of the entire process. The details of each step are presented in the following sections.

We first estimate the center of the first frame of a scene. The center point is supposed to be roughly located manually. The position of this tentative center point is then adjusted by iteratively applying a center estimation method (Section 6.4.1.3) 10 times. In the estimation process, the tentative center point is used to compute flows and then the position of the center point is updated using the computed flows. This circular process is repeated enough times until the position of the center point converge. Through simulations (Section 6.4.2.2), we found that this iterative estimation process converges quickly, and 10 iterations are sufficient. Once the center point is estimated, we simultaneously determine the innermost and outermost bins that are usable for RC estimation. We include a bin for estimation if the ratio of the flows of the school to all flows in the bin is greater than a threshold β (Table 4).

After the center point is located, and the innermost and outermost bins in the first frame are determined, we detect the flows of the school in each bin for each frame (Section 6.4.1.1). We then update the center point, innermost bin, and outermost bins for the next frame. In this update process, rather than replacing the data with new values,

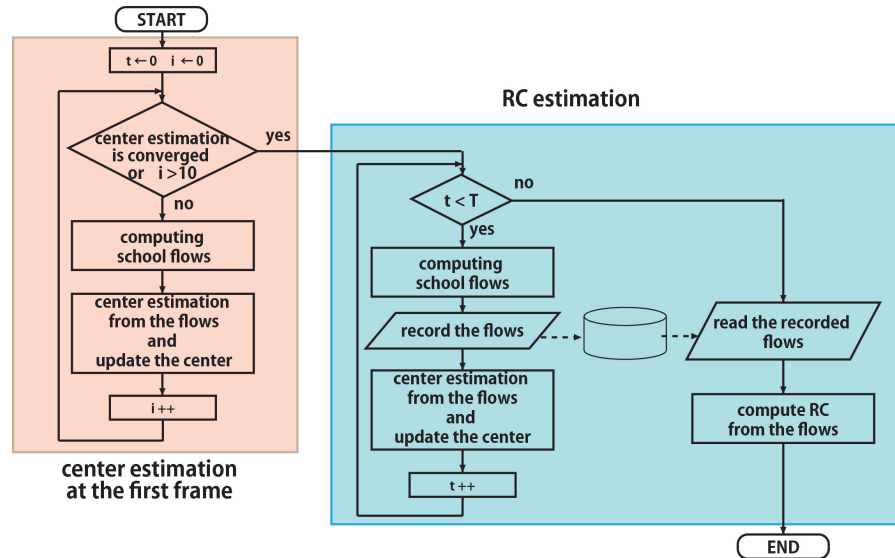


Figure 27: RC estimation framework

we take the average values of the previous 30 frames to stabilize the data.¹ These detection and update processes are repeated frame-by-frame. Once we have calculated school flows for each bin for all the T frames, we then compute the RC from the flows (Section 6.4.1.2).

We can successively estimate RCs for every T frames in a long time video by applying the above RC estimation process repeatedly. Note that we do not have to repeat the center estimation process for second or later RC estimation processes.

6.4.1.1 School Flow Detection

To estimate the RC of a school of fish properly, we must extract only the motion of the school. We detect motions as flows.

Before computing flows, we first apply a bilateral filter to each video frame to reduce block noise caused by the movie codec and wave noise from the water surface.

We then calculate a dense optical flow between frame t and frame $t + \Delta t (1 \leq \Delta t)$ and multiply $1/\Delta t$ for each flow. We do not calculate flows between two consecutive frames directly because the movements of fish between frames are sometimes negligible. We employ Gunnar Färneback's algorithm [37] to calculate dense optical flow. We compute flows for grid points at regular intervals of p pixels vertically and horizontally.

The obtained flows include the flows that are affected by noises and obstacles. We extract school flows by considering their expected conditions.

First, school flows are expected to move uniformly with the direction of rotation because the rotation direction of the school will not

¹ We use the data of the first frame if data for i th frame ($i < 0$) are required.

change during a short period. Second, a wandering fish, such as a sardine or tuna, always swims about its BL per second [8]. Therefore, we assume that extremely slow and extremely fast flows should not be considered as school flows.

From the above considerations in our work [IC3], we select flows that satisfy the following conditions: 1) the difference between flow direction and rotation direction is less than $\pm 3\pi/8$; 2) the speed derived from the flow is less than 4 BL/s; 3) the speed derived from the flow is greater than $s_L(n)$ BL/s, where n is the bin number ($n = 0, 1, \dots$):

$$s_L(n) = \begin{cases} 0.1 + 0.025 \times n & 0 \leq n < 20 \\ 0.6 & n \geq 20. \end{cases} \quad (12)$$

Flows that do not satisfy the above conditions are excluded from the calculation of RC. Flows around such excluded flows are also excluded because such flows may be affected by noise and obstacles. Thus, we define a flow as being in the school only if it and its 4-neighbor flows simultaneously satisfy the above conditions. We calculate RC from the extracted flows. Figure 28 shows an example of flows computed for scene A in Figure 32.

We have given a constant speed range for each bin as the above speed condition (3), however, speeds of fish vary not only from area to area and but also from time to time in rotating schools. We therefore need to determine adaptively the proper range of speed for each local area of each frame to exclude flows caused by small noises and obstacles such as large fish out of school. In our work [J1], we also proposed an extraction process that consists of two stages with adjusted speed condition.

In the first stage, we estimate the average speed of school flows for each bin for every T frames. We select flows from T frames by the three conditions and compute their average speed for each bin with a fixed center point in order to stabilize the results. Among the three conditions to be used here, we do not know the speed condition for school flows for each bin yet, but we can still provide constant thresholds that approximate minimum and maximum speeds for the whole school. In [J1], we use 0.15 BL/s and 5.0 BL/s respectively as the minimum and maximum speeds. It is expected that the average speeds computed in this way are not affected by noises and obstacles.

In the second stage of the extraction process, we adjust the speed condition for each bin according to the following criteria:

$$\text{minimum speed} = a_{\max}s + b_{\max} \quad (13)$$

$$\text{maximum speed} = a_{\min}s + b_{\min} \quad (14)$$

where s is the average speed of the bin obtained in the first stage and a_{\max} , b_{\max} , a_{\min} , b_{\min} are constants. We use $a_{\max} = 1.35$, $b_{\max} = 1.5$,

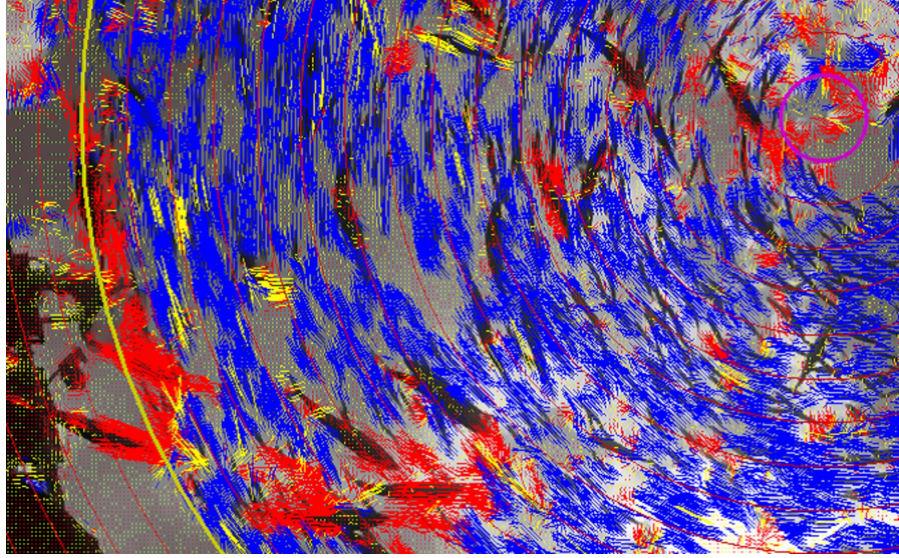


Figure 28: Optical flows of a frame in scene C: blue lines show flows that satisfy the conditions, red lines are flows that do not satisfy the direction condition, and yellow lines are extremely slow and fast flows

$\alpha_{\min} = 0.2$ and $b_{\min} = 0.15$ in $[J1]^2$. We then apply the adjusted speed condition together with the other two conditions to all the flows again and extract school flows from them.

The accuracy of RC estimation have been slightly improved with the extraction process in $[J1]^3$. We show the results according to the algorithm of $[IC3]$ in Section 6.4.2 and the ones according to the procedure of $[J1]$ in Section 6.5.

6.4.1.2 RC Computation from Flows

In frame t , we compute the mean speed of each bin of the school from the mean flow in each bin. We then obtain the RC by averaging the mean speeds in each bin for T frames. Accordingly, the mean speed RC_n of the n th bin can be computed by applying (11) to the bin as follows:

$$RC_n = \frac{1}{T} \sum_{0 \leq t < T} \left(\frac{1}{|F_{t_n}|} \sum_{i \in F_{t_n}} flow_i \right), \quad (15)$$

where F_{t_n} is the index set of the school flow of the n th bin at frame t and $flow_i$ is the value of the i th flow obtained in the school.

Equation (15) should work in principle; however, if there is a frame where we find only a small number of flows, this equation overesti-

² Note that here we allow to take flows faster than 5.0 BL/s. Although we assume the maximum speed in the first stage, it is given as an approximated value, and we can observe that there are exceptionally fast fish in schools.

³ The average relative errors of RC estimation for three scenes school of sardines in Section 6.4.2.3 have been improved from 3.4% to 3.1%.

mates the influence of the frame, and the mean speed obtained from the frame may result in incorrect fluctuations of the RC_n value. To mitigate such influence, we assume that we can compute RC_n by first summing all school flows found in the bin for all T frames and then dividing the sum by the total number of flows as follows:

$$RC_n = \frac{1}{\sum_{0 \leq t < T} |F_{n_t}|} \left(\sum_{0 \leq t < T} \sum_{i \in F_{n_t}} flow_i \right). \quad (16)$$

Table 4: parameters of our method

T	30	parameters of Färneback's algorithm	
p	3	scale to build image pyramids	0.5
Δt	6	number of pyramid layers	3
α	0.05	averaging window size	7
β	0.2	number of iterations at each layer	5
		size of the pixel neighborhood	5
		standard deviation for polynomial expansion	1.1

Fish in a school do not distribute over all bins evenly. Sparsely populated bins with many obstacles may not yield reliable results. Thus, we calculate the mean speed for a bin only when the ratio of school flows to the total number of flows found in the bin is greater than a threshold α .

Table 4 shows the parameters of our method. We implemented our method using the C++ programming language with OpenCV.

6.4.1.3 Center estimation

We propose a method that estimates the center of a rotating school of fish from flows of their movements with least-squares method. With our method, the center point is located accurately when the form of the rotating school is not heavily distorted.

We assume that each fish is expected to swim roughly along the rotation direction; thus, the line l_i , which is normal to the flow and goes through the origin of the flow, is expected to pass near the center point. Therefore, we can estimate the center point by minimizing the sum of squares of the distance from the center to line l_i of each flow.

For a normalized flow vector (u_i, v_i) at (x_i, y_i) , the distance from the center (x, y) to the line l_i is given by $|u_i(x - x_i) + v_i(y - y_i)|$ as shown in Figure 29. To determine the center point, we minimize the

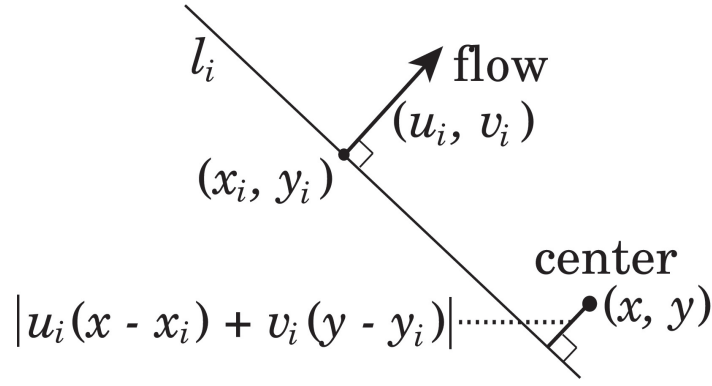


Figure 29: Overview of center estimation

following sum E of the distances from the center and normals of all the flows,

$$\begin{aligned}
 E &= \sum_i \{u_i(x - x_i) + v_i(y - y_i)\}^2 \\
 &= (\mathbf{x} - \mathbf{F}\mathbf{c})^T (\mathbf{x} - \mathbf{F}\mathbf{c}) \\
 &= \mathbf{x}^T \mathbf{x} - 2\mathbf{x}^T \mathbf{F}\mathbf{c} + \mathbf{c}^T \mathbf{F}^T \mathbf{F}\mathbf{c}
 \end{aligned} \tag{17}$$

where

$$\mathbf{x} = \begin{pmatrix} u_1 x_1 + v_1 y_1 \\ u_2 x_2 + v_2 y_2 \\ \vdots \\ u_n x_n + v_n y_n \end{pmatrix}, \mathbf{F} = \begin{pmatrix} u_1 & v_1 \\ u_2 & v_2 \\ \vdots & \vdots \\ u_n & v_n \end{pmatrix} \text{ and } \mathbf{c} = \begin{pmatrix} x \\ y \end{pmatrix} \tag{18}$$

The the sum of squares is found by setting the gradients to zero.

$$\frac{1}{2} \frac{\partial E}{\partial \mathbf{c}} = \frac{1}{2} \left(\frac{\partial E}{\partial x} \quad \frac{\partial E}{\partial y} \right)^T = \mathbf{F}^T \mathbf{F}\mathbf{c} - \mathbf{F}^T \mathbf{x} = 0 \tag{19}$$

From the above equation, we need to solve the following regular equation

$$\mathbf{F}^T \mathbf{F}\mathbf{c} = \mathbf{F}^T \mathbf{x}, \tag{20}$$

i.e., we solve the following matricial equation:

$$\begin{pmatrix} \sum_i u_i^2 & \sum_i u_i v_i \\ \sum_i v_i u_i & \sum_i v_i^2 \end{pmatrix} \begin{pmatrix} x \\ y \end{pmatrix} = \begin{pmatrix} \sum_i u_i (u_i x_i + v_i y_i) \\ \sum_i v_i (u_i x_i + v_i y_i) \end{pmatrix}. \tag{21}$$

We can estimate the center of school of fish quickly with this method because each term in (21) is calculated at a small cost.

After the estimation of the center (x, y) , we calculate the square sum of the residuals. It seems that this value is related with the degree of distortion of a school from torus shape. For example, if each of the

school flows aligns exactly with rotation direction, the value becomes zero. We call this value center estimation residuals (CER). The CER is employed as an index to estimate the degree of distortion in school's shape. Since the term $\mathbf{x}^T \mathbf{x}$ in (17) is a constant, i.e., $\sum_i (u_i x_i + v_i y_i)$, we can easily calculate this index according to (17). The details of how we use this index will be explained in Section 6.5.2.

6.4.2 Experimental Results

Here, we present experimental results. We first applied our method to 9 different simulation scenes and confirmed that it works in principle. To estimate RCs for real schools of fish, we recorded videos of schools of sardines at an aquarium. The process of recording the videos is explained in Section 6.4.2.3. To evaluate our method, RCs were estimated once by manually tracking sardines in the videos. The details of the manual tracking process are described in Section 6.4.2.4. We applied our method to the same videos. The results of our experiments are presented in Section 6.4.2.5. We also examine the accuracy of our method by comparing the obtained RCs with those obtained by manual tracking. Finally, we present the results of an experiment for a long video.

We prepared 9 simulation scenes and applied our method to confirm if it works in principle. Here, we describe how the scenes were created and present the results of the simulations, i.e., the accuracies of center estimations and RCs.

6.4.2.1 Simulation Scenes

To confirm that our method can estimate RCs under various conditions, we prepared 9 virtual scenes of rotating schools by changing RCs in three ways and the amount of obstacles (i.e., larger fishes) in three levels. In the simulations, the populations of schools, the sizes of fish, and the number of frames were determined so that the scenes have approximately the same values as the videos we obtained. Section 6.4.2.3 provides the details of the obtained videos. A school was represented by 4,000 black ellipses. Other fish were represented by larger black ellipses moving straight at 1 BL/s.

Table 5 details the parameters used in the simulations. RCs are given as lines with different parameters for inclinations and intercepts. The speed (BL/s) of fish in the n th bin of a school was controlled according to the given line equation. The simulation scenes are uniquely named, e.g., D-1. Scenes with the same symbol (i.e., D, E, and F) have equal RCs. The branch numbers 1, 2, and 3 indicate three different levels for the number of obstacles. No obstacles were added to level 1, whereas a small number of obstacles is added to level 2, and a larger number of obstacles is added to level 3. Figure 30 shows snapshots of simulation scenes D-1, D-2, and D-3.

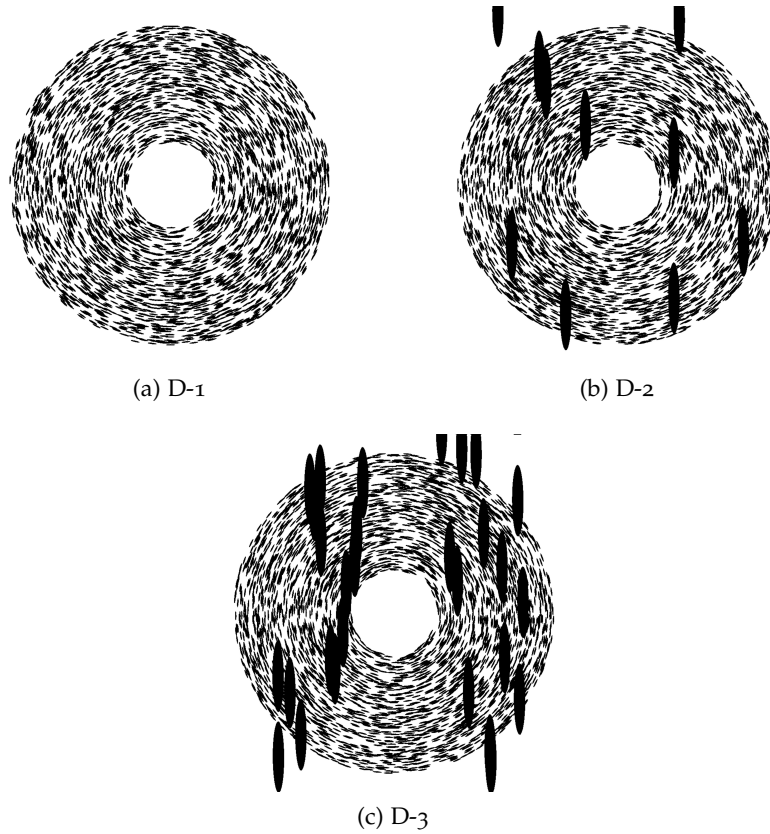


Figure 30: Snapshots of simulation scenes D-1, D-2 and D-3

6.4.2.2 Results of simulation scenes

Table 6 shows the results of center estimation in the first frame for each scene (Section 6.4.1.3). We repeated estimations by changing the locations of the initial point over the regions of the school for each scene. Note that the unit of length is always BL. The “error of center (%)” in Table 6 shows the error between the correct center points and estimated centers. The “ave. of conv. (1%)” and “max. of conv. (1%)” show the average and maximum number of iterations, respectively, when we obtained a point that nearly converged during estimation (within 0.01 BL from the estimated center point). The “ave. of conv.” and “max. of conv.” give the average and maximum number of iterations required for the process to converge, respectively. These results demonstrate good performance of the center estimation method. In these experiments, we require at most 10 iterations for estimation. This number of iterations was employed for the proposed RC estimation method (Section 6.4.1).

Figure 31 shows the estimated RCs obtained by our method. To quantify RC estimation errors, we also show the average relative errors (RE) and the root mean square of the relative errors (RMSRE) of our method in Table 7 with respect to the RCs given in Table 5. As

can be seen, both the average RE and average RMSREs are less than 2% of the BL. The “ave. of center errors” is the average error of the estimated center points in all frames for each scene. These results indicate that the proposed center estimation algorithm can locate the center points of schools of fish stably.

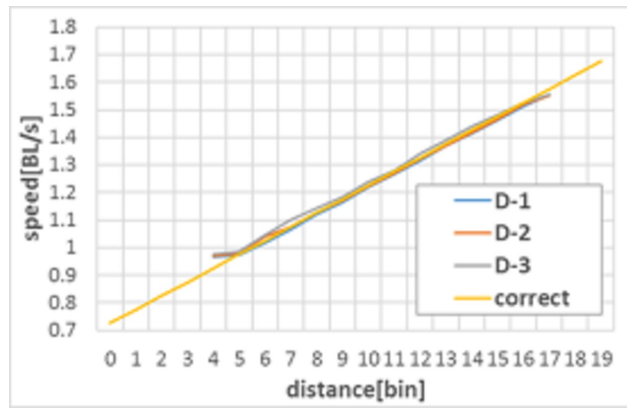
According to Figure 31, Table 6, and Table 7, accuracy tends to decrease as the number of obstacles increases. However, our method shows practical performance for various types of RCs even in the presence of obstacles.

Table 5: simulation scenes

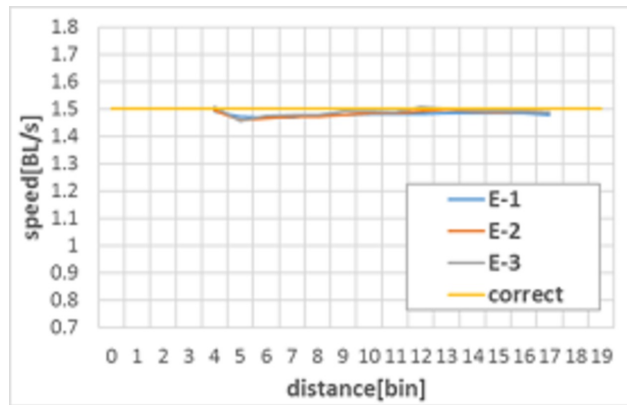
scene	inclination and intercept of RC	obstacles
D-1	$0.05n + 0.9$	none
D-2	$0.05n + 0.9$	few
D-3	$0.05n + 0.9$	many
E-1	1.5	none
E-2	1.5	few
E-3	1.5	many
F-1	$-0.04n + 1.8$	none
F-2	$-0.04n + 1.8$	few
F-3	$-0.04n + 1.8$	many

Table 6: Center estimation results

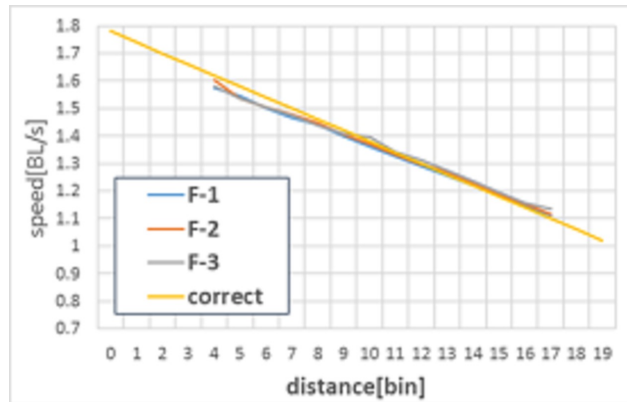
scene	center estimations				
	error of center(%)	ave. of conv.(1%)	max. of conv.(1%)	ave. of conv.	max. of conv.
D-1	1.41	2.71	3	5.92	8
D-2	0.66	3.00	4	5.61	7
D-3	2.27	3.04	4	6.08	9
E-1	0.63	2.62	3	5.92	8
E-2	1.18	2.98	4	5.47	7
E-3	2.77	3.05	4	5.46	8
F-1	0.49	2.68	3	5.12	6
F-2	1.59	3.01	4	5.37	8
F-3	4.97	3.05	4	6.33	8



(a) D-1,2,3



(b) E-1,2,3



(c) F-1,2,3

Figure 31: RCs Estimated by our method for simulation scenes

6.4.2.3 Schools of fish in an Aquarium

The videos of schools of fish were recorded in the largest tank at the Kujukushima Umikirara Aquarium, Nagasaki, Japan between March 2012 and March 2014, as explained in Chapter 3.

We submerged a commercially available HERO2 video camera to the bottom of the tank.

We extracted three scenes (30 frames each) wherein sardines were rotating in a relatively stable and solid torus formation. The population of each school was approximately equal (i.e., 3,000 individuals). Figures 32(a), (c), and (e) show snapshots of the scenes A, B, and C, respectively.

As stated previously, the unit of distance is measured in BL, which can vary for each school. To estimate BL for a given school, we randomly targeted 30 sardines from an image of the school and employed the average apparent BL. The left side of Table 8 shows basic data for each scene.

6.4.2.4 RC Estimation by Manual Tracking

To evaluate our method, we measured RCs for scenes A, B, and C by manually tracking sardines.

For each scene, we first estimated the center of the rotating school using the method explained in Section 6.4.1.3. We randomly selected approximately 170 sardines in each scene, recorded trajectories of their heads, and calculated the speed of each sardine. Note that not all sardines could be tracked in the scene because of occlusions caused by other sardines in the school and other fish in the tank.

Table 7: RC estimation results

scene	errors of RCs		
	ave. of RE(%)	RMSRE (%)	ave. of center errors(%)
D-1	0.99	1.42	0.82
D-2	0.82	1.44	0.73
D-3	1.39	1.90	2.47
E-1	1.37	1.44	0.43
E-2	1.17	1.40	1.92
E-3	0.94	1.19	2.20
F-1	1.32	1.55	0.34
F-2	1.09	1.29	2.48
F-3	1.61	1.79	3.86

Table 8: Basic data of schools of sardines and RC estimation results

scene	date	mean of BL(pixel)	ave. of RC(%)	RMSRE (%)
A	March, 26 2013	31.0	3.50	4.80
B	March, 27 2013	31.1	3.07	5.34
C	March, 21 2014	32.7	3.44	4.81

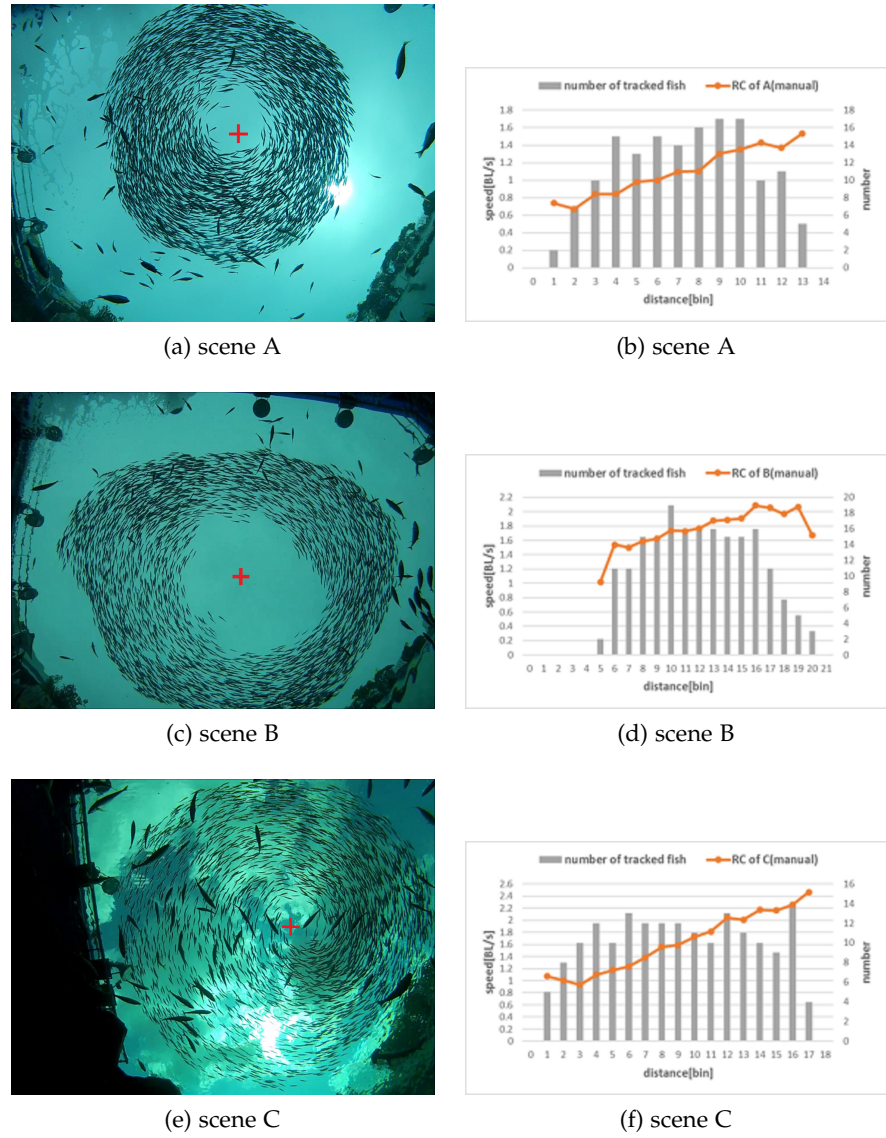


Figure 32: Snapshots of scenes and the estimated manually-tracked RCs: (a), (c), and (e) are snapshots of scenes A, B, and C, respectively. Red crosses are the centers estimated by our method. (b), (d), and (f) show the estimated RCs and number of tracked fish in each bin for scenes A, B, and C, respectively.

Figure 33(a) shows the trajectories recorded for scene A. Figure 33(b) shows the plotted speeds, where the x-axis is the bin number and the y-axis is speed [BL/s]. Figures 32(b), (d), and (b) show the RCs obtained by computing the mean speed for each bin from the tracked trajectories.

6.4.2.5 RC Estimation by Our Method

RCs were estimated using our method for the three scenes. The red crosses in Figures 32(a), (c), and (e) indicate the estimated centers. As can be seen, the centers are located correctly. Figure 34 shows the

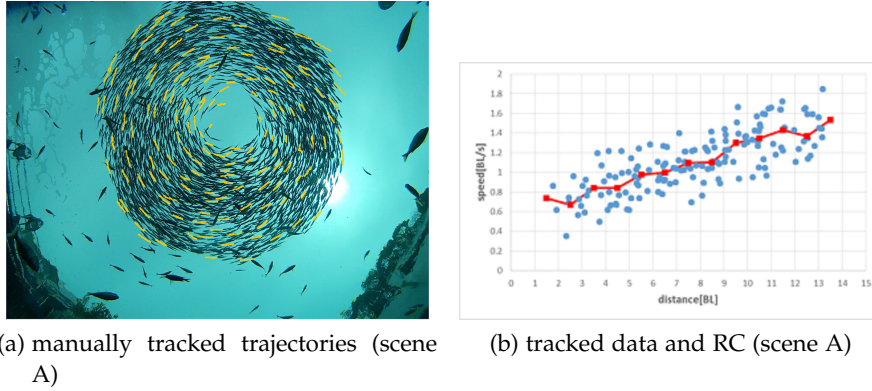


Figure 33: (a) Yellow lines are the 152 trajectories of the manually-tracked sardines in scene A. (b) Blue points represent tracked data for each sardine from (a), and the red line shows the average speed of each bin, i.e., rotation curve.

estimated RCs. We compared the results with the RCs obtained by manual tracking. The right side of Table 8 shows the average relative errors and the RMSRE with respect to the manually-tracked RCs. The average RE values are less than 4%, and those of RMSRE are approximately 5% for all scenes.

From Figure 34 and Table 8, it can be observed that the RCs obtained by our method and those obtained by manual tracking are sufficiently close, which indicates that our method works well for real scenes. The differences between RCs obtained manually and those estimated by our method can be explained as follows. Occlusions, waves on the water surface, and movements of tail fins can generate noise, which affect our estimations. The accuracy of RCs obtained by manual tracking is likely to be limited because we computed these values by sampling only approximately 5% of the fish in a school and tracking fish manually was not always possible. Accordingly, it is possible that the RC estimated by our method is closer to the correct RC.

In addition, the number of fish in the innermost and outermost bins was fewer than in-between bins, which may distort the estimated RCs obtained by both manual tracking and our method.

6.5 APPLICATIONS OF ROTATION CURVE ESTIMATION METHOD

In this section, we show two applications of our method. We first applied our method for a long time scene of a school of sardines. During the scene, we occasionally found frames not suitable for estimating RCs. For example, if the shape of the school is heavily distorted or not all of the school is observed, RCs estimated from such frames would be unreliable. In order to continuously measure RCs stably over a long period, it is important to automatically detect ill-conditioned frames and exclude such ones from computation. For

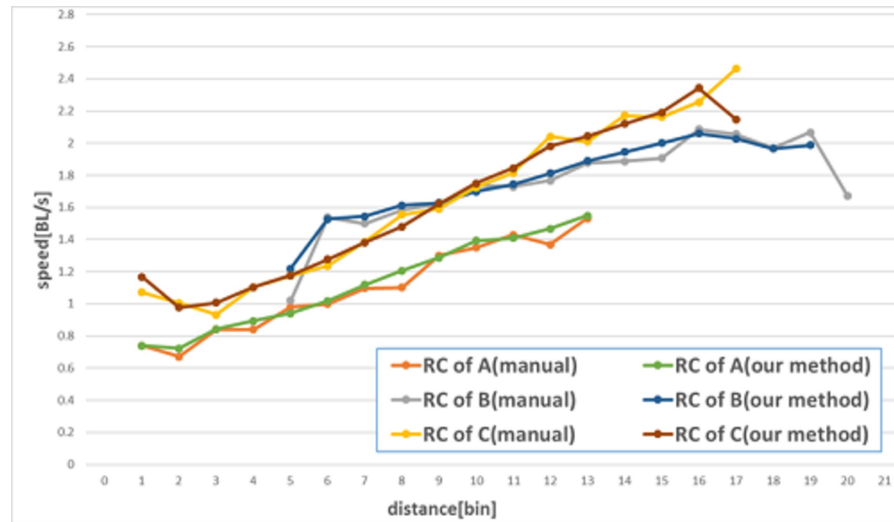


Figure 34: RCs estimated by our method and manually-tracked RCs. The 20th bin's value of B by our method was not computed because the ratio of the school flows was less than α .

this purpose two features of school flows have been introduced, with which we could successfully detect the center of the school and compute RCs through the long time scene. We next applied our method to a school of another kind of fish, anchovies, and confirmed that our method was well applicable to that school as for the case of sardines.

6.5.1 RC Estimation with a 20 minute Scene

Measuring the long time evolution of speed or velocity distribution of fish school, such as RC, is useful for analysis of school behavior and for analysis of the condition of them in fish farm. We recorded the rotational motion of a school of sardines for 20 minutes on 26th March 2013 at the Kujukushima Umikirara Aquarium. Our method was then applied to the whole scene and we could successfully detect the center of the school and compute RC time series through the long time scene. The results are shown in Section 6.5.1.1.

As shown in Figure 35, we cannot always expect to observe a school rotating in torus form stably. We occasionally find that the shape of the school is heavily distorted, for example, because the school is attacked by large fish (predators). It also happens that silhouettes of large fish crossing over near the camera and a part or all of the school is covered as a result. The school itself moves around and (a part of) it may go out of frame. It is impractical to check for those kinds of events through a long time movie by human eyes, and it is desirable to detect events automatically. By detecting such an event, for example, we can find that the estimated RC for a frame is unreliable.

Concerning this issue, we devise two features of school flows for estimating the state of a school as the degree of distortion of its form



(a) A banded houndshark is covering a part of the school

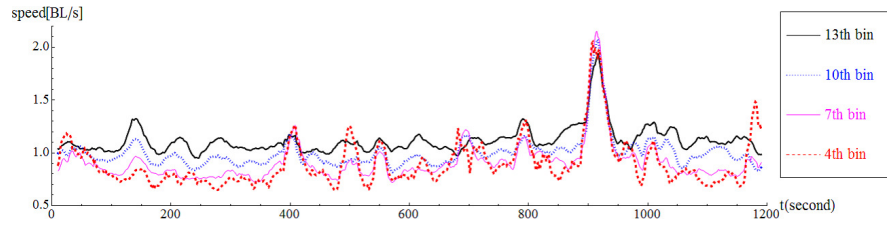


(b) The form of the school is distorted

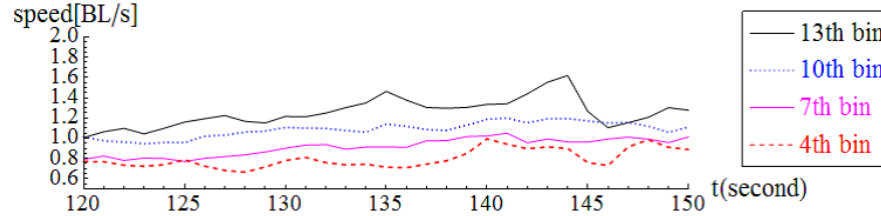


(c) A hammerhead shark is attacking the school

Figure 35: (a), (b) and (c) are snapshots of the long term scene at 153s, 24s and 898s respectively.



(a) 20s averaged speed series at 4th, 7th, 10th and 13th bins



(b) Speed series at 4th, 7th, 10th and 13th bins from 120s to 150s

Figure 36: RC time series of sardines

from torus shape. Several results we obtained from the 20 minute scene are described in Section 6.5.2.

6.5.1.1 RC Time Series of Sardines

As stated above, we computed RC time series for the 20 minute scene. Several results are shown in Figure 36. In Figure 36(a), the time series of 20-second averaged speed at 4th, 7th, 10th and 13th bins are shown respectively. It is almost impossible for us to obtain RCs from such a long scene by tracking manually enough many fish, whereas our method could automatically track the center of the school and compute RCs all through the frames without interruption.

To see the detail of RC time series, we show a part of the series in the period from 120 to 150 seconds in Figure 36(b). The shape of the school was relatively stable but the RCs were gradually changed during this period. The RC time series data reveal that fish at outer region of the school always swim faster than the ones near the rotation center even when the rotating speed of the whole school vary. Such behavioral feature of schools of sardines has never been reported, but is interesting for considering the efficiency of collective swimming and mathematical modeling of collective motion. Although these data have just been computed, our data seem informative and actually we could detect noticeable events from the data by our school flow features as we will show in Section 6.5.2.

6.5.2 Event Detection by School Flow Features

For characterizing collective motions, statistical features such as the group polarization and angular momentum have been invented [29,

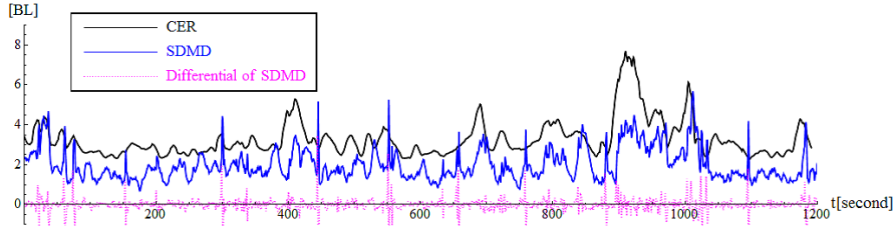


Figure 37: 10s averaged time series of CER and 1s averaged time series of SDMD and differential of SDMD.

111]. However, including these ones, there are no statistical features suitable for measuring distortion of torus shape of the school as far as we know. Therefore, we constructed two features for estimating the shapes and states of schools. The first one is the center estimation residuals (CER) defined in Section 6.4.1.3. This feature represents a degree of distortion of the school form from torus shape. The other is also for evaluating distortion degree of the school form as a statistical quantity. The latter can also be employed for detecting events in which a part of the school is not observable. The details are explained below.

We assume that the positions of the school flows represent the positions of fish. We first divide the disk area whose center coincides the rotation center into 24 equal circular sectors. We then calculate the mean distance from the center to each flow position in each circular sector. The standard deviation of the mean distances of all the circular sectors is called SDMD and is employed as a school flow feature.

The SDMD becomes small when the school form is near torus shape, while it becomes large when the form is distorted, because the mean distances are varied from a circular sector to another for such a case. The SDMD thus represents a distortion degree from torus shape.

In Figure 37, we present the time series of CER values of our 20 minute movie. By comparing the movie and the CER time series, we could find that the shape of school was distorted while CER values were high. In the period from 900 to 1020 seconds, the CER values were high because sardines were stimulated by predators and swam in disorder. From our observations, when the value of CER exceeded 4 BL, the shape of school was heavily distorted. This can be confirmed for the CER values of six snapshots shown in Table 9. We can see that the CER values for Figure 35(b) and (c) were 4.07 and 7.13.

The time series of SDMD and the differential of SDMD are also shown in Figure 37. We picked up prominent spikes in the time series of SDMD and found that they were corresponded to events when the school was covered by large fish. The details are as follows. We first looked through the movie for events in which the silhouettes of large fish such as banded hound sharks, eagle rays covered the school. The number of such events was 32 in total. On the other hand, we detected spikes of SDMD by taking the points for which differentials of SDMD

were over 0.5 BL. We then compared the time when events happened with the detected spikes, and obtained the precision and recall were 0.84 and 0.81 respectively. This result demonstrates that the SDMD feature is useful.

Although our analysis of time series of RC and other features of schools is just the first step toward the empirical investigation of collective fish behavior, but the results we obtained indicate that our method is useful for analyzing the behavior and state of schooling fish for a long term.

6.5.3 RC Estimation of School of Anchovies

In order to evaluate applicability of our method, we measured the RC time evolution of rotating school of different kind of fish, anchovies in the same aquarium. Figure 38 shows the school of anchovies. Anchovies are smaller than sardines. The mean apparent BL of anchovies in the scene was 18.8 pixels.

We calculated RCs of the school by our method and estimated RCs by tracking 172 anchovies manually. All the parameters of our method were kept the same as for the case of sardines (Table 4).

Figure 39(a) shows the trajectories of anchovies we tracked. Both the estimated RCs by our method and the one by manual tracking are shown in Figure 39(b). The RE and the RMSRE of RC estimation errors were 4.99% and 6.32% respectively. The results demonstrate that our method is applicable to the school of anchovies.

We also computed the RC time evolution of the school of anchovies (Figure 40(a)). From the observation of RC time series of anchovies, we find that the fish in outer region of the rotating school swim faster than the ones near the center like sardines. These results suggest that such behavioral feature is universal for rotational collective motion irrespective of kinds of fish.

We show the time series of the CER, the SDMD and the differential of SDMD in Figure 40(a). Figure 41 shows the events of banded

Table 9: The CER and SDMD values of the first frame of the scene A, B and C and the snapshots

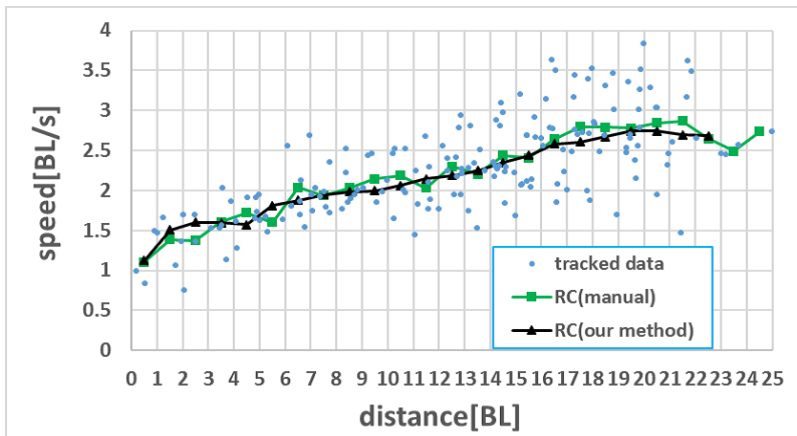
frame	CER(BL)	SDMD(BL)
the first frame of scene A	2.07	2.29
the first frame of scene B	2.84	3.12
the first frame of scene C	2.35	2.57
Figure 35 (a)	2.77	2.74
Figure 35 (b)	4.07	3.06
Figure 35 (c)	7.13	2.61



Figure 38: Rotating school of anchovies from the bottom of the tank



(a)



(b)

Figure 39: (a) White lines are the 172 trajectories of manually-tracked anchovies in Figure 38. (b) Estimated RCs by manual tracking and our method.

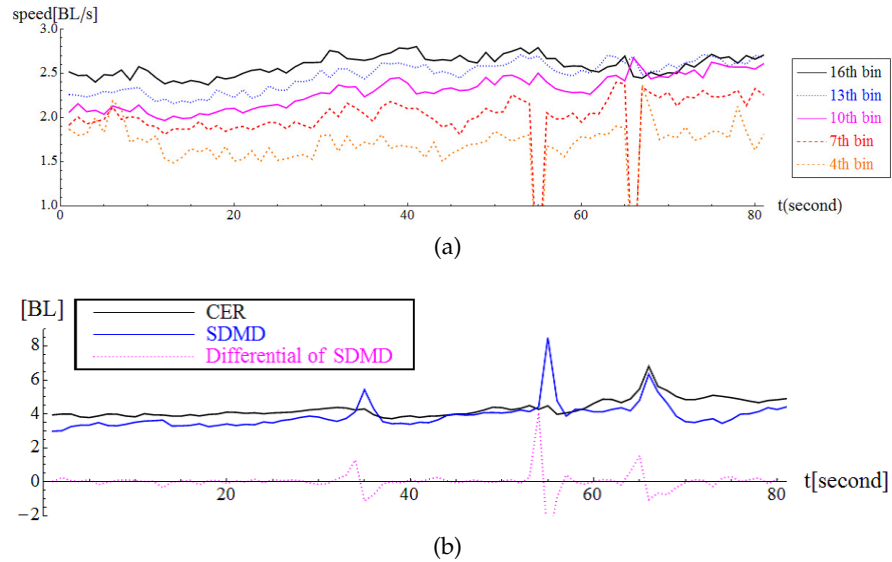


Figure 40: (a) RC time evolution of the anchovies and (b) CER, SDMD and differential of SDMD time series of the anchovies

houndsharks covered the school. For those events, we confirmed that there were spikes of time series of SDMD that corresponded to the events. These results demonstrate that the CER and SDMD features are useful for detecting events.

In order to apply our method to other kinds of fishes and animals, we may need, for each case, to optimize the parameters and modify the conditions for detecting flows relevant to target motions. However, as shown for the case of anchovies, it is expected that our basic framework works well for various cases. Measuring speed distributions of many kinds of animals with our method would enable us to analyze the differences of collective behaviors over a long time period, which would be valuable for animal behavior research.

6.6 CAKE-CUT DISTRIBUTION

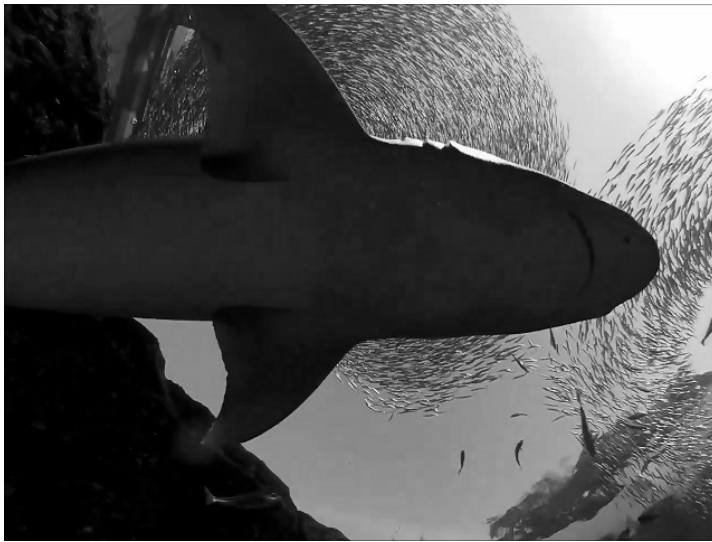
In order to detect information transfer along to circumferential direction, we propose another division of space, and speed and angle distribution estimation on the division.

6.6.1 Speed and Angle distribution on Cake-Cut Regions

We first divide the disk area into 24 equal circular sectors. We call each region of the circular sectors a cake-cut (cut) and assign numbers counterclockwise as shown in Figure 42. The center position of the disk is calculated by our center estimation method from flows. We also estimate the velocity distribution on the cake-cuts on the basis of our basic idea. In addition to the averaged speed of the cake-cuts,



(a)



(b)



(c)

Figure 41: Snapshots of the school of anchovies. (a), (b) and (c) are snapshots of the scene at 34s, 54s and 65s respectively.

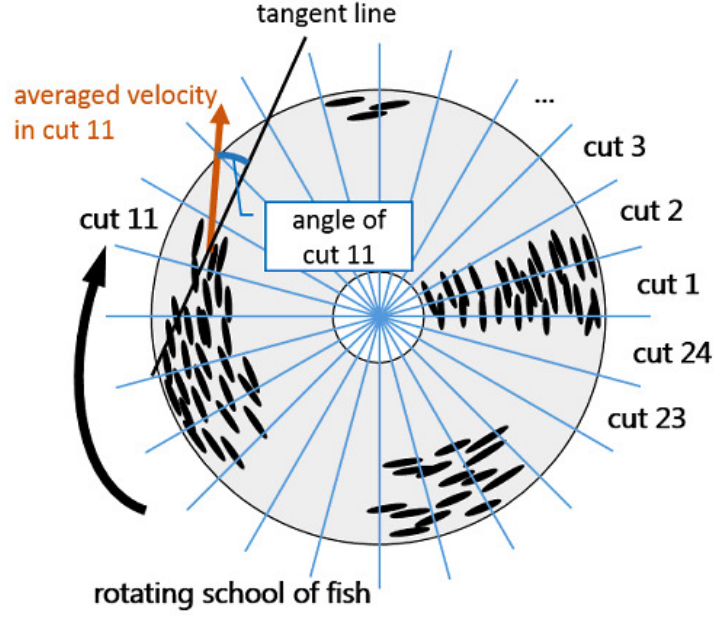


Figure 42: An overview of the velocity distribution on the cake-cuts.

directions of the averaged velocities seems to be important. For each cake-cut, the angle of the averaged velocity is defined as follows. We consider a center axis which goes outward through the middle of the cake-cut from the center of the torus. Then a tangential axis are set to be perpendicular to the center axis and put toward the direction of rotation of the torus. We define an angle of the averaged velocity of each cake-cut to be that between the averaged velocity and the tangential axis. This means that if the torus have complete circular motion, the angles of the averaged velocities of all cake-cuts vanish. Ranges of the angles are set to be $[-\pi, \pi]$, and they are positive (negative), when the direction of the velocity are outward from the center (inward toward the center). Furthermore the angles are divided by π to define the normalized angles having a range $[-1, 1]$. We show an example of the angle of cut 11 in Figure 42.

We have conducted experiments to show the accuracy of the velocity (speed and direction) distribution on the cake-cuts with optical flow. We prepared the same three scenes (30 frames each) A, B, and C in Figure 32. Figure 43(a), (c), and (e) show the same snapshots of the

Table 10: The estimation result of angles and speeds.

scene	RE of speed	RMSRE of speed	ave. of angle errors (degree)	RMSE of angle (degree)
A	0.079	0.102	1.670	2.043
B	0.063	0.075	1.909	2.155
C	0.087	0.112	1.412	1.807

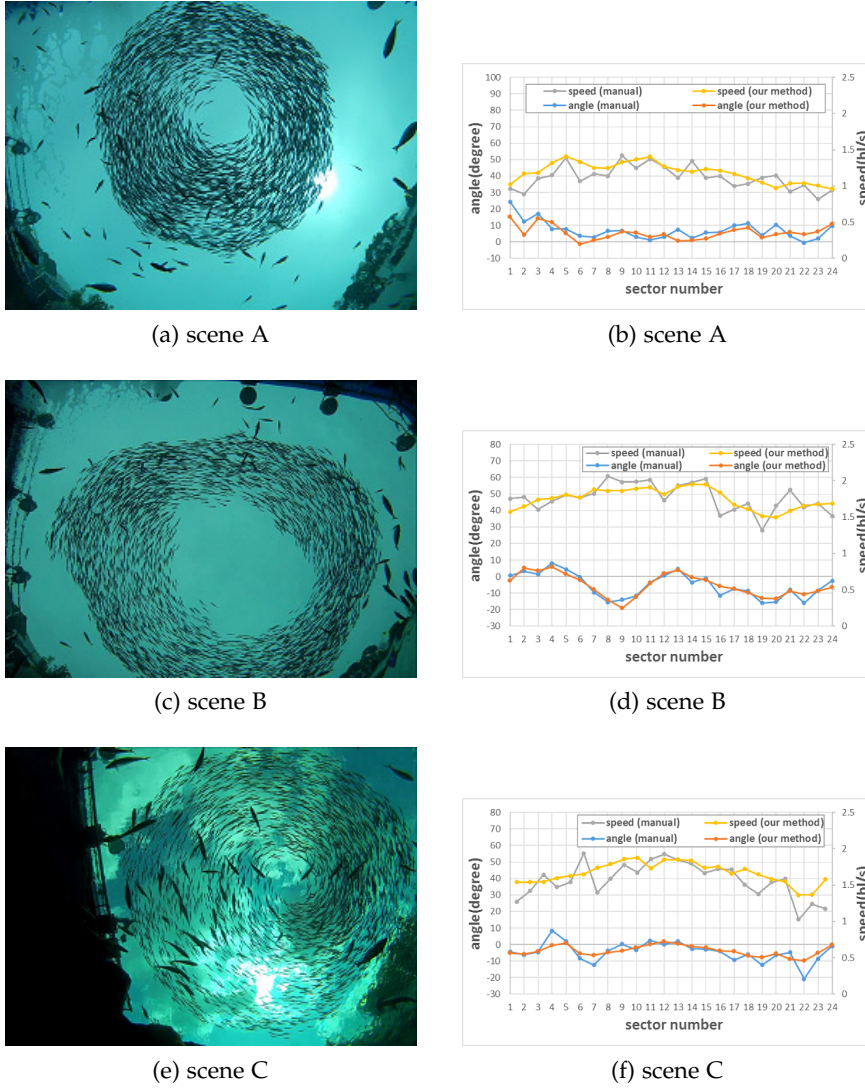


Figure 43: Snapshots of scenes and the result of the speed and velocity distributions by hand and by our method: (a), (c), and (e) are snapshots of scenes A, B, and C, respectively. (b), (d), and (f) show the estimated speed and angle in each cut for scenes A, B, and C, respectively.

scenes. To evaluate our method, we measured the mean speeds and directions of the cake-cuts by manually tracking. We randomly selected approximately 200 sardines in each scene, tracked their heads manually, and calculated the averaged speeds and directions of the cake-cuts. The manually estimated speeds and directions are shown in Figure 43(b), (d), and (f).

We have estimated the speeds and directions using our method for the three scenes. The parameters and flow conditions are the same as ones of our work in [IC3]. We show the results by our method in Figure 43(b), (d), and (f). Table 10 shows the averaged RE of speeds, the RMSRE of speeds, the average errors of angles, and the root mean-

square error (RMSE) of angles with respect to the manually tracked speeds and angles. The average REs of speeds are less than 0.1 (BL/s), and the average values of angle errors are less than 2 (degree) for all scenes.

From Figure 43 and Table 10, the speed and angle measurement method on the cake-cuts seems to be practically useful. The accuracy of the speeds and angles obtained by manual tracking is likely to be limited because we computed these values by sampling only less than 10% of the fish in a school and tracking fish manually was not always possible.

6.7 CONCLUSION

We have proposed a speed distribution measurement method for collective motions of RD type schools of fish with optical flow. We applied our method to rotating schools of sardines and measured their RCs and velocity distributions on the cake-cut. To compute these distributions automatically, we also proposed a center estimation method from the school flows. Experimental results show that our method is accurate for simulation scenes of rotating schools and that it works well for real scenes. Our method facilitates automatic estimation of RCs over a longer period of time with practical accuracy, even when individual tracking is difficult. This measurement method will be useful for observation of schools of fish and determination of proper mathematical models and their parameters.

VELOCITY STRUCTURES OF ROTATING FISH SCHOOLS AND THEIR EVOLUTIONS

In this chapter, we investigate the velocity structure of a school of sardines rotating in solid torus shape. We also study time development of rotation curves with the method proposed in Chapter 6. We found speed structure in a rotating school with analysis of a long (about 2 hours) time series data. Collective motion of the fish changes non-stationarity and continuously in several seconds. However, if we average the rotation curves by a dynamical time required for each circling movement in torus, universal structure of rotation curve appears.

Most of the results presented in this chapter have been published in [IC2, DC2]. The research of this chapter have been done with Prof. Masa-aki Sakagami. The author of this thesis designed the research, developed methods, calculated and analyzed the time series data, and wrote these papers.

7.1 INTRODUCTION

Collective Behaviors of animal groups such as flocks of birds and fish schools have been intensively investigated biologically, physically and mathematically. However, for dense and large schools of fish as shown in Figure 44 their behavior have not sufficiently been studied as stated in Chapter 2. In this chapter, we analyze velocity structure (rotation curve) of a large and dense rotating school of sardines (Figure 44) as a first step to study behaviors of dense and large schools of fish.

We have estimated three RCs of schools of sardines (Figure 34) with the proposed method and manually in Section 6.4.2.5. However, we need to measure RCs for long term to characterize and discuss the velocity structure of the rotating school. And we also need to measure distribution of body length in the school, because it is well known that the swimming speed is directly proportional to the body length at the same tail beat frequency [8] and distribution of body length may just cause the velocity structure of the school. Therefore, in Section 7.2, we first measure positions, body lengths and speeds for the relatively sparse rotating school with the methods proposed in Chapter 4. In Section 7.3, we also measure the time series of the RC for a long video (about 2 hours) which was recorded in March 2015. Figure 44 shows a snapshot of the video. We propose an averaging procedure over 60 seconds to discuss the feature of time evolution of the RCs in Section 7.4. Finally, we summarize this chapter in Section 7.5.

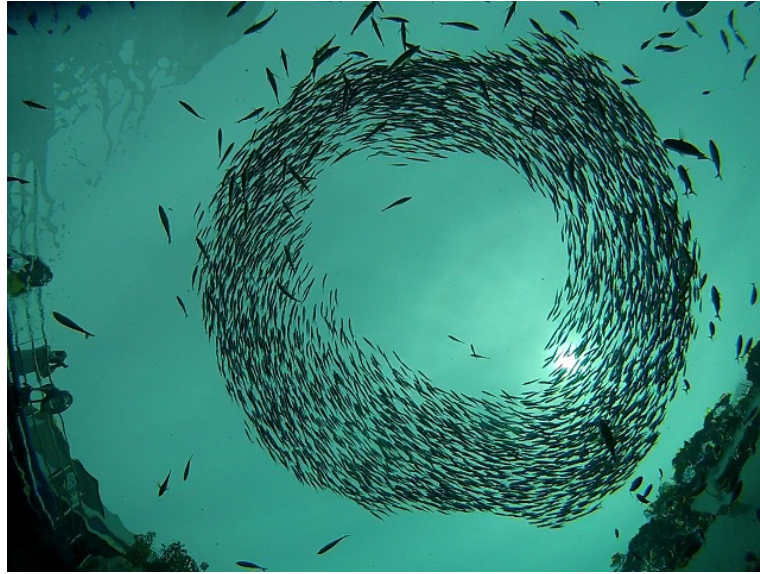


Figure 44: A large and dense school of sardines

7.2 DISTRIBUTIONS OF BODY LENGTH, SWIMMING SPEED AND TAIL BEAT FREQUENCY IN A ROTATING SCHOOL OF SARDINES

In this section, we measure distributions of body length and swimming speed in the RS type rotating school of sardines with the measurement methods proposed in Chapter 4.

We extracted a 10 seconds relatively RS type scene from the videos of a school of sardines which were recorded in March 2015, as explained in Chapter 3. We call the scene RSS. Figure 45(a) shows a snapshot of the RSS. Since the scene is RS type, we can measure the features of the school with the proposed method in Chapter 4.

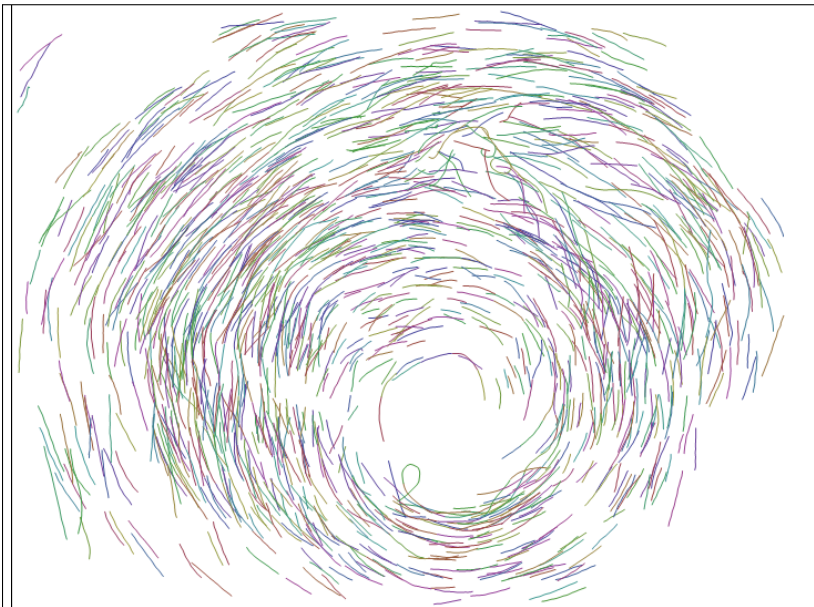
We first tracked isolated fish in the RSS using the tracking method proposed in Chapter 4. Figure 45(b) shows the trajectories of the isolated fish which are tracked over 30 frames (1 second) with the tracking method. We obtained 1507 trajectories from the RSS.¹

We measured the body lengths of the tracked 1507 fish with the body length estimation method in Chapter 4. Figure 46(a) shows the frequency distribution of body lengths in the RSS. The mean and S.D. of the body lengths were 57.52 [pixel] and 6.145 [pixel] relatively. We use the mean of the body lengths as the unit of body length (BL) in this section. Figure 46(b) shows the body length distribution against the radial distance from the rotation center. The rotation center was calculated with the center estimation method in Chapter 6. We also show the plotted speeds [BL/s] against the body length [pixel] in Figure 46(c). Figure 47(a) and 47(b) show the rotation curve of the RSS. The unit of the speed in Figure 47(a) is the BL and the unit of each fish in Figure 47(b) is each body length of the fish.

¹ Note that the same fish were counted twice or more in the RSS.



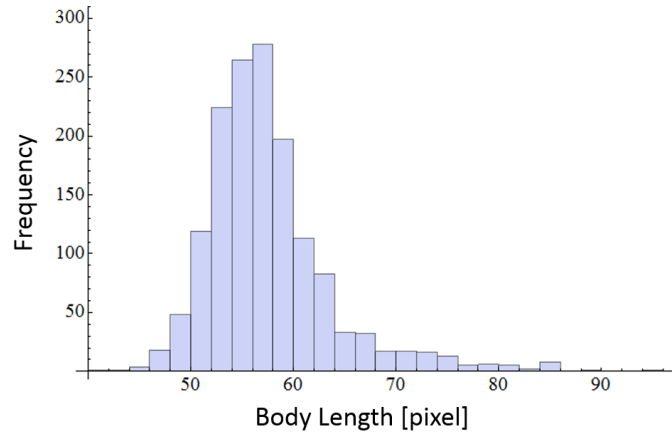
(a)



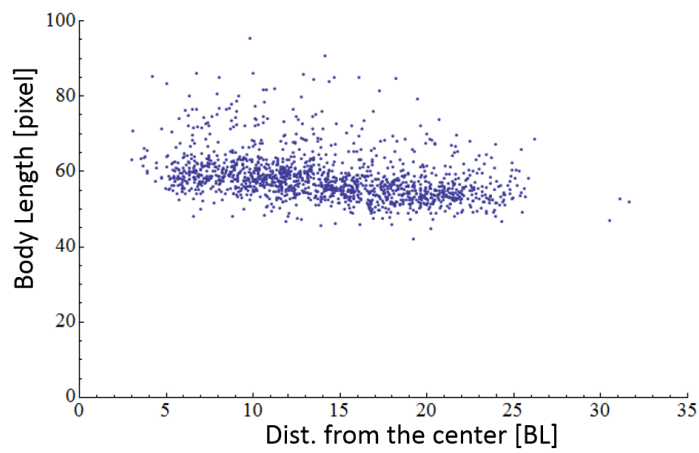
(b)

Figure 45: (a) A snapshot of the RSS. (b) The trajectories of the isolated fish in the RSS obtained by the tracking method in Section 4.3.2.

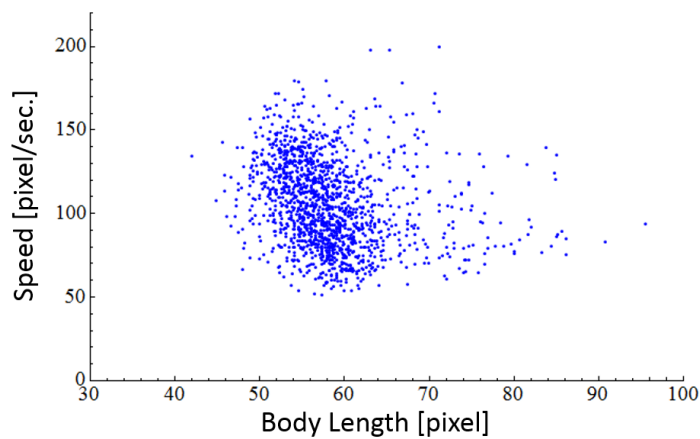
From Figure 46(b), it is suggested that the rotating school does not have clear structure of speed distribution. Figure 46(c) shows that larger fish don't swim faster than smaller ones, although it is known that the larger fish always swim faster as stated in Section 7.1. Figure 47(a) and 47(b) show that outer fish swim faster than inner ones. From these results, it was suggested that outer fish in a rotating school of sardines really swim faster than inner ones regardless their body lengths.



(a)

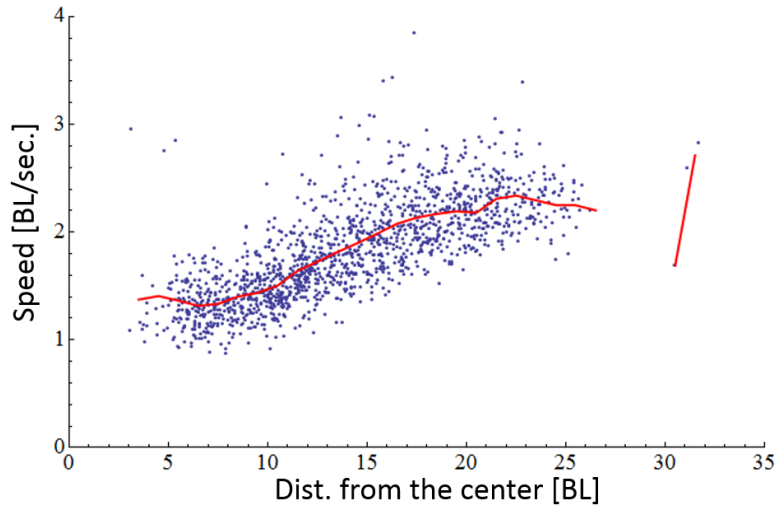


(b)

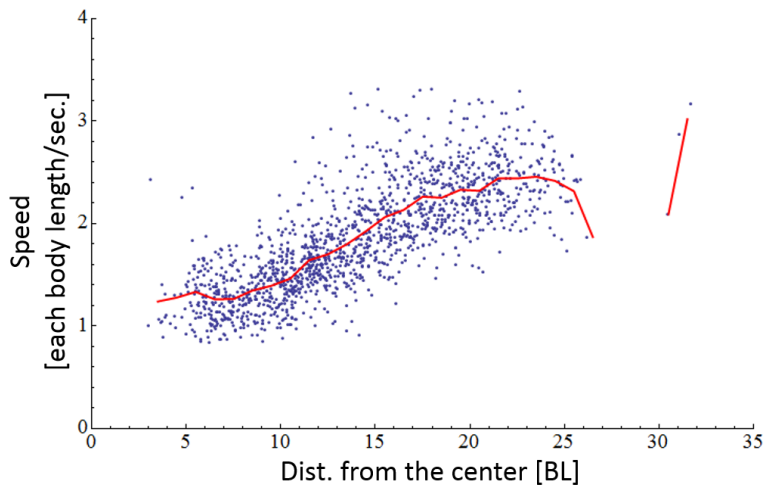


(c)

Figure 46: (a) The frequency distribution of body lengths of the RSS. (b) The body length distribution against the radial distance from the rotation center. (c) The plotted speeds [BL/s] against the body length [pixel].



(a)



(b)

Figure 47: (a) The plotted speeds [BL/s] against the radial distance [BL] from the center. The red line shows the averaged speed of each bin. (b) The plotted speeds [each body length/s] against the radial distance [BL] from the center. The red line is the averaged speed of each bin.

7.3 ROTATION CURVES OF SARDINE'S SCHOOLS AND TIME EVOLUTION OF THEIR VELOCITY STRUCTURE

We estimated three RCs of schools of sardines (Figure 32) with the proposed method and manually in Section 6.4.2.5. The forms of the estimated RCs in Figure 34 are briefly summarized that the mean speed almost linearly grows with respect to the radius. Although the RCs in Figure 34 for the three snapshots suggest that linearly growing form of RCs might be universal, we should remind that these snapshots in Figure 32 represent a regular state of the torus. The tori change their shape within a time scale of a few second and are sig-

nificantly distorted from their regular state as shown in Figure 11. In order to discuss the speed structure of the rotating school of sardines, we need to measure and analyze RCs of long time movies.

We calculated time series of RCs for a long video by means of our RC measurement method in Chapter 6.

In this section, we first show the time series of the averaged speed at the 9th bin. We then show the time development of the velocity structure of the rotating school. Finally we briefly discuss the speed structure of the rotating school and averaged tori.

7.3.1 *Time Development of Averaged Speed at the 9th Bin*

In Figure 48(a), we show the time series of the averaged velocity at the bin of radius $r = 9$ BL over two time scales. This bin ($r = 9$ BL) locates almost middle of torus so that its velocities seems to represent kinetic properties of the whole torus. The one second average velocity (green) shows quite rapid change within the time scale from a few to 10 seconds. Oscillations in this time scale represent the deviations from the regular state.

For much longer time scale (from 1 to 2 hours), fish schools exhibit larger fluctuation as shown in Figure 48(b). We recognize that prominent spikes of the one second average in Figure 48(b) correspond to significant deviations from the regular torus shape caused by severe predations. On the contrary, origins of small fluctuations in Figure 48(a) seem to be intrinsic dynamics of the fish schools and modest predations.

7.3.2 *Time Development of the Velocity Structure of the Rotating School*

We show the long term evolutions of the averaged velocities at several radii $r = 3, 6, 9, 12, 15$ BL in Figure 49(a) (60 s average) and Figure 49(b) (600 s average). Locations of inner and outer edges of the torus significantly varies in time, especially outermost radius exceeds 20 BL in some occasions. However the averaged velocities at radii $r = 3$ and 15 BL characterize kinematical nature of inner and outer parts of the torus. These figures clearly show that the time scale for changing the averaged velocity is rather long and its magnitude small in outer part of the torus. In rapidly changing regimes where averaged velocities have spikes, this insensitivity at $r = 15$ BL suggests the form of RC deviates from the linearly growing shape at the outer part of the torus. On the contrary, except the rapidly changing regimes, the averaged velocities at several radii are co-moving simultaneously so that RCs can keep the linearly growing shape as similar as RCs for the regular tori shown in Figure 44.

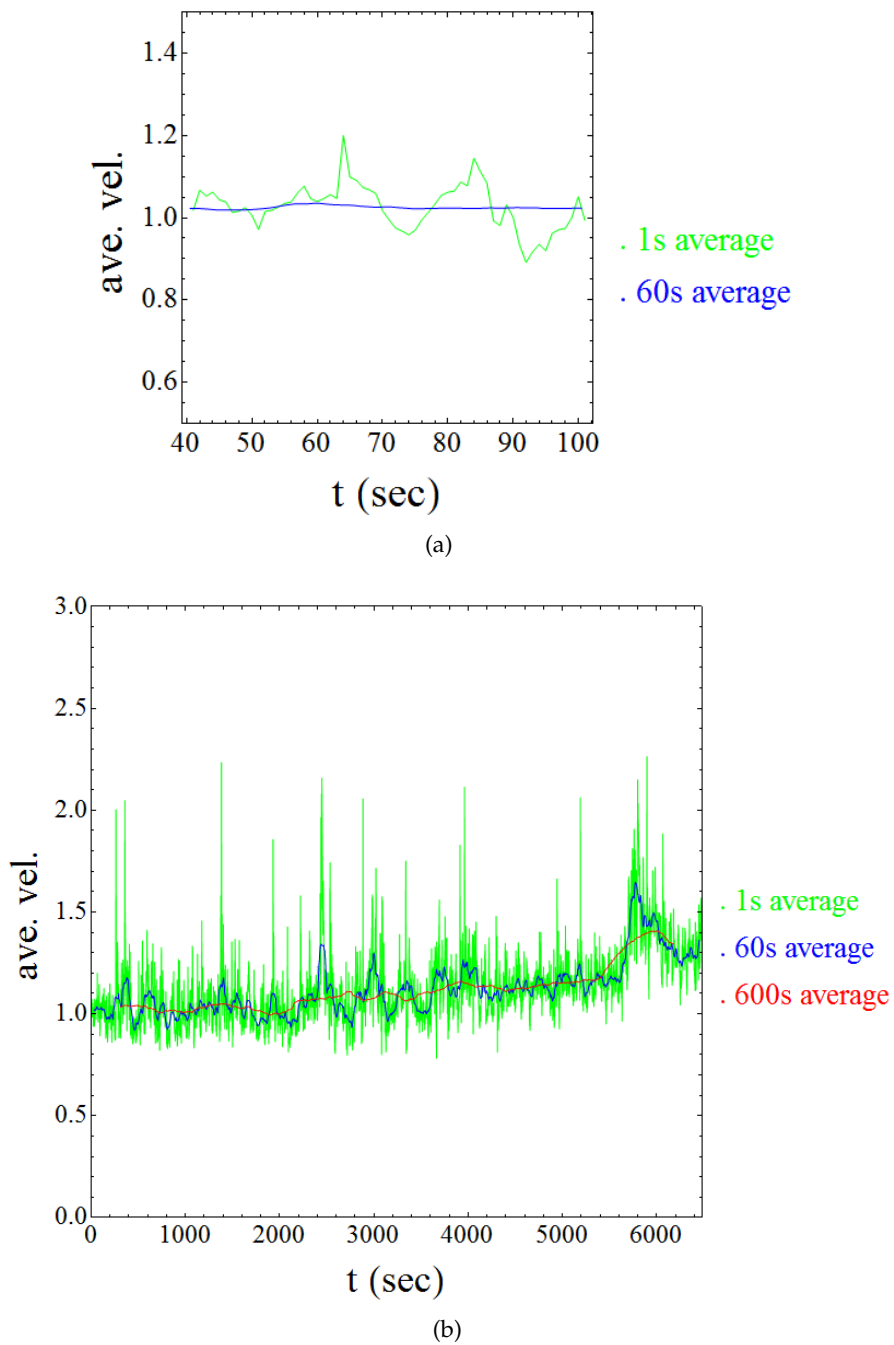


Figure 48: (a) A short term time series of the averaged speed at the 9th bin.
 (b) The time series of the averaged speed at the 9th bin for the long video.

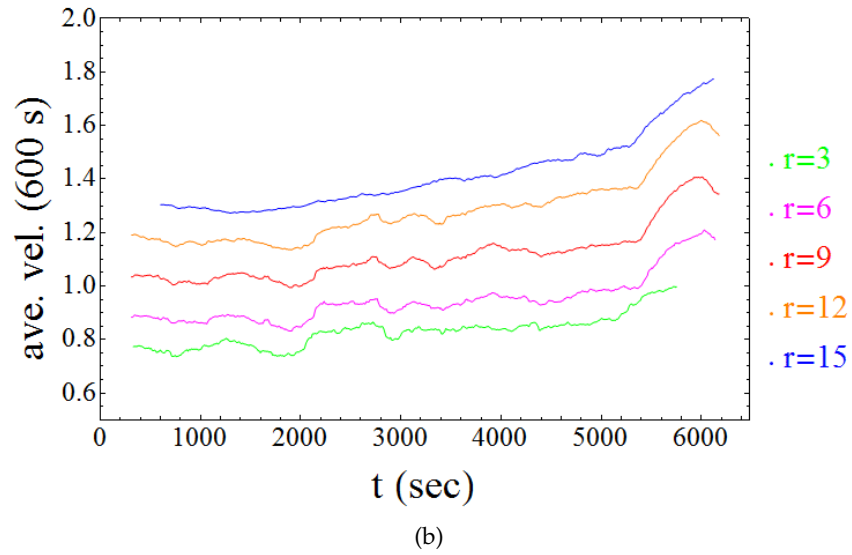
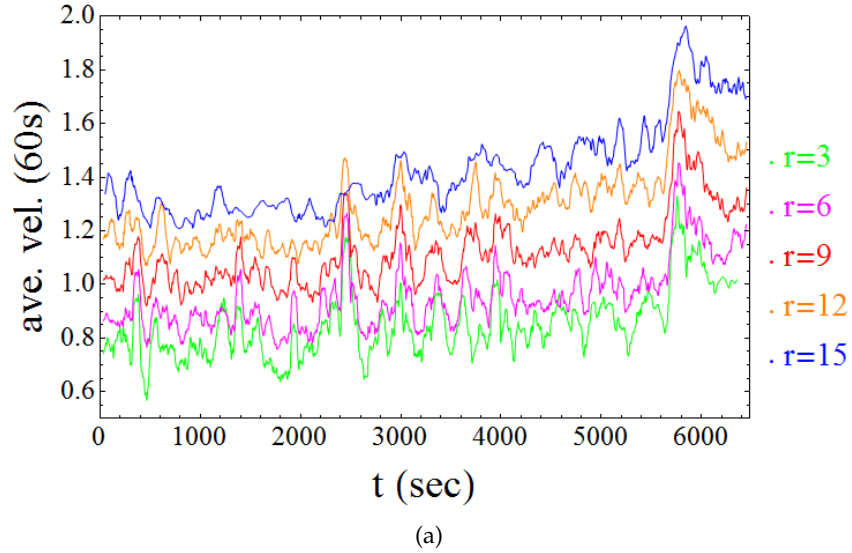


Figure 49: (a) Long term evolution of 60s averaged velocities at several radius. (b) Long term evolution of 600s averaged velocities at several radius.

7.4 EXISTENCE OF AVERAGED TORI OVER THE DYNAMICAL TIME

According to the discussion in Section 7.3, although the torus states of the fish schools are far from equilibrium and have large fluctuations, it is suggested that averaging procedure over 60 second works well for RC to recover its universal shape as similar as the regular tori. We note that choice of the time scale is not necessarily ad hoc, since this corresponds to the so called dynamical time [15] within which each fish has single rotation in the torus. Here we would like to present two arguments which support validity of averaging procedure over the dynamical time and the existence of the averaged torus.

Suppose that we evaluate the time development of the averaged velocity over the time τ . Figures 49(a) and 49(b) are typical examples for $\tau = 60$ s and $\tau = 600$ s. The values of the averaged velocities distribute around their mean values. In Figure 50(a), we show how the variances depend on the averaging time τ . It follows that the longer averaging time we take, the smaller the fluctuation of the averaged velocity. Furthermore the variances fall rapidly with the time scale τ 10 seconds for middle part of the torus $r = 3, 6, 9, 12, 15$ BL.

In Figure 50(b), we show log-log plot of the variance ($r = 9$ BL) with averaging time. And the red line is a fitting by a following power law,

$$\text{Variance} = a(\tau + b)^{-c} \quad (22)$$

with $a = 0.043$, $b = 3.6$ and $c = 0.22$, respectively. The rapid power law decay of the variance terminates and slower behavior appears in the dynamical time scale ~ 60 seconds.

Finally we evaluate a velocity correlation function,

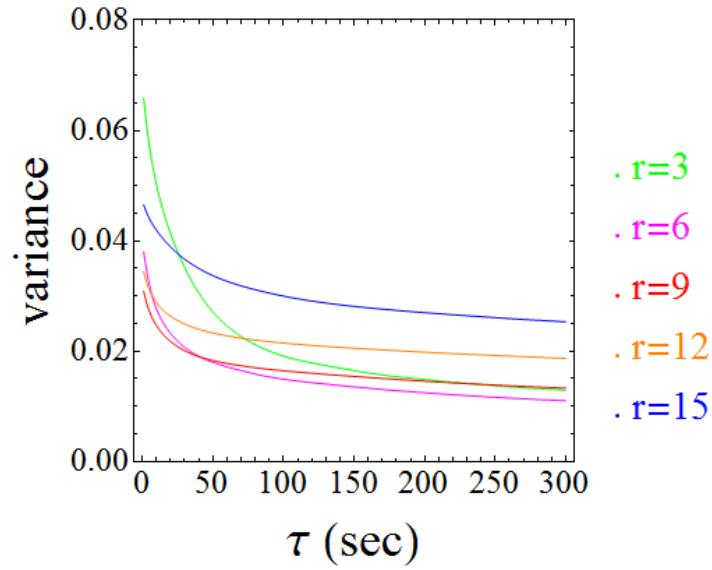
$$\text{Correlation}(\tau) = \frac{C(\tau)}{C(0)}, \quad C(\tau) = \frac{1}{T} \sum_{0 \leq t < T} (v(t + \tau) - \bar{v})(v(t) - \bar{v})$$

where \bar{v} is the averaged velocity over time T . Here $v(t)$ is velocity at $r = 9$ BL and averaging time $T = 600$ seconds. Figure 51 clearly shows a decay of the velocity correlation within the dynamical time scale. Although small oscillation remains, the behavior of the velocity correlation suggests that $v(t)$ became almost independent beyond the dynamical time scale. The decay of variance (Figure 50(a) and Figure 50(b)) and the velocity correlation (Figure 51) strongly support the validity of averaging procedure over the dynamical time and the existence of the averaged.

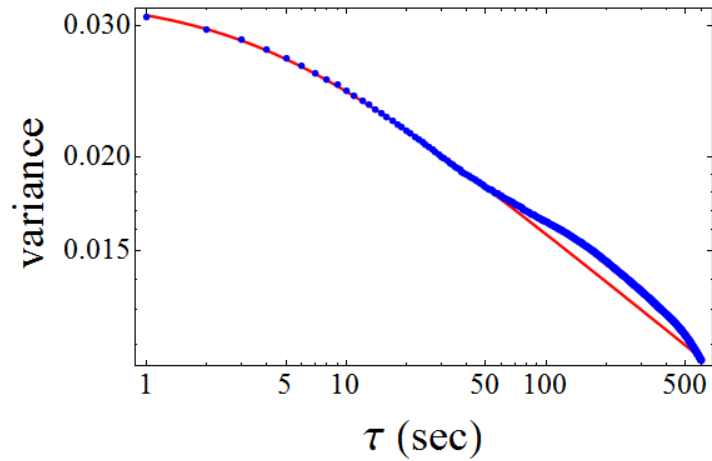
7.5 DISCUSSION AND CONCLUSION

We measured the distributions of body length and swimming speed in short term (10 second) video of the RS type rotating school of sardines. From the results, we found that outer fish in the rotating school swim faster than inner ones regardless their body lengths.

We have also investigated the long-term evolution and fluctuations of the RCs of the RD type rotating schools of sardines by means of our RC estimation method. From observations of the long-term evolution of estimated velocity structure, we note that tori of fish schools have the non-stationary nature which cause both of rapid (a few seconds) and slow (an hour) changes of their velocity profiles. In spite of existence of this difficulty, the averaging procedure over the dynamical time scale have been shown to work well in order to analyze kinematical nature of tori of fish schools. And it was suggested that RCs for the averaged tori keep their universal form, i.e. the linearly growing



(a)



(b)

Figure 50: (a) The variances of the averaged velocity distributions over time τ . (b) Log-Log plot of the variance of the averaged velocity distributions over time τ at $r = 9$ BL.

shape. Finally we also discussed the existence of averaged tori from viewpoints of the decay of velocity correlation and the convergence of the averaged velocity. The evolution and fluctuations of the RCs of rotating school of sardines can be examined in more detail, including investigations about the cause of growth of the mean rotational velocity with respect to the radius, and by constructing mathematical model that explains how the RCs of the schools behave.

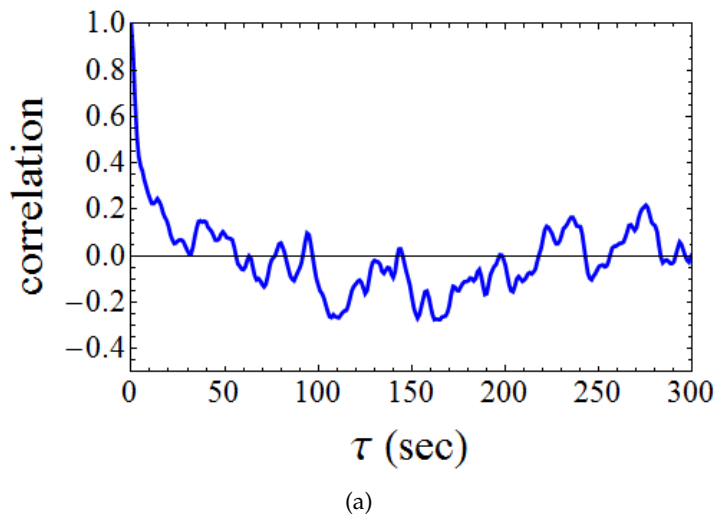


Figure 51: Velocity correlation function at $r = 9$ BL

CONCLUSION

8.1 SUMMARY

In this thesis, we first briefly reviewed research of collective behaviors in Chapter 2 and explained the data of schools of fish we used to measure and analyze their behaviors in Chapter 3. In Chapter 1, we set development of measurement methods for large and dense schools of fish as the primal goal in this thesis. For RS type schools, we established the tracking and measuring method for isolated fish in Chapter 4 and proposed the appearance-based tracking method for multiple fish in Chapter 5. For RD type schools, we developed the speed distribution measurement method with optical flow in Chapter 6. The second goal of this thesis was to find and analyze characteristic features of schools of fish. We analyzed the behaviors of a rotating school of sardines with the proposed measurement methods and then found the speed structure in the rotating schools and the averaged tori in Chapter 7. We summarize each chapter as follows.

In Chapter 2, we briefly reviewed research into collective behaviors, especially for behaviors of fish schools. Measurement methods for collective behaviors were also summarized. We pointed out that automatic measurement methods had not been sufficiently developed, particularly for schools of fish.

In Chapter 3, we explained the way videos of schools of fish were recorded in the Kujukushima Umikirara Aquarium. We also stated that the water tank and the school of sardines in the tank have a lot of advantages, mainly because the water tank is open air and has a large school of sardines throughout the year.

In Chapter 4, we established the tracking method for isolated fish and proposed the measurement method for tail beat frequency and the estimation method of coast phase for isolated fish in a school of fish. In our experiments, we recorded a large school of sardines and applied our method to a scene taken from the video. The average difference of the tail beat frequencies using our method and using manually estimated data was 0.126 (Hz). For estimation of the coast phase, the precision and recall of the classification result were 0.945 and 0.879. These results indicate that our method is practically useful. We expect that our method is useful for observation of individual behaviors in school of fish.

In Chapter 5, we proposed the appearance-based tracking method for multiple fish in a relatively sparse school. For the test scenes in which two or three fish overlap with each other, our tracking method

exhibited practical performance (80% for Type B and 100% for Type C), although the FP-LK method failed in all the scenes. The trajectories tracked by our method were also accurate, because the average differences between the trajectories of our method and the ground-truth in the three scene types were less than 4% of the BL of the school. However, our algorithm is still slow due to combinations of parameters. We need to accelerate our algorithm in order to track thousands of fish.

In Chapter 6, we proposed the speed distribution measurement method for collective motions of highly dense homogeneous groups with optical flow. The main idea was that we could measure a speed distribution by extracting flows that are relevant to fish behaviors with a number of proposed constraints. We applied our method to rotating schools of sardines and measured their RCs. To compute RCs automatically, we also proposed a center estimation method from the school flows. Experimental results show that our method is accurate for simulation scenes of rotating schools and that it works well for real scenes as well. Our method facilitates the automatic estimation of RCs over a longer period of time with practical accuracy, even when individual tracking is difficult. This measurement method will be useful for the observation of schools of fish and determination of proper mathematical models and their parameters.

In Chapter 7, with the method proposed in Chapter 6, we investigated the time development of the rotation curve for the solid torus shape of fish schools. We found the speed structure in rotating schools of fish through analysis of the long time development data. The existence of the averaged tori is also demonstrated in this chapter.

To summarize this thesis, the proposed methods enable us to analyze some aspects of fish schooling behavior such as body length distribution, speed distribution, and time development of speed distribution. As stated in Chapter 2, measurement methods for large and dense schools of fish have not sufficiently been developed. It should also be noted that manual measurement of the behaviors of thousands of fish for hours is hard or almost impossible. Therefore, our method opens up the possibility for a new research field into measurement and analysis for behaviors of large and dense fish schools. However, there remains problems for the analysis of the collective behavior of fish. For example, our algorithm described in Chapter 5 has not yet tracked all members of large schools of fish because the algorithm is still slow and not accurate for occlusions of multiple fish. Moreover, as a fundamental problem, we measured behaviors of fish in projected (2D) images, but in the future the 3D positions of fish should be measured in order to analyze in detail their behaviors and construct interaction models between neighbors.

8.2 FUTURE WORK

In future, this research can be extended in the following three directions.

IMPROVEMENTS OF MEASUREMENT METHODS

First of all, individual tracking is essentially important for measurement of the behaviors of fish schools. We plan to introduce a parametrised appearance model of fish, a probabilistic multi-object tracking framework, a data association framework, and a number of interaction models between fish to improve tracking performance. It is also worth accelerating our algorithm in order to track thousands of fish in schools.

For relatively dense schools of fish, tracking individuals is almost impossible, even using manual methods. Thus, methods that measure the velocity distributions of school behaviors approximately like the proposed method in Chapter 6 are important for automatic observations. However, there are some problems for further analysis of schooling behaviors with the proposed method. For example, we still cannot analyze information transfers such as agitations in fish schools, because the spatial and temporal resolution of our method are low. We plan to improve the accuracy of velocity distribution measurement at high spatial and temporal resolution. It is worth speeding up the proposed method with optical flow by calculating flows in parallel with GPUs for monitoring systems of school behaviors of fish in aquariums or fish farms.

In order to analyze fish behaviors in more detail, techniques for measuring the 3D positions of the individuals of a school is essential. We are attempting to develop such techniques in the aquarium with a stereo camera system and our tracking methods.

BEHAVIOR ANALYSIS WITH MEASUREMENT METHODS

The behavior of large and dense schools of fishes have not sufficiently been studied because measurement methods for such schools have not been developed as stated in Chapter 2. In Chapter 7, we applied the proposed measurement method of speed distribution to a rotating school of sardines for analysis of the speed structure of the school and the time evolution of the structure. This analysis is just the first step for investigating the collective behavior of large fish schools. The proposed methods enable us to study the details of schooling behaviors such as information transfers in schools, interaction manners with neighborhood members, and predator-avoidance behaviors.

APPLICATIONS OF MEASUREMENT METHODS

As stated in Chapter 2, a number of devices and techniques have been utilized to measure collective motions for many kinds of animals. We believe that the proposed measurement methods for collective motions, especially for schools of fish, have applications in a wide range of fields. In the field of biology, zebrafish (*Danio rerio*) are widely used to examine relationships between their genome and their behaviors, or to study the effects of medicines and drugs. Automatic measurement of zebrafish behavior and methods for tracking individuals are essential in the field. In the future, we plan to apply our methods to measure the behaviors of zebrafish. As another practical application, it is expected that our method could be utilized in fish farms to observe the health and growth of fish automatically, which may help improve productivity. We would also like to apply our speed distribution measurement method to collective motions other than those of rotating schools of fish, such as those of other species of animals and dense crowds of people.



LIST OF PUBLICATIONS

Journal article related to this thesis

- [J1] K. Terayama, H. Hioki and M. Sakagami, "A measurement method for speed distribution of collective motion with optical flow and its applications to school of fish," *International Journal of Semantic Computing*, vol.9, no.2, pp. 143-168, 2015.

Journal article

- [J2] K. Terayama and H. Tsuiki, "A Stream Calculus of Bottomed Sequences for Real Number Computation" *Electronic Notes in Theoretical Computer Science*, Vol.298, pp.383-402, 2013.

Refereed International Conference Papers related to this thesis

- [IC1] K. Terayama, K. Hongo, H. Habe and M. Sakagami, "Appearance-based Multiple Fish Tracking for Collective Motion Analysis," The Third IAPR Asian Conference on Pattern Recognition (ACPR 2015), Kuala Lumpur, Nov, 2015.
- [IC2] K. Terayama and M. Sakagami, "Measurement of Velocity Fields of Schools of Sardines and Existence of Averaged Tori," The First International Symposium on Swarm Behavior and Bio-Inspired Robotics (SWARM 2015), pp.324-325, Kyoto, Oct, 2015.
- [IC3] K. Terayama, H. Hioki and M. Sakagami, "A Measurement Method for Speed Distribution of Collective Motion with Optical Flow and its Application to Estimation of Rotation Curve," in Proceedings of the IEEE International Symposium on Multimedia (ISM 2014), pp.32-39, Taichung, Dec, 2014.

Refereed International Conference Paper

- [IC4] K. Terayama and H. Hioki, "A Practical Classifier for Photographs and Non-Photographic Images Based on Local Visual Features," in Proceedings of the 14th IAPR Conference on Machine Vision Applications (MVA 2015), pp.307-311, Tokyo, May, 2015.

Refereed Domestic Conference Paper related to this thesis

- [DC1] M.Sakagami and K.Terayama, "Swift response and fluctuation of fish schools," Proceedings of the Symposium on Simulation of Traffic Flow, Vol.21, pp.91-94, 2015. (in Japanese)

- [DC2] M.Sakagami and K.Terayama, "Velocity structures of fish schools and existence of averaged tori," Proceedings of the Symposium on Simulation of Traffic Flow, Vol.20, pp.27-30, 2014. (in Japanese)

Refereed Domestic Conference Paper

- [DC3] K.Terayama and H. Hioki, "A method classifying digital images into photographs and non-photo images based on visual characteristics of hand-drawn images," The 17th Meeting on Image Recognition and Understanding (MIRU2014), OS3-7, Okayama Convention Center, Jul 2014.

International Conferences related to this thesis

- [C1] M. Sakagami and K. Terayama, "Averaged Torus and fluctuation of fish schools," International Conference on Mathematical Modeling and Applications 2014 'Crowd Dynamics'(ICMMA 2014), Tokyo, January.
- [C2] K. Terayama, D. Tadokoro, K. Shimatani and M. Sakagami, "Analysis of a long-time evolution and fluctuations in the average torus shape of fish school," The 6th International Symposium on Aero Aqua Bio-mechanisms (ISABMEC 2014), pp.66-72, Honolulu, November, 2014.

BIBLIOGRAPHY

- [1] EthoVision. <http://www.noldus.com/animal-behavior-research/products/ethovision-xt>.
- [2] Kujukushima aquarium - umi kirara. <http://www.pearlsea.jp/english/aquarium.html/>.
- [3] Nissan eporo robot car “goes to school” on collision-free driving by mimicking fish behavior. http://www.nissan-global.com/EN/NEWS/2009/_STORY/091001-01-e.html.
- [4] SwisTrack. <http://disal.epfl.ch/page-32500-en.html>.
- [5] VideoTrack. <http://www.viewpoint.fr/en/p/software/videotrack>.
- [6] S. Ali and M. Shah. Floor fields for tracking in high density crowd scenes. In *ECCV*, pages 1–14. 2008.
- [7] I. Aoki. A simulation study on the schooling mechanism in fish. *Bulletin of the Japanese Society of Scientific Fisheries*, 48(8):1081–1088, 1982.
- [8] R. Bainbridge. The speed of swimming of fish as related to size and to the frequency and amplitude of the tail beat. *Journal of Experimental Biology*, 35(1):109–133, 1958.
- [9] M. Ballerini, N. Cabibbo, R. Candelier, A. Cavagna, E. Cisbani, I. Giardina, V. Lecomte, A. Orlandi, G. Parisi, A. Procaccini, M. Viale, and V. Zdravkovic. Interaction ruling animal collective behavior depends on topological rather than metric distance: Evidence from a field study. *Proc. of the National Academy of Sciences of the United States of America*, 105(4):1232–1237, 2008.
- [10] M. Ballerini, N. Cabibbo, R. Candelier, A. Cavagna, E. Cisbani, I. Giardina, A. Orlandi, G. Parisi, A. Procaccini, M. Viale, et al. Empirical investigation of starling flocks: a benchmark study in collective animal behaviour. *Animal behaviour*, 76(1):201–215, 2008.
- [11] M. Bando, K. Hasebe, A. Nakayama, A. Shibata, and Y. Sugiyama. Dynamical model of traffic congestion and numerical simulation. *Physical Review E*, 51(2):1035–1042, 1995.
- [12] S. Bazazi, J. Buhl, J. J. Hale, M. L. Anstey, G. A. Sword, S. J. Simpson, and I. D. Couzin. Collective motion and cannibalism in locust migratory bands. *Current Biology*, 18(10):735–739, 2008.

- [13] C. Becco, N. Vandewalle, J. Delcourt, and P. Poncin. Experimental evidences of a structural and dynamical transition in fish school. *Physica A: Statistical Mechanics and its Applications*, 367:487–493, 2006.
- [14] J. Berclaz, F. Fleuret, E. Türetken, and P. Fua. Multiple object tracking using k-shortest paths optimization. *IEEE Transactions on Pattern Analysis and Machine Intelligence*, 33(9):1806–1819, 2011.
- [15] J. Binney and S. Tremaine. *Galactic Dynamics*. Princeton Univ. Press, 1987.
- [16] D. Biro, D. Sumpter, J. Meade, and T. Guilford. From compromise to leadership in pigeons homing. *Current Biology*, 16(21):2123–2128, 2006.
- [17] C. M. Breder. Studies on the structure of the fish school. *Bulletin of the American museum of natural history*, 98(1):1–28, 1951.
- [18] C. M. Breder. Equations descriptive of fish schools and other animal aggregations. *Ecology*, 35(3):361–370, 1954.
- [19] D. Bumann, J. Krause, and D. Rubenstein. Mortality risk of spatial positions in animal groups: the danger of being in the front. *Behaviour*, 134(13):1063–1076, 1997.
- [20] S. Butail and D. A. Paley. Three-dimensional reconstruction of the fast-start swimming kinematics of densely schooling fish. *Journal of The Royal Society Interface*, 9(66):77–88, 2012.
- [21] A. Cavagna, A. Cimarelli, I. Giardina, G. Parisi, R. Santagati, F. Stefanini, and M. Viala. Scale-free correlations in starling flocks. *Proceedings of the National Academy of Sciences*, 107(26):11865–11870, 2010.
- [22] A. Cavagna, I. Giardina, A. Orlandi, G. Parisi, A. Procaccini, M. Viale, and V. Zdravkovic. The STARFLAG handbook on collective animal behaviour: 1. Empirical methods. *Animal Behaviour*, 76(1):217–236, 2008.
- [23] H. Chaté, F. Ginelli, G. Grégoire, and F. Raynaud. Collective motion of self-propelled particles interacting without cohesion. *Physical Review E*, 77:046113, 2008.
- [24] D. Comaniciu and P. Meer. Mean shift: A robust approach toward feature space analysis. *IEEE Transactions on Pattern Analysis and Machine Intelligence*, 24(5):603–619, 2002.
- [25] D. Comaniciu, V. Ramesh, and P. Meer. Kernel-based object tracking. *IEEE Transactions on Pattern Analysis and Machine Intelligence*, 25(5):564–577, 2003.

- [26] I. Couzin. Collective minds. *Nature*, 445:715–715, 2007.
- [27] I. D. Couzin and N. R. Franks. Self-organized lane formation and optimized traffic flow in army ants. *Proceedings of the Royal Society of London B: Biological Sciences*, 270(1511):139–146, 2003.
- [28] I. D. Couzin, J. Krause, N. R. Franks, and S. A. Levin. Effective leadership and decision-making in animal groups on the move. *Nature*, 433:513–516, 2005.
- [29] I. D. Couzin, J. Krause, R. James, G. D. Ruxton, and N. R. Franks. Collective memory and spatial sorting in animal groups. *Journal of theoretical biology*, 218(1):1–11, 2002.
- [30] A. Czirók, E. Ben-Jacob, I. Cohen, and T. Vicsek. Formation of complex bacterial colonies via self-generated vortices. *Physical Review E*, 54(2):1791–1801, 1996.
- [31] A. Czirók, H. E. Stanley, and T. Vicsek. Spontaneously ordered motion of self-propelled particles. *Journal of Physics A: Mathematical and General*, 30(5):1375–1385, 1997.
- [32] A. Czirók, M. Vicsek, and T. Vicsek. Collective motion of organisms in three dimensions. *Physica A: Statistical Mechanics and its Applications*, 264(1):299–304, 1999.
- [33] J. Delcourt, C. Becco, N. Vandewalle, and P. Poncin. A video multitracking system for quantification of individual behavior in a large fish shoal: Advantages and limits. *Behavior Research Methods*, 41(1):228–235, 2009.
- [34] J. Delcourt, M. Denoël, M. Ylieff, and P. Poncin. Video multitracking of fish behaviour: a synthesis and future perspectives. *Fish and Fishers*, 14(2):186–204, 2013.
- [35] M. J. B. Duff. Clip4: A large scale integrated circuit array parallel processor. In *Proc. of 3rd International Joint Conference on Pattern Recognition*, pages 728–732, 1976.
- [36] J. J. Faria, J. R. Dyer, C. R. Tosh, and J. Krause. Leadership and social information use in human crowds. *Animal Behavior*, 79(4):895–901, 2010.
- [37] G. Farneäck. Two-frame motion estimation based on polynomial expansion. In *Image Analysis*, pages 363–370. 2003.
- [38] F. Fish, J. Fegely, and C. Xanthopoulos. Burst-and-coast swimming in schooling fish (*Notemigonus crysoleucas*) with implications for energy economy. *Comparative Biochemistry and Physiology Part A: Physiology*, 100(3):633–637, 1991.

- [39] E. Fontaine, D. Lentink, S. Kranenbarg, U. K. Müller, J. L. van Leeuwen, A. H. Barr, and J. W. Burdick. Automated visual tracking for studying the ontogeny of zebrafish swimming. *Journal of Experimental Biology*, 211(8):1305–1316, 2008.
- [40] N. Gordon, D. Salmond, and A. Smith. Novel approach to nonlinear/non-Gaussian Bayesian state estimation. *IEE Proc. F (Radar and Signal Processing)*, 140(2):107–113, 1993.
- [41] H. Hashimoto, S. Aso, S. Yokota, A. Sasaki, Y. Ohyama, and H. Kobayashi. Cooperative movement of human and swarm robot maintaining stability of swarm. In *Proceedings of the 17th IEEE International Symposium on Robot and Human Interactive Communication*, pages 249–254, 2008.
- [42] Y. Hayakawa. Spatiotemporal dynamics of skeins of wild geese. *Europhysics Letters*, 89:48004, 2010.
- [43] D. Helbing, F. Illés, and T. Vicsek. Simulating dynamical features of escape panic. *Nature*, 407:487–490, 2000.
- [44] D. Helbing, A. Johansson, and H. Z. Al-Abideen. Dynamics of crowd disasters: An empirical study. *Physical Review E*, 75(4):046109, 2007.
- [45] C. K. Hemelrijk and H. Hildenbrandt. Self-organized shape and frontal density of fish schools. *Ethology*, 114(3):245–254, 2008.
- [46] C. K. Hemelrijk, H. Hildenbrandt, J. Reinders, and E. J. Stamhuis. Emergence of oblong school shape: models and empirical data of fish. *Ethology*, 116(11):1099–1112, 2010.
- [47] C. K. Hemelrijk and H. Kunz. Density distribution and size sorting in fish schools: an individual-based model. *Behavioral Ecology*, 16(1):178–187, 2005.
- [48] C. K. Hemelrijk, D. A. P. Reid, H. Hildenbrandt, and J. T. Padding. The increased efficiency of fish swimming in a school. *Fish and Fisheries*, 16(3):511–521, 2014.
- [49] L. F. Henderson. The statistics of crowd fluids. *Nature*, 229:381–383, 1971.
- [50] F. H. Heppner. *Three-dimensional structure and dynamics of bird flocks*. Cambridge University Press, 1997.
- [51] H. Hexmoor, B. McLaughlan, and M. Baker. Swarm control in unmanned aerial vehicles. In *Proc. of International Conference on Artificial Intelligence*, pages 911–917, 2005.

- [52] J. K. Hodgins, W. L. Wooten, D. C. Brogan, and J. F. O'Brien. Animating human athletics. In *Proc. of SIGGRAPH*, pages 71–78, 1995.
- [53] J. R. Hunter and J. R. Zweifel. Swimming speed, tail beat frequency, tail beat amplitude, and size in jack mackerel, *Trachyrus symmetricus*, and other fishes. *Fishery Bulletin*, 69(2):253–266, 1971.
- [54] A. Huth and C. Wissel. The simulation of the movement of fish schools. *Journal of theoretical biology*, 156(3):365–385, 1992.
- [55] A. Huth and C. Wissel. The simulation of fish schools in comparison with experimental data. *Ecological modelling*, 75:135–146, 1994.
- [56] Y. Inada and K. Kawachi. Order and flexibility in the motion of fish schools. *Journal of theoretical Biology*, 214(3):371–387, 2002.
- [57] M. Isard and A. Blake. Condensation — conditional density propagation for visual tracking. *International journal of computer vision*, 29(1):5–28, 1998.
- [58] M. Kang. Semiautomated analysis of data from an imaging sonar for fish counting, sizing, and tracking in a post-processing application. *Fisheries and Aquatic Sciences*, 14(3):218–225, 2011.
- [59] S. Kato, T. Nakagawa, M. Ohkawa, K. Muramoto, O. Oyama, A. Watanabe, H. Nakashima, T. Nemoto, and K. Sugitani. A computer image processing system for quantification of zebrafish behavior. *Journal of neuroscience methods*, 134(1):1–7, 2004.
- [60] Y. Katz, K. Tunstrom, C. C. Ioannou, C. Huepe, and I. D. Couzin. Inferring the structure and dynamics of interactions in schooling fish. *Proceedings of the National Academy of Sciences*, 108(46):18720–18725, 2011.
- [61] E. Keller and L. Segel. Model for chemotaxis. *Journal of Theoretical Biology*, 30(2):225–234, 1971.
- [62] Z. Khan, T. Balch, and F. Dellaert. Mcmc-based particle filtering for tracking a variable number of interacting targets. *IEEE Transactions on Pattern Analysis and Machine Intelligence*, 27(11):1805–1819, 2005.
- [63] J. Krause, D. Hoare, S. Krause, C. K. Hemelrijk, and D. I. Rubenstein. Leadership in fish shoals. *Fish and Fisheries*, 1(1):82–89, 2000.

- [64] H. Kunz and C. K. Hemelrijk. Artificial fish schools: Collective effects of school size, body size, and body form. *Artificial Life*, 9(3):237–253, 2003.
- [65] M. Kupilik and T. Petersen. Imaging sonar tracking of salmon for size and tail beat frequency. In *Proc. of IEEE Global Conference on Signal and Information Processing*, pages 1127–1131, 2014.
- [66] B. J. Laurel, C. J. Laurel, J. A. Brown, and R. S. Gregory. A new technique to gather 3-d spatial information using a single camera. *Journal of fish biology*, 66(2):429–441, 2005.
- [67] J. C. Liao. A review of fish swimming mechanics and behavior in altered flows. *Philosophical Transactions of the Royal Society B*, 362(1487):1973–1993, 2007.
- [68] J. Liu and Y. Liu. Multi-target tracking of time-varying spatial patterns. In *CVPR*, pages 1839–1846, 2010.
- [69] B. D. Lucas and T. Kanade. An Iterative Image Registration Technique with an Application to Stereo Vision. In *IJCAI*, pages 674–679, 1981.
- [70] P. F. Major. Predator-prey interactions in two schooling fishes, *Caranx ignobilis* and *Stolephorus purpureus*. *Animal Behaviour*, 26(3):760–777, 1978.
- [71] N. C. Makris, P. Ratilal, D. T. Symonds, S. Jagannathan, S. Lee, and R. W. Nero. Fish population and behavior revealed by instantaneous continental shelf-scale imaging. *Science*, 311(5761):660–663, 2006.
- [72] R. Mikel, S. Ali, and T. Kanade. Tracking in unstructured crowded scenes. In *ICCV*, pages 1389–1396, 2009.
- [73] N. Y. Miller and R. Gerlai. Oscillations in shoal cohesion in zebrafish (*Danio rerio*). *Behavioural brain research*, 193(1):148–151, 2008.
- [74] H. Min and Z. Wang. Design and analysis of Group Escape Behavior for distributed autonomous mobile robots. In *Proc. of the IEEE International Conference on Robotics and Automation*, pages 6128–6135, 2011.
- [75] A. V. Moere. Time-varying data visualization using information flocking boids. In *Proc. of IEEE Symposium on Information Visualization*, pages 97–104, 2004.
- [76] K. Nagel and M. Schreckenberg. A cellular automaton model for freeway traffic. *Journal de Physique I*, 2(12):2221–2229, 1992.

- [77] M. Nagy, Z. Ákos, D. Biro, and T. Vicsek. Hierarchical group dynamics in pigeon flocks. *Nature*, 464(7290):890–893, 2010.
- [78] H.-S. Niwa. Self-organizing dynamic model of fish schooling. *Journal of theoretical Biology*, 171(2):123–136, 1994.
- [79] K. Okuma, A. Taleghani, N. De Freitas, J. J. Little, and D. G. Lowe. A boosted particle filter: Multitarget detection and tracking. In *ECCV*, pages 28–39, 2004.
- [80] B. L. Partridge. Internal dynamics and the interrelations of fish in schools. *Journal of Comparative Physiology*, 144(3):313–325, 1981.
- [81] B. L. Partridge. The structure and function of fish schools. *Scientific american*, 246(6):114–123, 1982.
- [82] B. L. Partridge and J. M. Cullen. A low-cost interactive coordinate plotter. *Behavior Research Methods & Instrumentation*, 9(5):473–479, 1977.
- [83] B. L. Partridge, T. Pitcher, J. M. Cullen, and J. Wilson. The three-dimensional structure of fish schools. *Behavioral Ecology and Sociobiology*, 6(4):277–288, 1980.
- [84] B. L. Partridge and T. J. Pitcher. The sensory basis of fish schools: relative roles of lateral line and vision. *Journal of Comparative Physiology*, 135(4):315–325, 1980.
- [85] L. A. Pipes. An operational analysis of traffic dynamics. *Journal of applied physics*, 24(3):274–281, 1953.
- [86] T. J. Pitcher. *Functions of shoaling behaviour in teleosts*. Springer US, 1986.
- [87] T. J. Pitcher, A. E. Magurran, and I. J. Winfield. Fish in larger shoals find food faster. *Behavioral Ecology and Sociobiology*, 10(2):149–151, 1982.
- [88] T. J. Pitcher and C. J. Wyche. Predator-avoidance behaviours of sand-eel schools: why schools seldom split. In *Predators and prey in fishes*, pages 193–204. Springer Netherlands, 1983.
- [89] Z.-M. Qian, X. E. Cheng, and Y. Q. Chen. Automatically detect and track multiple fish swimming in shallow water with frequent occlusion. *PLOS ONE*, 9(9):e106506, 2014.
- [90] D. V. Radakov. *Schooling in the Ecology of Fish*. Wiely, 1973.
- [91] C. W. Reynolds. Flocks, herds and schools: A distributed behavioral model. *ACM SIGGRAPH Computer Graphics*, 21(4):25–34, 1987.

- [92] W. Sakamoto, I. Aoki, and T. Kuroki. Studies on the schooling behaviour of fish. 1: Spectral analyses of interaction between two individuals of fish in locomotion. *Bulletin of the Japanese Society of Scientific Fisheries*, 41:945–952, 1975.
- [93] W. Sakamoto, T. Inagaki, and T. Kuroki. Studies of the schooling behaviour of fish. 4: Some discussions concerning continuity of swimming speed and response time of individuals. *Bulletin of the Japanese Society of Scientific Fisheries*, 42:1983–191, 1967.
- [94] M. Saska, J. Vakula, and L. Preucil. Swarms of micro aerial vehicles stabilized under a visual relative localization. In *Proc. of IEEE International Conference on Robotics and Automation*, pages 3570–3575, 2014.
- [95] T. C. Schneirla. A unique case of circular milling in ants, considered in relation to trail following and the general problem of orientation. *American Museum Novitates*, 1253:1–26, 1944.
- [96] E. Shaw. Schooling fishes. *American Scientist*, 66:166–175, 1978.
- [97] J. Shi and C. Tomasi. Good features to track. In *CVPR*, pages 593–600, 1994.
- [98] M. F. Steinhausen, J. F. Steffensen, and N. G. Andersen. Tail beat frequency as a predictor of swimming speed and oxygen consumption of saithe (*Pollachius virens*) and whiting (*Merlangius merlangus*) during forced swimming. *Marine Biology*, 148(1):197–204, 2005.
- [99] A. Strandburg-Peshkin, C. R. Twomey, N. W. Bode, A. B. Kao, Y. Katz, C. C. Ioannou, S. B. Rosenthal, C. J. Torney, H. S. Wu, S. A. Levin, et al. Visual sensory networks and effective information transfer in animal groups. *Current Biology*, 23(17):R709–R711, 2013.
- [100] Y. Sugiyama, M. Fukui, M. Kikuchi, K. Hasebe, A. Nakayama, K. Nishinari, S. ichi Tadaki, and S. Yukawa. Traffic jams without bottlenecks-experimental evidence for the physical mechanism of the formation of a jam. *New Journal of Physics*, 10(3):033001, 2008.
- [101] D. Sumpter, J. Buhl, D. Biro, and I. Couzin. Information transfer in moving animal groups. *Theory in Biosciences*, 127(2):177–186, 2008.
- [102] D. J. Sumpter, J. Krause, R. James, I. D. Couzin, and A. J. Ward. Consensus decision making by fish. *Current Biology*, 18(22):1773–1777, 2008.

- [103] K. Suzuki, T. Takagi, and T. Hiraishi. Video analysis of fish schooling behavior in finite space using a mathematical model. *Fisheries Research*, 60(1):3–10, 2003.
- [104] J. C. Svendsen, J. Skov, M. Bildsoe, and J. F. Steffensen. Intra-school positional preference and reduced tail beat frequency in trailing positions in schooling roach under experimental condition. *Journal of Fish Biology*, 62(4):834–846, 2003.
- [105] J. A. Tipton. Aristotle’s observations of the foraging interactions of the red mullet (Mullidae: *Mullus* spp) and sea bream (Sparidae: *Diplodus* spp). *Archives of natural history*, 35(1):164–171, 2008.
- [106] J. Toner and Y. Tu. Long-range order in a two-dimensional XY model: How birds fly together. *Physical Review Letters*, 75(23):4326–4329, 1995.
- [107] J. Toner and Y. Tu. Flocks, herds, and schools: A quantitative theory of flocking. *Physical Review E*, 58:4828–4858, 1998.
- [108] N. Ukita, T. Kitajima, and M. Kidode. Estimating the positions and postures of non-rigid objects lacking sufficient features based on the stick and ellipse model. In *Computer Vision and Pattern Recognition Workshop*, page 5, 2004.
- [109] J. Vermaak, A. Doucet, and P. Pérez. Maintaining multimodality through mixture tracking. In *ICCV*, pages 1110–1116, 2003.
- [110] T. Vicsek, A. Czirók, E. Ben-Jacob, I. Cohen, and O. Shochet. Novel type of phase transition in a system of self-driven particles. *Physical review letters*, 75(6):1226–1229, 1995.
- [111] T. Vicsek and A. Zafeiris. Collective motion. *Physics Reports*, 517(3):71–140, 2012.
- [112] J. J. Videler. *Fish Swimming*. Chapman and Hall, 1993.
- [113] S. V. Viscido, J. K. Parrish, and D. Grünbaum. Individual behavior and emergent properties of fish schools: a comparison of observation and theory: Emergent properties of complex marine systems: a macroecological perspective. *Marine ecology. Progress series*, 273:239–249, 2004.
- [114] D. Weihs. Hydromechanics of fish schooling. *Nature*, 241:290–291, 1973.
- [115] D. Weihs. Energetic advantages of burst swimming of fish. *Journal of Theoretical Biology*, 48(1):215–229, 1974.

- [116] Z. Yin and R. Collins. Belief propagation in a 3D spatio-temporal MRF for moving object detection. In *CVPR*, pages 1–8, 2007.
- [117] M. Y. Ylieff and P. Poncin. Quantifying spontaneous swimming activity in fish with a computerized color video tracking system, a laboratory device using last imaging techniques. *Fish Physiology and Biochemistry*, 28(1):281–282, 2003.